Electronic Thesis and Dissertation Repository

12-15-2022 10:00 AM

Wind-Borne Debris Resistance of Façades: Identification of Alternative Impact Test Requirements

Angela Mejorin, *The University of Western Ontario*

Supervisor: Kopp, Gregory A., *The University of Western Ontario*
Joint Supervisor: Trabucco, Dario, *Iuav University of Venice, Italy*
A thesis submitted in partial fulfillment of the requirements for the Doctor of Philosophy degree in Civil and Environmental Engineering
© Angela Mejorin 2022

Follow this and additional works at: https://ir.lib.uwo.ca/etd

Part of the Civil and Environmental Engineering Commons

Abstract

Climate change effects are causing a steady increase of previous records both in terms of monetary losses and in fatality occurrence due to severe storms. The frequency and intensity of disaster events are increasing worldwide and areas that were excluded from these extreme weather scenarios in the past, are now looking for solutions to increase the urban resilience. Among others, extreme winds are endangering the built environment, often leading to the breakage of the primary barrier to protect people and property: the building envelope. On May 22nd, 2011, the Joplin tornado killed 161 people, and 14 of those were receiving treatments at the St. John's Regional Medical Center. At the hospital, most of the windows were broken by the impact of wind-borne debris. The structure of the hospital has remained intact and only one section of the building was not affected by façade breakage: the Behavioral Health Unit, a result that was ensured by breakage-resistant windows. To avoid façade breakage, in areas hit almost every year by tropical cyclones and hurricanes, code and standard requirements have been developed in the last five decades, to provide wind-borne debris impact resistance to the building envelope. This thesis develops a performance-based design framework to identify alternative impact test criteria, to verify the resilience of façades to wind-borne debris, in specific contexts. The design framework is, therefore, set for case-specific wind-borne debris types, to explore the design possibility given by the code and standard best practices. The analysis considers building aerodynamics, and the trajectory and velocity of specific debris elements to implement performance-based façade technologies. The reference target buildings of the thesis are essential facilities, to avoid disruption of essential services, especially in the post-event scenario. If new buildings and façade retrofit projects can improve their resilience to wind-borne debris impacts, there can be a notable mitigation of the overall consequences of extreme wind events. The current widely adopted testing equipment to conduct wind-borne debris impact testing is presented in its implementation to work out alternative impact tests. Adopting performance-based design impact tests, building envelope solutions can sustainably address local needs to improve urban resilience.

Keywords

Summary for Lay Audience

The effects of climate change are causing an increase of windstorms worldwide that are reported on at least a weekly basis by major news organizations. The extreme winds are known as tornadoes, hurricanes, tropical cyclones, typhoons, depending both on the wind characteristics and on the location of the disaster event in the Globe. During these events, one of the major risks is related to wind-borne debris that could lift from its position and subsequently fly, impacting building envelopes and urban objects such as cars, houses, and anything in its path. Wind-borne debris impact could, therefore, cause window and façade breakage and, consequently, damage the entire building structure, all the mechanical and electrical systems, and its contents. For essential facilities such as hospitals, if these problems occur, it means that primary services cannot be guaranteed in emergency circumstances such as the immediate aftermath of an event. To mitigate the negative consequences of wind on the building envelopes, and to avoid breakage of windows, doors, and façade solutions in general, there are testing procedures to verify if these building components can withstand wind-borne debris impacts. These procedures have been developed in the last fifty years through damage observation, without considering the aerodynamic behavior of free-to-fly objects in specific urban environments. This thesis proposes an alternative design framework for window and façade design, to make these building envelope technologies resistant to the impacts of local debris that is seen in specific contexts. The results are especially addressed to essential facilities, to avoid in the future dramatic outcomes such as the May 22nd, 2011, Joplin tornado that killed 161 people, of which 14 were receiving treatments at the St. John's Regional Medical Center. The hospital's structure was not affected by any damage, but almost all the windows were broken by wind-borne debris. When the windows were not protecting the interior of the building anymore, the patients turned to be victims, and the facility did not help the Joplin population to recover from the event.

Acknowledgements

Table of Contents

List of Tables

List of Figures

Symbols & Abbreviations

a	acceleration
A	influence area of the debris component
AR	aspect ratio of the plate
B	exposed width of the roof tile
c	center of pressure on the plate
C_D	drag coefficient
C_{DR}	rotational drag coefficient
C_{DS}	static drag coefficient
C_e	exposure factors (= $K_z K_{zt} K_d K_e$, defined in ASCE 7-22 2022)
C_g	gust effect factor
$C_g Cp_N$	peak pressures coefficient referenced to a 3-s gust-wind speed at roof height
C_L	lift coefficient
C_{L_IBC}	lift coefficient. The lift coefficient for concrete and clay tile shall be 0.2 or shall be determined by test in accordance with Section 1504.3.1 of IBC (2021)
C_{LR}	rotational lift coefficient
C_{LS}	static lift coefficient
C_M	moment coefficient
C_{MR}	rotational moment coefficient
C_{MS}	static moment coefficient
C_N	static normal coefficient on the plate
Cp	pressure coefficient
Cp_N	peak pressures coefficient referenced to a 3-s gust-wind speed at roof height (= ($Cp_e - Cp_i$), defined in ASCE 7-22 2022, Section 30.3)
D	drag force
F_a	aerodynamic force
F_H	total hold-down force on the debris element
$F_{HoldDown}$	hold-down force of the restraint system type
F_m	hold-down force given by the weight of the debris element

FS	fixing strength
g	gravity acceleration
GCp	3-second gust net pressure coefficient acting on the building component, determined from Chapter 30 of ASCE 7-22 (2022)
h	thickness of the plate
H	mean roof height
he	height of fenestration assembly
I	moment of inertia of the plate
I*	non-dimensional moment of inertia of a plate
K	kinetic energy
K_d	wind directionality factor (defined in ASCE 7-22 2022, Section 26.6)
K_e	ground elevation factor (defined in ASCE 7-22 2022, Section 26.9)
K_z	velocity pressure exposure coefficient (defined in ASCE 7-22 2022, Section 30.3)
K_{zt}	topographic factor (defined in ASCE 7-22 2022, Section 26.8)
ℓ	side dimension of the plate
L	lift force
L_t	maximum overall dimension of the tile measured parallel to the water course
L_{at}	moment arm from the axis of rotation to the point of uplift on the roof tile. The point of uplift shall be taken at 0.76 L_t from the head of the tile and the middle of the exposed width
m	mass of the debris
M	pitching moment
M_a	aerodynamic uplift moment acting to raise the tail of the tile
$N_{impacts}$	number of debris impact on target façade
N_{total}	number of Monte Carlo simulations
p	surface pressure
P_{impact}	probability of façade impact
p_0	static pressure
q	dynamic wind pressure (= 0.5 $\rho_a V_b^2$)
q_h	wind velocity pressure determined from Section 26.10.2 of ASCE 7-22 (2022)

S	spin parameter of the plate
S_0	spin parameter of the plate at the point of stable autorotation
S_{up}	speed-up factor
t	time
$\bar{t}$	non-dimensional time
T_a	Tachikawa number
u	horizontal velocity of the plate
U	horizontal wind velocity
$\bar{u}$	non-dimensional horizontal velocity of the plate
U_{rel}	relative velocity of the plate
$\bar{U}_{rel}$	non-dimensional relative wind velocity
V	vertical wind velocity
$\bar{V}$	non-dimensional vertical wind velocity
$V_{10,000}$	3-s gust regional wind speed (V_R) for a 10,000 annual recurrence interval (AS/NZS 1170.2 2021)
$V_{failure}$	failure wind speed
V_b	basic wind speed [1]
V_{b_ref}	reference wind speed [2]
V_{b_ini}	minimum basic wind speed to have debris failure
V_{imp}	impact velocity
V_{mean_ini}	10-min mean wind speeds to have debris failure
V_r	flight initialization wind speed for the restrained debris element
V_R	3-s gust regional wind speed (AS/NZS 1170.2 2021)

---

[1] Basic wind speed (V_b): it is intended to represent the 3-s gust wind speed design such as used to describe a 50-year recurrence period or annual 0.02 probability of being exceeded (ASCE 7-22 2022, Section 26.5 = 3-s gust speed at 10 m in open terrain). Conversion factors based on worldwide design best practices and wind engineering literature are given to report the described basic wind speed to another context such as the European (ISO 4354 2009).

[2] 3-s gust reference wind speed for target building design. It considers the basic wind speed (V_b) without the load factor used in the building codes (i.e. ASCE 7-22 2022).

V_s	flight initialization wind speed for the unrestrained debris element
$V_{T=1h}$	1-hour mean wind speed
$V_{T=10min}$	10-minute mean wind speed
$V_{T=3s}$	3-second gust wind speed
w	vertical velocity of the plate
$\bar{w}$	non-dimensional vertical velocity of the plate
x	horizontal distance of the debris element
$\bar{x}$	non-dimensional horizontal displacement of the debris element
z	vertical distance of the debris element
$\bar{z}$	non-dimensional vertical displacement of the debris element
α	angle of attack of the relative wind velocity with reference to the horizontal axis
β	angle of attack of the relative wind velocity to the plate
Δ	non-dimensional plate inertia
θ	angle of rotation of the debris element
$\bar{\theta}$	non-dimensional angular rotation of the debris element
τ	thickness ratio of the plate
ρ_a	air density
ρ_m	density of the debris element
φ	buoyancy parameter
Ω	dimensionless parameter
ω	angular velocity of the plate
ω_0	angular velocity of the plate at the point of stable autorotation

Chapter 1. Introduction

1.1 Background

Evidence of climate change is now clear and convincing worldwide, and one of the major consequences is in the increasing intensity and quantity of extreme weather events (IPCC 2022; Munich RE 2022; Gergis 2019; Sisco et al. 2017). There is an upward trend in natural disasters, in terms of economic losses and people injured or death (Munich RE 2021; Lu et al. 2019; Brody et al. 2008; Eckstein et al. 2021). Extreme weather is the second most severe risk on a global scale over the next decade identified by the World Economic Forum Global Risks Perception Survey 2021-2022 (World Economic Forum 2022a). "Extreme weather" and "climate action failure" are among the top five short term risks to the world according to the Survey, and the climate action intend to contain the in-progress increasing effects of climate change.

Extreme weather events are represented by extreme wind events such as hurricanes, typhoons, tornadoes, floods, wildfires, etc. and their occurrence is related to loss of human life, damage to ecosystems, property damage, and/or financial loss, at a global scale. Climate action failure identifies the failure of governments and businesses to enforce, enact or invest in effective climate change adaptation and mitigation measures, preserve ecosystems, protect populations, and transition to a carbon-neutral economy. If we consider the Top Five Risks Identified by the Executive Opinion Survey (World Economic Forum 2022a) for Italy, Canada, and the United States "extreme weather events" are the third risk for these three countries, and the "climate action failure" is respectively the first risk for Italy and the second risk for Canada and the United States. China, the world's largest carbon emitter, finally set down a plan to achieve carbon neutrality by 2050 (World Economic Forum 2022b), and in the Top Five Risks Identified by the Executive Opinion Survey, "extreme weather events" represent the first risk (World Economic Forum 2022a). It is necessary that Canada, China, and the United States strictly follow directions to contain carbon emissions due to the concentration of production industries in these territories (Weber 2015; IPCC 2018; Jacobson et al. 2019).

When it comes to wind-related extreme weather events, these are defined with different naming conventions depending on the geographical area they occur in, even if the consequences are equally threatening. Tropical cyclones are called hurricanes in the Atlantic Ocean, in the Caribbean Sea, in the Gulf of Mexico, and East of the International Date Line. The same events are named cyclones in the South-West Pacific Ocean. Typhoon is a third term adopted on the West side of the International Date Line in the Pacific

area (Figure 1). Moreover, other extreme wind phenomena are constantly recorded worldwide, such as tornadoes and downbursts. The major tornado records are in the United States and Canada, but their recurrence has been noted in Argentina, Australia, Bangladesh, Brazil, Chile, France, Germany, India, Italy, Japan, Malta, New Zealand, Paraguay, Poland, Russia, South Africa, Spain, Ukraine, United Arab Emirates, United Kingdom, and Uruguay (Brooks et al. 2003; Chmielewski et al. 2013; Goliger & Milford 1998; Piscitelli et al. 2022; Zhang et al. 2020).
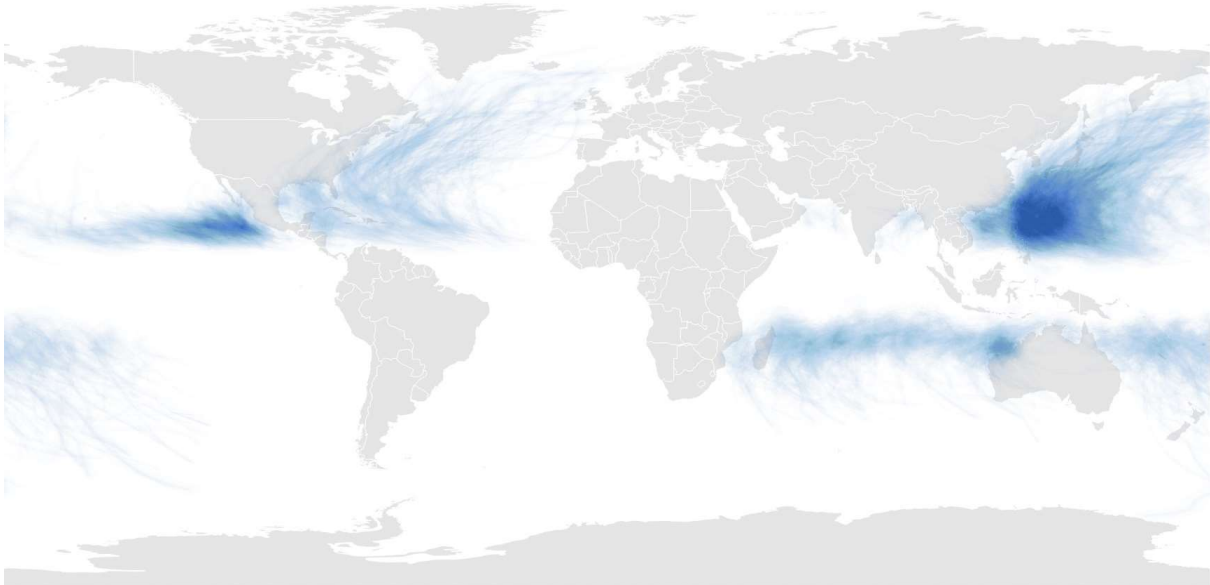
Figure 1 - World map of tropical cyclones-prone areas. GIS analysis based on UNEP (2017).

In the past decades, Europe was relatively less prone to severe winds, but an increase in both frequency and peak wind speed has been recorded in recent years (Chronis et al. 2015). The 2019 Annual Report of the European Severe Storms Laboratory reports 22,216 severe weather events (ESSL 2020). Most of the records are related to "severe wind gusts": 12,098 in total (ESSL 2020). In 2017 the recorded severe wind gusts have been 14,650 (ESSL 2018) with a three-fold increase from 2013 (ESSL 2014). In Italy, 946 extreme-weather events were reported in the 2010-2020 period, with 257 events being connected with strong winds (Legambiente 2020).

Extreme wind events affect the urban environment heavily damaging buildings (Minor et al. 1972) and one of the major causes of building damage is due to wind-borne debris[3] impact (Nishimura et al. 2009),

---

[3] Wind-borne debris: objects carried by the wind in windstorms.

especially on the building envelope (Minor 1994). It is useful to remember the May 22nd, 2011, Joplin tornado that hit Missouri as the costliest tornado in the United States history, that set the record of 3 billion U.S. dollars in damage. The same event is also the deadliest tornado event in the new millennium, with 161 fatalities, 14 of which recorded at the St. John's Regional Medical Center (Kuligowski et al. 2014). The hospital is an essential facility (ASCE 2022) that is supposed to help people to recover, especially in the post-event scenario when it comes to natural disasters. The structure of the hospital remained intact through the tornado, but most of the windows were broken. Consequently, wind-borne debris entered in the building, and the St. John's Regional Medical Center turned to be a cage for 14 patients that were receiving treatments. It is interesting to notice what has been highlighted by the Final Report of the National Institute of Standards and Technology on the Joplin tornado (Kuligowski et al. 2014): the fifth floor of this building, the Behavioral Health Unit, had breakage-resistant window solutions and most of these windows did not break. This example is one of the cases where performance-based design, to mitigate the effect of extreme wind events, would have made the difference in the victim records and also in helping the local population in the recovery phase. The debris elements that were found inside the building and that were considered cause of window breakage were primarily roof gravel (Kuligowski et al. 2014).

In extreme wind events, debris can originate from the failure of materials and pieces from source buildings and other man-made structures. Roof gravel, roof tiles, façade elements, antennas, and other urban components such as street signs can be blown away, becoming wind-borne debris that can endanger people and property, hitting surrounding buildings at high speed (ASCE 2014; Butler and Kareem 2012). In this scenario, building envelope is the first barrier to protect or at least to mitigate the effects of extreme wind events on people and property (Minor 2005).

Wind has been investigated extensively to prevent the failure of major building elements. Accordingly, codes and standards have been developed over decades (Florida Building Code 2020; ASCE 2022; AS/NZS 2021), but recent extreme wind events in territories that were not used to hurricanes and tornadoes such as Italy prove that also European buildings are vulnerable to extreme winds (Figure 2). The combination of increased wind actions, an old building stock, and meteorological events with different characteristics from the past (e.g., downbursts; Figure 4) are the main reasons for wind-induced damages, for which research is required.

Figure 2 - Extreme winds in Verona, Italy. August 29th, 2020. In this event, roof tiles were recorded flying from building roofs.

Currently, in National and European Codes, the wind-borne debris impact resistance of the building envelope is not considered. In contrast, other countries have developed design guidelines, testing, and certification systems to improve the resistance to wind-borne debris (Laboy et al. 2012), preventing the breach of the building envelope, systemic failures, and wind-driven water infiltration (Henderson et al. 2018; Herseth et al. 2012). The ASTM standards are the current best practices for impact testing to replicate wind-borne debris in destructive windstorm events[4] (ASTM 2019, 2020). Standard debris elements (missiles[5]) and impact

---

[4] Destructive windstorm: severe weather event with high winds and turbulent gusts, such as a tropical cyclone, having a reference wind speed capable of generating wind-borne debris.

[5] Missiles: objects that are propelled towards a test specimen – i.e. lumber missile, steel ball, roof tile, etc..

velocities are used in these testing procedures, to classify building envelope components such as windows and curtain wall solutions. The impact energies, that the products have to absorb without breaking to pass the impact tests that are simulating wind-borne debris, are not based on the aerodynamics of wind-borne debris in local contexts, due to the absence of a database of wind-borne debris speeds in hurricane and tropical-cyclone winds (Kordi 2009). However, the ASTM standard criteria allow façade designers to go through engineering analysis[6] to conduct ad hoc wind-borne debris impact tests for their projects, using "other missiles" for the impact test (ASTM 2019). In practice, designers and/or window and façade suppliers are unlikely to investigate this possibility because their competence does not extend to wind engineering.

Figure 3 - Downburst winds in Dunnville, Ontario, Canada. November 11th, 2020. Roof tile failure was recorded (Northern Tornadoes Project 2022).

---

[6] Engineering analysis is the demonstrated or documented performance through a review of materials that predicates a minimum of equivalent performance (ASTM 2019).

At an international level, there is an emerging interest from the International Standard Organization for the introduction of testing requirements to consider wind-borne debris impacts on building envelopes, and Technical Committee 162 "Doors, Windows, and Curtain Walling" formed an ad hoc group between the Working Group 4 (Windows and Doors) and the Working Group 5 (Curtain Walling) in 2021 to set down various levels of resistance of the building envelope when it comes to wind-borne debris impact. This group is developing a draft standard 'Windows, Doors and Curtain Walling - Impacted by Wind-Borne Debris in Windstorms - Test Method', which the author is coordinating. The standard will contribute to the Sustainable Development Goals (International Organization for Standardization 2018; UN 2022) 9 "Industry, Innovation and Infrastructure: Build resilient infrastructure, promote inclusive and sustainable industrialization and foster innovation", and 11 "Sustainable Cities and Communities: Make cities and human settlements inclusive, safe, resilient and sustainable".

This thesis aims to provide a performance-based design tool for façade designers, to estimating impact energies though trajectory and velocity analysis of specific debris after its failure occurs from source locations. The method proposed uses a fragility analysis to assess building component failure from a source building and it considers different wind-borne debris types. Past research has used fragility analyses to develop impact risk assessments and vulnerability models (Grayson et al. 2012; Zhang et al. 2014), whereas this thesis aims to highlight and propose a design framework for façade design. It presents, furthermore, suitable testing apparatus based on widely commercialized testing equipment, to handle the alternative tests that consider local debris.

The outcome can be used to implement both testing standards and design code requirements, presenting a specific case study for roof tile failure and impact of the surrounding target buildings. In extreme wind events roof tile failure and flight significantly influence a target buildings' window damage due to their impacts. In the U.S. context, building envelopes with surrounding roof coverings led to double the amount of damage if compared to target buildings surrounded by shingle-covered buildings (Gurley et al. 2006).
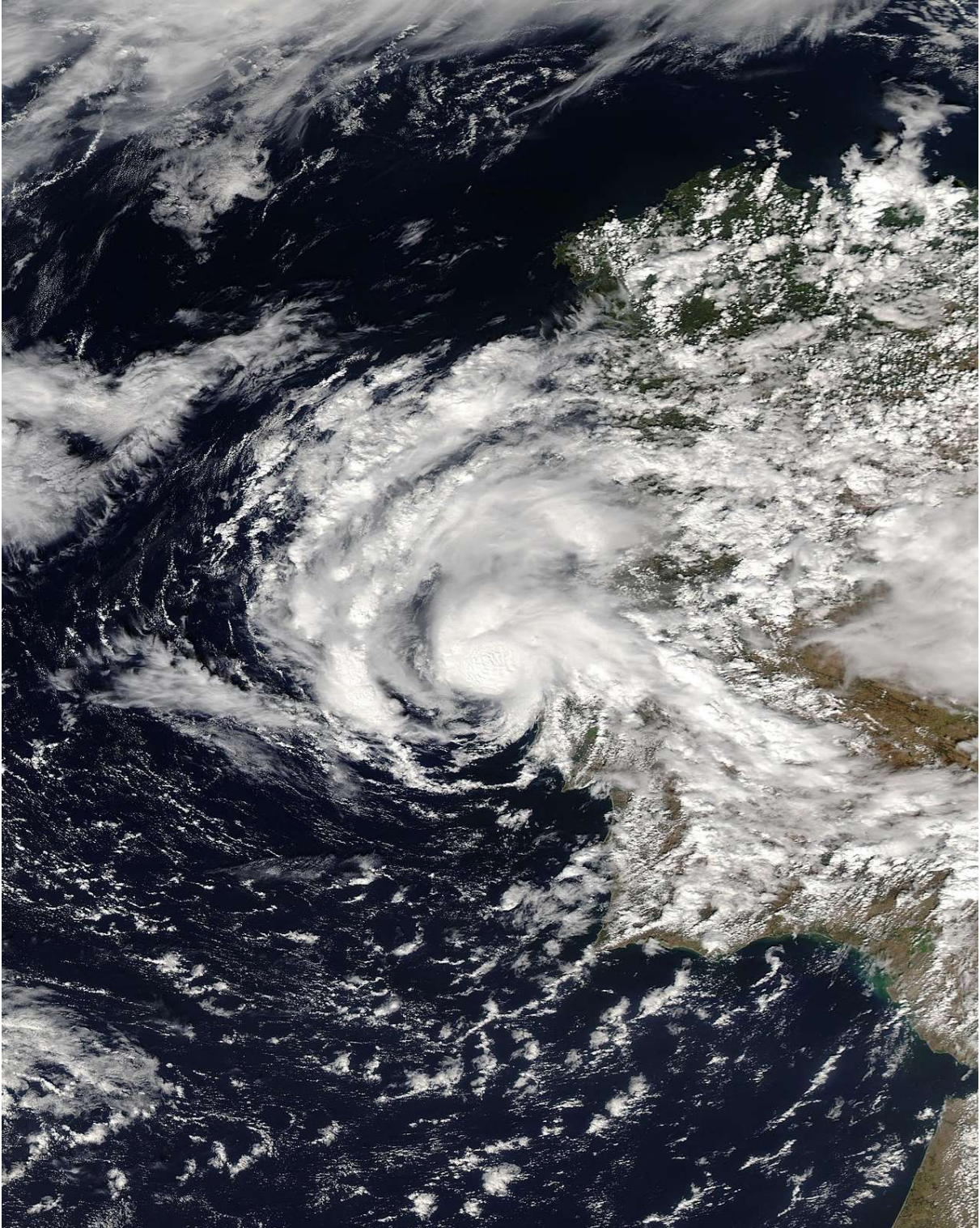
Figure 4 - Subtropical Storm Alpha, Portugal, September 18th, 2020 (NASA 2020).

1.2   Problem Statement, Aims, and Scope

As discussed above, one of the major causes of building damage in extreme winds is due to wind-borne debris impact (Minor 1994; ASCE 2014; Butler & Kareem 2012; Nishimura et al. 2009). This thesis presents a performance-based design framework for wind-borne-debris-resistant façades, based on the current understanding of the aerodynamics of wind-borne debris, wind-induced failures, wind loading, and impact dynamics. A specific case study of roof tile failure, flight, and impact is presented. The tool is generalized so that designers can consider case-specific building environments to enable impact-resistant design of building envelopes.

The current best practices in terms of impact testing to certify building façade components to resist wind-borne debris impacts are based on the ASTM standard procedures (ASTM 2019, 2020). These standards adopt standard "missiles" and impact velocities. The impact energies are, therefore, not based on the aerodynamics of wind-borne debris in local environments, also because there is no available database about wind-borne debris speeds in windstorms of various intensities (Kordi 2009). The ASTM standard requirements give, however, façade designers the chance to go through engineering assumptions and calculations to develop ad hoc wind-borne debris impact tests for their projects, using "other missiles" for the impact tests.

The objective of the thesis is to provide a site-specific wind-borne debris impact design framework for façade design. It is primarily addressed to primary importance buildings in an urban environment such as hospitals, that are required to have "enhanced protection" (IBC 2021). Through a case study section, the methodology to develop alternative wind-borne debris-resistance[7] test requirements is discussed with a specific example. The discussed design tool could be implemented for any object that could fail in windstorms, in local environments. Analyzing a specific building component in its failure mechanism, this method opens a discussion about other materials such as roof gravel, shingles, sheathing, and structural members, the most common sources of wind-borne debris (Kordi 2009).

---

[7] Wind-borne debris-resistance: performance of a window, a door, curtain walling or a windstorm protective system, to resist the impact of wind-borne debris and cyclic test load without occurrence of specified failure (ASTM 2019, 2020).

1.3   Structure of the Thesis

This Thesis is articulated in 7 main chapters. In **Chapter 1** the Introduction is presented, discussing the problem statement, the aim, and the scope of the research. In **Chapter 2** the Critical Literature Review of the thesis is presented. The codes and standards development for wind-borne debris resistance of façades are discussed. Moreover, the uplift capacity and aerodynamics of wind-borne debris are examined, based on the literature review: wind-borne debris failure, flight, and impacts are described through the building technology best practices and the wind engineering research developments. Current building codes and standards requirements for wind-borne debris impact resistance of façades are presented, together with the adopted testing equipment to conduct wind-borne debris impact tests on windows, doors, and curtain walling. The alternative testing equipment to perform impact tests to simulate the impacts of projectiles other than the standardized ones is described, based on existing literature. Chapter 2 ends with a summary of this examination of the literature, with reference to the thesis objectives.

In **Chapter 3** the Research Objectives and Methodology are articulated and the Design Tool for the identification of wind-borne debris origin, type, and flight trajectory is discussed. This design tool leads to the definition of alternative façade impact tests. This part of the thesis goes through all the steps of the presented performance-based design framework, to find the alternative impact tests for wind-borne debris-resistance of the building envelope:

- target building risk category;

- building location analysis;

- reference wind speed for target building design;

- analysis of the surrounding environment;

- identification of potential wind-borne debris;

- wind-borne debris characteristics;

- debris failure analysis: wind speeds at the initiation of flight;

- debris flight analysis: wind-borne debris velocity and trajectory;

- synthesis of the result to set wind-borne debris impact test requirements;

- impact test equipment and test definition.

Chapter 4 presents a case study. Through the proposed performance-based design framework, the impact tests to conduct on the façade of an essential facility is analyzed. The case study considers the failure of U.S. concrete roof tiles from a source building located in the design area, and accordingly, the failure and

flight of the debris element is assessed. The impact kinetic energy of the roof tiles on the building envelope of the essential facility is presented, to define the impact test requirements. Chapter 5 is articulated in the following sections:

- premise;
- design building for case study;
- analysis of surrounding of the design building;
- wind-borne debris identification;
- failure analysis of low-profile roof tiles (in this section, the uplift capacity of low-profile roof tiles is analyzed, to calculate the wind speeds for roof tiles' flight initialization);
- flight trajectory analysis of low-profile roof tiles (debris flight distances and impact velocities on the target building envelope are calculated);
- wind-borne low-profile roof tiles' impacts on façades (the impact velocities, locations, and trajectories are identified, and the test equipment characteristics are proposed, to conduct the performance-based impact test);

Chapter 5 presents the current design solutions for wind-borne debris resistance of façades and propose alternative design approaches to discuss the thesis case study. **Chapter 6** concludes the thesis, discussing the results and contributions of the research. The final part of the chapter describes the limitations of the thesis, suggesting further steps in the research field of wind-borne debris façade design. The thesis ends with the references.

Chapter 2. Literature Review

2.1 Wind-Borne Debris-Resistance of Façades: Code and Standard Development

On December 25th, 1974, Tropical Cyclone Tracy struck Darwin, in the Northern Territory of Australia, causing significant damage and fatalities with recorded gusts of 217 km/h (Walker 2010). The city of Darwin had previously been hit by cyclones in January 1897 and March 1937, and in these episodes significant damage had already been recorded. The Australian Department of Housing commissioned a report (Walker & Reardon 1987), which highlighted the loss of roof cladding as significantly contributing to the extensive damage to housing. It was weakening the structure of the building causing in many cases the collapse of the whole building, and was also generating a significant amount of debris, which had a vital role in the further destruction of structures and set off a domino effect. It was clear that damage to windows caused by wind-borne debris represented a serious threat to building occupants' safety (Murphy 1984) and increasing the post-event recovery costs. It had been therefore decided to give more importance on enhancing the performance and integrity of structures in cyclonic areas, subject to extreme winds (Mason & Haynes 2010).

After Cyclone Tracy, the Darwin Area Building Manual (Darwin Reconstruction Commission 1975) introduced requirements for any construction material to be tested by a laboratory certified with the National Association of Testing Authorities, if it was not possible to certify and test the material according to an Australian Standard. Due to this, Australia came up with a technologically advanced method of shielding windows from wind-borne debris in tropical cyclone-prone regions. The Manual stated that the protection of doors, windows, and cladding for cyclonic regions would have been considered adequate for their installation in cyclonic regions based on a performance criteria. These building envelope technologies had to resist a 4-kilogram lumber mass with a 100x50-millimeter impacting cross section at any angle, at a velocity of 20 m/s (Darwin Reconstruction Commission 1975). The impact energy to be absorbed by the building envelope systems, to avoid the projectile penetration, would have been, therefore, equal to 800 Joules.

Following these first wind-borne debris-resistance performance requirements, in Australia, at the Pilkington factory, the original so-called "cyclone-resistant glazing" was developed in 1975. After the impact of the 100x50 mm lumber missile, this glass type had to withstand the entire design wind pressure of its cyclonic zone. The design wind pressure had to be applied to the impacted glass. If the glass edges were correctly secured to the frame using an adhesive glazing solution, the glass would have been able to withstand the pressure without any air escape (Mejorin et al. 2019).

Figure 5 - Damaged houses after the passage of Cyclone Tracy on Christmas day 1974 in Darwin, Australia (Wikimedia Commons).

Guidelines for the Testing and Evaluation of Products for Cyclone-Prone Areas were issued as Technical Record (TR) 440 by the Experimental Building Station, Department of Construction, in 1978 (EBS 1978). Using the 100x50 millimeter lumber projectile, TR 440 stipulated that the debris protection performance should be decreased from an impact at 20 m/s projectile (of the Darwin Manual, Darwin Reconstruction Commission, 1975) to a 15 m/s projectile (EBS 1978; Mejorin et al. 2019). In TR 440, it was also agreed that metal roof cladding in cyclone-prone areas must endure the impacts of dynamic wind loading, but there was no mention of the need for pressure cycling for windows, doors, or curtain walling. Although TR 440 was not a legislative document, it was adopted as a reference standard for cyclone-prone Australian locations like the State of Queensland shortly after it was published. The events that followed Cyclone Tracy led to the revision of the Australian Standard 1170.2 "Minimal Design Loads on Structures: Wind Actions" (1971), and in the 1989 edition of the code (AS 1989), the cyclone-prone areas were required to have building envelopes able to withstand the impact of wind-borne debris.

Hurricane Andrew hit Florida, the Bahamas, and Louisiana in the middle of August 1992, 18 years after the Darwin event in Australia. The strongest wind gusts reached 270 km/h on August 23rd and 24th, 1992, in Miami-Dade County, Florida. Hurricane Andrew was a Category Four hurricane (Saffir-Simpson Scale) and it killed 44 people in Florida alone and damaged local properties to $25 billion. After Andrew, 250,000 people were left homeless, the infrastructure for communication and transportation was severely damaged, and 1.4 million people were left without electricity for up to six months (Cochran & Levitan 1994). The psychological impact was severe and instead of fixing their houses and businesses, many individuals chose to relocate to other towns and states. When individuals chose to rebuild their structures, the process took years to complete.

Figure 6 - After Hurricane Andrew 1992. These clay tiles were mortar-set. Three failure modes are illustrated: Separation of the mortar from the cap sheet, separation of the tile from the mortar and debris impact damage (photo courtesy of TLSmith Consulting Inc.).

Post-disaster event evaluations identified a number of problems with severe wind occurrences (Powell & Huston 1996; FEMA 1993). Similar to Australia, the Florida Building Code added curtain-wall regulations in the years following the catastrophic occurrence, TAS 201 (1994), TAS 202 (1994), TAS 203 (1994), include

provisions to add protection against wind-borne debris (FBC 2001). When it comes to impact-resistant façade systems, the Miami-Dade rules and, any updates since then, continue to be the most demanding in the U.S. (Marshall et al. 2012).

The Florida impact test procedure for windows, doors, and curtain walls impacted by wind-borne debris were an improvement over Australia's, as reported in Technical Record 440 (EBS 1978). The procedure differed from the Australian document in the requirement for the test specimen[8] to withstand a cycling of positive and negative pressure[9] after the impact test. Façade performance criteria set in the 1994 revision of the Florida Building Code are the Testing Specification Standards TAS 201-94, TAS 202-94, TAS 203-94 (FBC 2001). Furthermore, the U.S. testing procedure defined the missile impact locations on the specimen. Other non-mandatory reference standards such as the SSTD 12-94 "Test Standards for Determining Impact Resistance from Windborne Debris" published in 1994 by the Alabama-based Southern Building Code Congress International (SBBCI 1997), also served as the foundation for the formulation of the Florida Building Code requirements (FBC 2001). Following TAS 201-94, TAS 202-94, TAS 203-94 (FBC 2001), ASTM standards were developed:

- ASTM E1996 (2020) Standard Specification of Exterior Windows, Curtain Walls, Doors, and Impact Protective Systems[10] Impacted by Wind-Borne Debris in Hurricanes;

- ASTM E1886 (2019) Standard Test Method for Performance of Exterior Windows, Curtain Walls, Doors and Impact Protective Systems Impacted by Missile(s) and Exposed to Cyclic Pressure Differentials[11].

---

[8] Test specimen: the entire assembled unit submitted for test.

[9] Cyclic test load: beginning at a specified air pressure differential, the application of a positive (and negative) pressure to achieve another specified air pressure differential and returning to the initial air pressure differential (ASTM 2019, 2020).

[10] Impact protective systems: construction assemblies applied, attached, or locked over an exterior glazed opening system to protect that system from wind-borne debris during destructive windstorm events. Windstorm protective system includes types that are fixed, operable, or removable.

[11] Air-pressure differential: specified maximum pressure differential in cyclic test load across the specimen, creating an inward or outward load. Select P_{pos} and P_{neg} for the maximum inward (positive) and maximum outward (negative) air pressure differential for which qualification is sought (ASTM 2019, 2020). The air-pressure differential is expressed in Pascal or its multiples.

These ASTM standards provide additional criteria including the range of temperatures to conduct the test weren't included in TAS 201-94, TAS 202-94, and TAS 203-94 (FBC 2001). Currently, according to ASCE 7-22 (2022), buildings erected in U.S. wind-borne debris regions must follow ASTM E1886 (2019) and ASTM E1996 (2020) specifications, or local standards requirements, whichever is more demanding. These testing procedures are discussed in the thesis since they have been identified as the international benchmark when it comes to wind-borne debris impact testing of the building envelope. The weights and velocity of the testing projectiles change according to the building's wind zone and level of protection (ranging from Wind Zone 1, the least wind-prone, to Wind Zone 4, the most wind-prone, following ASCE 2022).

The design wind pressure (inward and outward) from the Building Code is used to determine the pressure cycling to be performed on the façade once the impact test passes. It is necessary to do 4,500 cycles of positive and negative pressure, with each cycle lasting 1-3 seconds. Through a process of consensus-building, the ASTM E1886 (2019) standard test method was created with the participation of manufacturers, consultants, building code authorities, and other specialists. The permitted tolerances for the testing criteria for both debris' projectile impacts, and the pressure cycle program have been developed, and the testing loading sequence[12] and conditions have been defined.

In Australia, the 2002 revision of AS 1170.2 "Structural Design Actions: Wind Actions" led to the first unified Australian and New Zealand design wind code (AS/NZS 2002). Again, a number of substantial modifications were made to AS/NZS 1170.2 in the 2011 revision (AS/NZS 2011) including the introduction of criteria for impact loading of wind-borne debris. The latest studies on wind profiles in tropical storms and hurricanes developed in the United States served as the basis for Amendment 4 of AS/NZS 1170.2 (2016).

These studies found a significant correlation between horizontal missile velocity and distance traveled (Holmes et al. 2012).

The study "Trajectories of Wind-Borne Debris in Horizontal Winds and Applications to Impact Testing" provides the foundation for the specifications for windows and façades (Lin et al. 2007), and it has been developed through experimental studies at the Texas Tech University wind tunnel. In terms of wind gust speeds, the research develops ratios for missile speed based on the wind zone of the building to be designed and tested in its impact performance for wind-borne debris (ASCE 2018). Plots by Lin et al. (2007) show that the terminal velocity of the projectiles is represented by the $0.4 \times V_R$, the regional wind velocity. V_R is, therefore,

---

[12] Test-Loading Sequence: after the lumber missile and/or steel ball, the air pressure cycles are applied (ASTM 2019, 2020).

used to calculate the missile impact velocity in the Design Guidelines for Queensland Public Cyclone Shelters (DPW, 2006). These studies consider wind-borne debris flight in uniform flow and, since the regional velocity does reach 316 km/h for the Australian Severe Cyclonic Region D, the impact velocity of the 4-kilograms projectile reaches impact speeds of 130 km/h. This impact velocity is more than double the previous one adopted in Australia, which was equal to 54 km/h (= 15 m/s). The fenestration assembly[13], according to AS/NZS 1170.2 (2011) is supposed to be wind-borne debris-resistant for a height of 25 meters above the ground level[14] (Figure 7), and no provisions are in place for cyclic stress testing post-debris impact for glass façades and debris screens.

The small projectile, a 2-gram steel ball[15], was chosen since it is a representation of roof gravel and may go up to 25 meters in altitude. AS/NZS 1170.2 (2011) does not specify any testing method or acceptance criteria that *"may vary according to the purpose of the test. An appropriate test method and acceptance criteria for debris tests are given in Technical Note No. 4, 'Simulated windborne debris impact testing of building envelope components', Cyclone Testing Station, James Cook University"* (Clause 2.5.8, Amendment 4, AS/NZS 1170.2:2011, 2016). The steel ball impact test followed Minor's (1974) observations about high-rise building window breakage. He observed that it was from the impact of wind-borne gravel originating from one and two-storey roofs upwind of the damaged building (Williams & Redgen 2012). Florida requirements and the ASTM standard procedures that are widely adopted to test hurricane/cyclone-resistant windows, doors, and curtain walls, include the pressure cycling test following the impact phase because it is considered a good representation of the natural phenomenon. Pressure cycling testing is present in Australian requirements when it comes to roofing testing for cyclonic areas. But it is not in place for wind-borne debris resistance, and it is not even mentioned in the last revision of Technical Note No. 4 (CTS 2017).

---

[13] Fenestration assembly: glazing system intended to be installed in a building; i.e. exterior windows (including skylights), doors, and curtain walling.

[14] Height above ground level of assembly: for any location of a building component, it is intended to be the minimum distance between the ground level and the head of the building component itself. In the case of different ground levels for a single front of a building, the ground level is the lower altitude line referred to each front of the building (see Figure 7). Head of a window: a top horizontal member of a window frame (ISO 2021).

[15] Steel ball: a solid steel ball weighing 2 g ± 5 %, with an 8 mm nominal diameter (ASTM 2019, 2020).
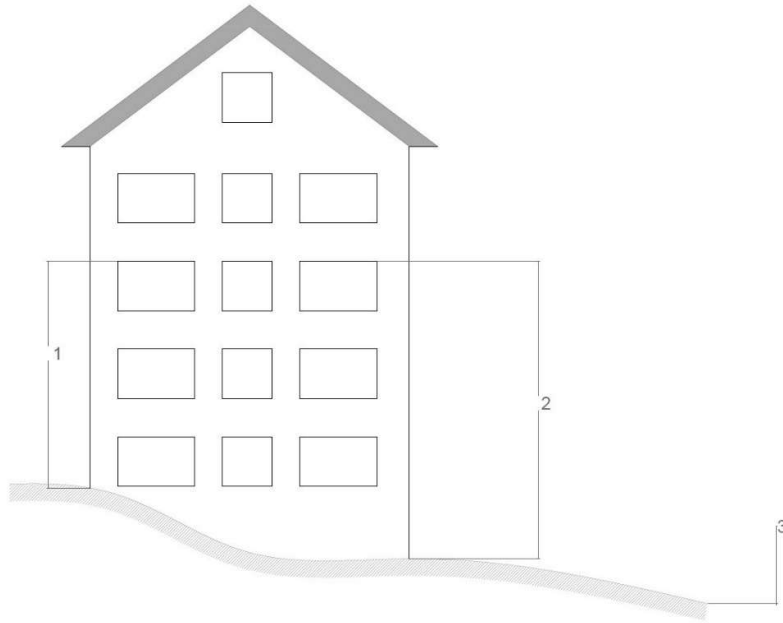
Figure 7 - Schematic examples of height above ground level of assembly depending on the different fronts of a building.

Key

1	height above ground level of assembly for the back of the building
2	height above ground level of assembly for the front of the building
3	ground level not relevant for the fronts of the building

In the Asia-Pacific Region, different countries are currently increasing their level of preparedness for climate change and to issues related to building envelope breakage due to wind-borne debris impact (Mejorin et al. 2019), pushed especially by the requests of insurance companies to lower the annual premiums to insure the buildings. These regions are, respectively, either considering design practices achieved through having experienced a significant number of typhoon events and collected in façade manuals, either leaving to façade consultants design choices based on the professionals' experience, or developing testing procedures and certification protocols inspired by, or finally, different from to U.S.-based approach to the topic, represented by the set of ASTM norms (Mejorin et al. 2018a). In Japan, the Disaster Prevention Research Institute (DPRI) at Kyoto University investigated the behavior of wind-borne objects in typhoon winds and several impact tests have been conducted on building envelope glazing panels (Figure 20).

Currently, there are no requirements for wind-borne debris resistance in Europe because the continent has experienced relatively few extratropical cyclones and tornadoes but in the last years, there have been an increased number of such events as noted earlier. This trend led to the term "medicanes", which are "hurricanes" occurring in the Mediterranean Sea (Figure 9). The necessity to use this new terminology occurred in the last two decades to localize these phenomena to areas where extreme wind events did not happen in the past.

Figure 8 - Manila, 2016. When Typhoon Glenda hit the Philippines capital in 2016, building envelopes have been heavily damaged, especially the glazed panels, due to wind-borne debris impact (photo courtesy of Joe Khoury).

Figure 9 - Medicane Ianos, 17 September 2020 at 10:48 CEST (contains modified Copernicus Sentinel data 2020, processed by ESA, CC BY-SA 3.0 IGO).

2.2 Building Code and Standard Requirements for Wind-Borne Debris Impact Resistance

Governing bodies in areas that are prone to extreme weather events (e.g., Florida, Hong Kong, Japan, and Australia) have implemented measures to mitigate the effect of wind on the built environment. Studies and field observations have been conducted on the consequences of major hurricanes, typhoons, and tornadoes on the built environment and human safety (FEMA 1993; CTS 2017). Such measures have one single goal: preventing injury to people and damage to property due to debris impacts. Such an objective is sought by adopting two sets of measures: on the one hand, reducing the likelihood of the wind-borne debris phenomenon by improving the resistance of building elements to the wind; on the other hand, mitigating the consequences of wind-borne debris by setting design guidelines and testing methodologies to ensure the resistance of the building envelope to the debris impact. These measures apply to buildings in areas prone to hurricane and cyclonic winds: less demanding target performances are requested for houses, while essential facilities (such as hospitals, emergency services, schools, etc.) are required to meet demanding standards, especially for the building envelope (AS/NZS 2021; ASCE 2022).

Regarding building envelope resilience, the main international reference standards for façades are (Letchford 2018):

- ASTM E 1886 (ASTM 2019);
- ASTM E 1996 (ASTM 2020);
- FEMA P-361 (FEMA 2015);
- AS/NZS 1170.2:2021 (AS/NZS 2021).

At the international scale, the International Code Council regulates through the International Building Code (IBC 2021) areas with wind speeds of 209 km/h or above, which are known as wind-borne debris regions, and establishes the necessary debris missile resistance in areas prone to hurricanes, typhoons, tropical cyclones, tornadoes. The ASTM E1886 (2019) and ASTM E1996 (2020) standards are referred to in the International Building Code (IBC 2021). Other international product standards related to wind-borne debris resistance have been developed, such as ISO 16932 (2020), which outlines the specifications for damaging the windstorm-resistant glass. The procedure follows the ASTM (ASTM 2019, 2020) requirements for the classification of the construction material (glass) but it differs when it comes to the testing approach in general. The ISO standard currently doesn't test the window, door, or curtain walling assembly, but just the glass. It considers the glass put in a standardized iron frame, without therefore considering the actual assembly of the

glass in the window/curtain walling, not even the shape of the product. Generally, the norms are based on the evidence of practical experience (Miami-Dade County 2006) and, despite working effectively, lack systematic theoretical work in support of the aerodynamics of wind-borne debris (Lin et al. 2006). In regards to an expected return period, façades must withstand design wind loads based on the location, shape, and height of the building.

Flying debris resilience of façades is currently widely assessed in the United States wind-borne debris regions (ASCE 2016) and Australian wind regions C and D (AS/NZS 2016). The impact testing is conducted using two different impactor typologies to be shot through an air cannon either on the spandrel or the glass panel. The U.S. façade test procedures are currently the international benchmark requirements for façade impact resistance to wind-borne debris caused by windstorm events (Trabucco et al. 2017).

According to ASCE 7 (2022), the wind zone map is shown to identify the wind-borne debris regions and the boundary for hurricane-prone regions. ASTM E1886 (ASTM 2019) and ASTM E1996 (ASTM 2020) requirements, or local standards requirements, whichever is more stringent, must be followed by buildings constructed in these United States areas. The two ASTM standards dictate the building envelope impact resistance, as well as the air infiltration control during extreme wind events. The testing missile weights and speeds vary on the level of importance of the building (Level 4 requires "enhanced protection" for essential facilities, such as hospitals, police stations, etc.) and on the wind zone location of the building, ranging from Wind Zone 1, the least wind-prone, to Wind Zone 4, the most wind-prone (ASCE 2022). The impact locations include the center of each type of infill; 150 mm from supporting members at the corner; 150 mm from supporting members at a diagonally opposite corner; integral mullion; meeting stile; combination mullion; meeting rail/check rail (ASTM 2020). The impact testing procedure shall be conducted on the single specimen if the building envelope component is designed to be installed as a single element. The test should be repeated for three test specimens, both for the lumber[16] and the steel ball missiles (ASTM 2019, 2020; Figure 10, Figure 11). The pressure cycling to conduct on the façade after the successful impact tests are based on the design wind pressure (inward and outward) from the building code, based on an intact building envelope. A total of 4,500 positive and 4,500 negative pressure cycles have to be conducted, and the duration of each cycle is 1-3 s.

---

[16] Lumber missile: a pressed piece of surface-dried, soft-wood, structural timber that impacts the glazing surface of the specimen (ASTM 2019, 2020).
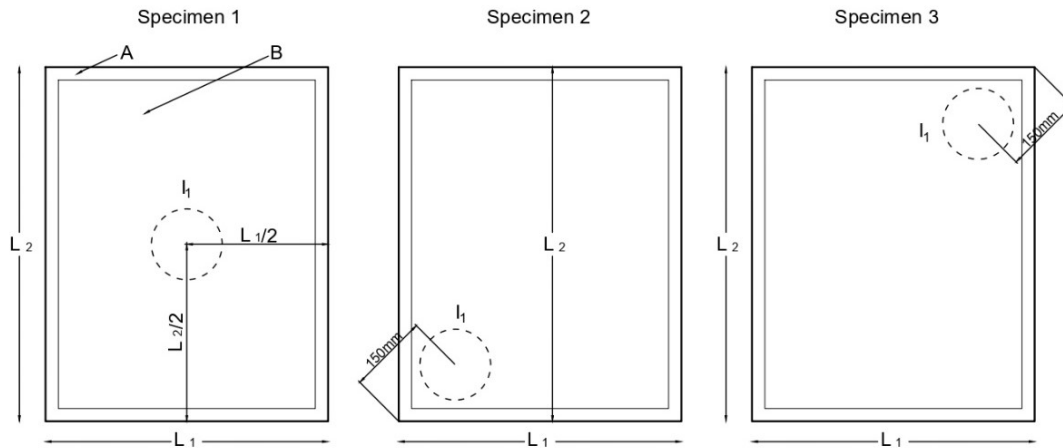
Figure 10 - Impact area of wood lumber missile impact test for individual windows, doors, curtain walling or windstorm protective systems tested separately (following ASTM 2020).

Key

I = impact area of each specimen
L = dimension of each specimen
A = frame of the specimen
B = panel of the specimen
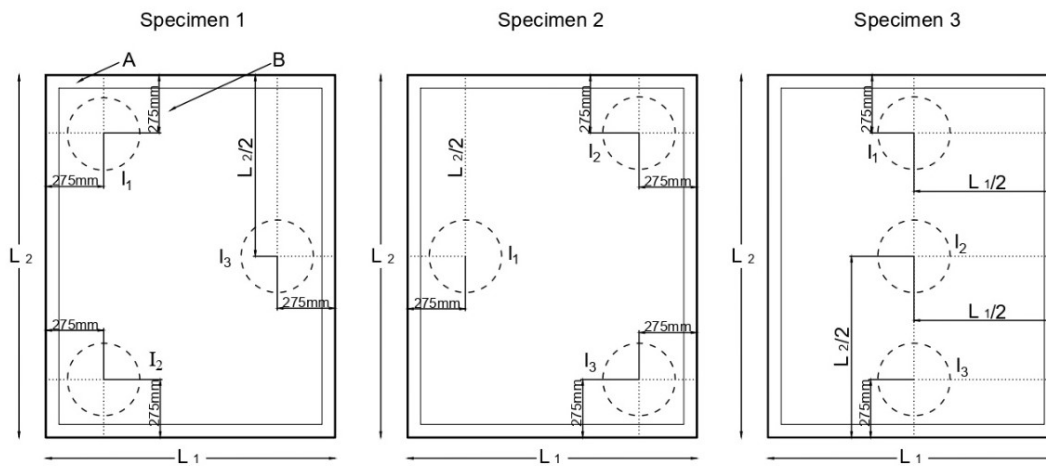
Figure 11 - Impact area of steel ball impact test for individual windows (incl. skylights), doors, curtain walling or windstorm protective systems tested separately (following ASTM 2020).

Key
I = impact area of each specimen
L = dimension of each specimen
A = frame of the specimen
B = panel of the specimen

Considering the impact performances of façades in wind-borne debris-prone areas, according to ASTM standards, depending on missile weight and impact speed, the façade has to withstand different impact energies that are of about 1.5 J for the small missile, and in the range of 150 to 1220 J for the large missile.

When it comes to window or curtain wall assemblies, at least three panels should be tested together and that has been shown in being an important parameter to classify the façade products (Figure 12, Figure 13). The success of the building envelope solution can be significantly impacted by the characteristics of the glass, the interlayer for the glass lamination process, the mullion and transom features, and the fastening method chosen, also between the various elements. The assembly must pass the impact tests and the subsequent application of pressure cycle tests, following the same procedure as the single building components. For the glazed surfaces' design, wind loads dictate the glass thickness and the interlayer thickness and typology, but the impact resilience is almost entirely reliant on the interlayer type and its thickness, ensuring glass retention when breakage occurs.
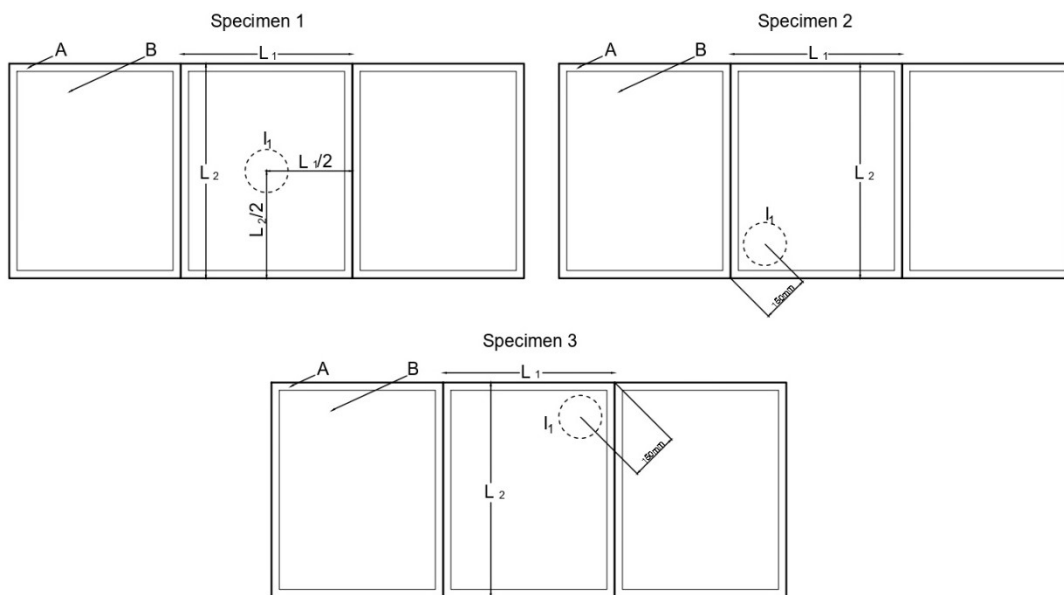
Figure 12 - Impact area lumber missile impact test for windows, doors, curtain walling or windstorm protective systems intended to be installed combined together and tested by joining at least three lites into one mounting frame (following ASTM 2020).

Key
I = impact area of each specimen
L = dimension of each specimen
A = frame of the specimen
B = panel of the specimen

Specimen 1

Specimen 2

Specimen 3
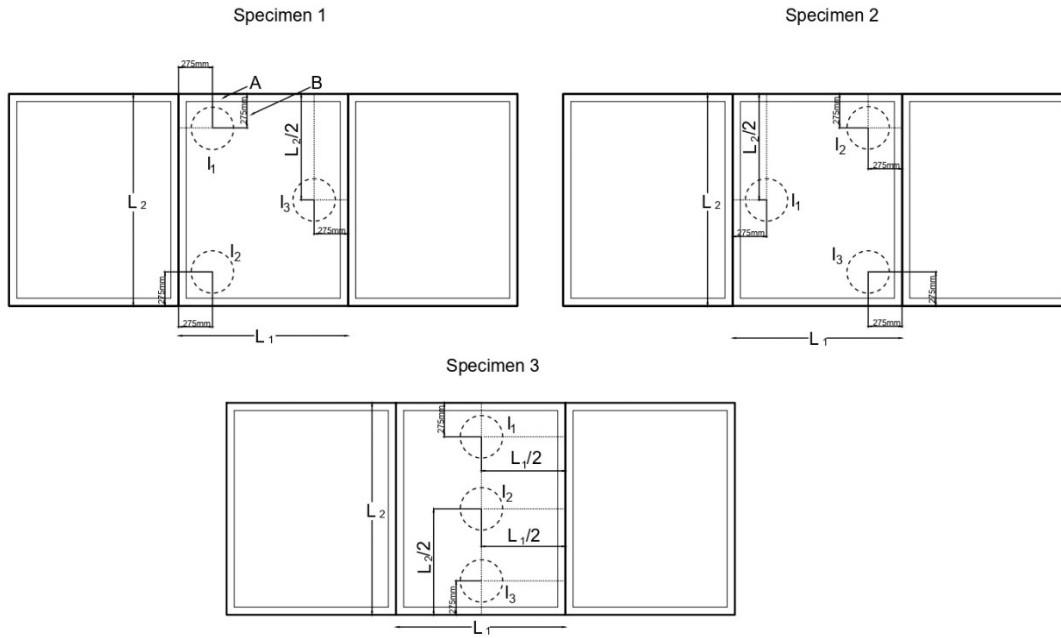
Figure 13 - Impact area of steel ball impact test for windows, doors, curtain walling or windstorm protective systems intended to be installed combined together and tested by joining at least three lites into one mounting frame (following ASTM 2020).

Key
I = impact area of each specimen
L = dimension of each specimen
A = frame of the specimen
B = panel of the specimen

A different design approach is in place in cyclone-prone Australian regions, where doors, windows, and claddings must withstand the impact of a:

- Timber member of 4-kg mass with a nominal 50-by-100-mm impacting cross-section, impacting on-end at 0.4 V_R for horizontal trajectories, and 0.1 V_R for vertical trajectories.

- Spherical steel ball 8-mm diameter (2-g mass) impacting at 0.4 V_R for horizontal trajectories, and 0.3 V_R for vertical trajectories.

In Australia, the impactors' velocities are based on wind engineering research, that establishes ratios for missile speed in terms of wind gust speeds (Lin et al. 2007; Prevatt & Desai 2018). The velocity is 0.4 x $V_{10,000}$ ratio ($V_{10,000} = V_R$) for horizontal trajectories, for both lumber and steel balls projectiles (AS/NZS 2021). This Standard does not specify a test method or acceptance criteria, which may vary according to the purpose

of the test. However, an appropriate testing method and approval process for these resilience tests are given in Technical Note No. 4 (CTS 2017).

Differently from the United States testing, there is no provision for cyclic load testing post-debris impact for façades in AS/NZS 1170.2 (AS/NZS 2021). According to Australian Standard's requirements, the building envelope components are required to be flying debris-resistant for a height of only 25 meters from the ground level. This last criterion is based on research, fixing the upper limit for flight initiation at 20 meters (Moghim & Caracoglia 2012), but the small projectile (2-gram steel ball) has been chosen because it is representative of roof gravel, thus it could be higher than 25 meters.

Figure 14 - Hong Kong, 1999. Typhoon York damaged the curtain walls of many buildings in the Wan Chai area. Wind-borne debris caused the breakage of glazed panels in the highest tall building floors (photo courtesy of Joe Khoury).

In Japan, the JIS R 3109 (JIS 2018) standard references the international ISO 16932 (ISO 2007) standard. Both these two standards differ from the previously discussed ASTM and AS/NZS testing procedures, considering the testing of the glazing instead of the entire system constituting the building envelope. The JIS and ISO standards consider a normalized glass installed in a standard metallic frame to conduct the test, whereas the ASTM tests the actual installation that will be used on-site. Usually, laminated glass could be defined as "cyclone/hurricane glass" when it guarantees a precise level of performance so, based on ISO or JIS standards, the impact energies could reach 1700 J for the 6.8-kg impactor.

In Europe, the design of façades against wind actions follows currently Eurocode 1 (EN 2005), but extreme loading configurations, including natural hazard events, are only marginally considered. Nevertheless, some past extreme weather events highlighted the insufficiency of such regulation in terms of maximum design values for wind. It has been revealed lower than values recorded in the past years. Moreover, no specific regulations are provided for curtain systems because of conventional assumptions in use. Curtain walls are conventionally regarded as non-structural components (CPR 2011), but as building elements not designed to contribute to the structural capacity of the load-bearing frame (Bedon et al. 2018). The only European mandatory requirements, when it comes to impact performances of the building envelope, are the related to safety in use requirements and expected design performances (Bedon et al. 2019).

The testing procedures are EN 12600 (EN 2002), EN 14019 (EN 2016), EN 13049 (EN 2004), and ISO 7892 (ISO 1988), and the testing rig and equipment normally involve a certain mass making into a pendulum motion (Figure 15), to verify the façade resistance to different types of impacts, varying the mass of the body (impactor), its nature, drop height, impact location, and impact direction (acting from the outside or inside of the building). The mass of the body varies from a minimum of 0.5 to 1 kg in the case of the hard body impact test, up to a maximum of 50 kg for the soft body impact test. The two different natures of the impactors are respectively representative of a hard object accidentally falling against the panel, or of a human impacting the façade. Depending on drop height and on the mass of the body, the façade has to withstand different impact energies, and these are in the range of 3 to 10 J for the hard body and in the range of 120 to 500 J for the soft body. The variation in the required façade performance in terms of impact resistance depends on the impact classification design of the curtain wall to be certified. Therefore, key impact locations of the façade are tested: its central region, the midpoint section, the panel edges, the fixings' area, and other ones, identified as weak locations by the designer (Mejorin et al. 2020).
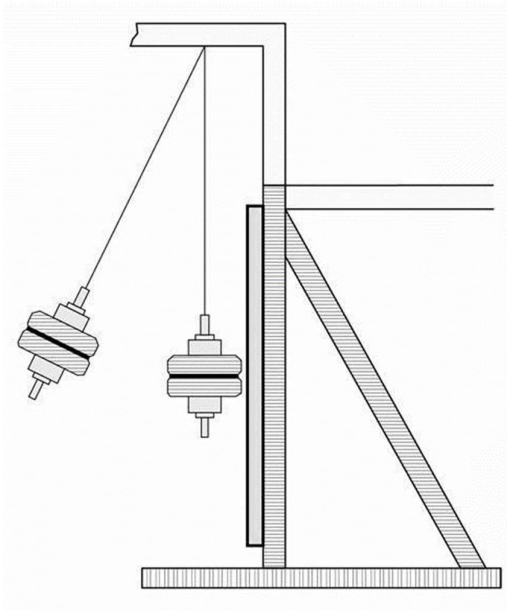
Figure 15 - Pendulum test scheme (based on EN 12600).

2.3 Testing Equipment to Conduct Wind-Borne Debris Impact Tests

To perform the impact tests on façades, there is widely adopted testing equipment (ASTM 2019; CTS 2019). In Figure 17 and Figure 18, the schematic diagrams of respectively the lumber and steel balls testing apparatus configurations are reported and this equipment is used to certify products according to ASTM standard procedures (ASTM 2019, 2020).

2.3.1 Missile Propulsion Device

Any device capable of propelling the missile at a specified speed, orientation, and impact location could be defined as a missile propulsion device. The missile shall not be accelerating upon impact due to the force of gravity along a line normal to the specimen when shot using a missile propulsion device, following the testing procedure for wind-borne debris simulation. The cannon assembly shall be comprised of a compressed-air supply, a remote firing device, a barrel, and a timing system.

The large missile cannon shall consist of four major components: a compressed-air supply, a pressure-release valve, a barrel and support frame, and a speed-measuring system for determining missile speed. The

end of the missile that impacts the target is denoted as the missile's impact end. The end of the missile opposite to the impact end is denoted as the missile's trailing edge. A sabot shall be used at the trailing edge of the missile to facilitate launching.

The small-missile cannon shall be mounted on a frame designed to permit movement of the cannon so that it can propel missiles to impact the test specimen at specified locations. The photoelectric sensors shall be positioned to measure missile speed within 150 cm of the impact point on the test specimen.

Figure 16 - Lubbock, Texas Tech University. Lumber projectile missile propulsion device (based on ASTM 2019). In the figure, the test specimen used to conduct the test is a concrete panel. Wind-borne debris impact test is used to test products that can be different from windows, doors, and curtain walling. The test goals are the assessments of the wind-borne debris impact performance of case study building technologies. The specimen area is surrounded by transparent vertical panels that are protecting who is attending the test from wood splinters.
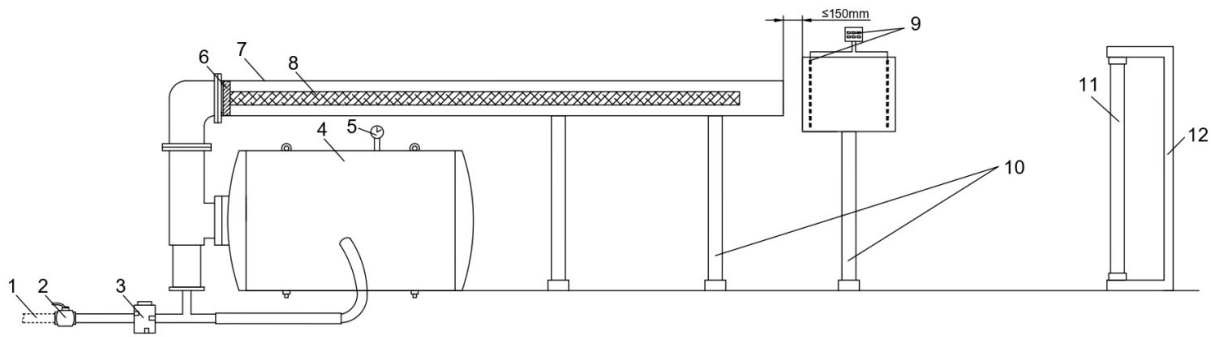
Figure 17 - Schematic diagram of lumber testing apparatus configuration (based on ASTM 2019).

Key

1	air pipe
2	valve
3	solenoid valve
4	pressure gage
5	pressure vessel
6	circular base of missile
7	launching tube
8	wood lumber
9	velometer
10	support
11	specimen
12	pressure chamber
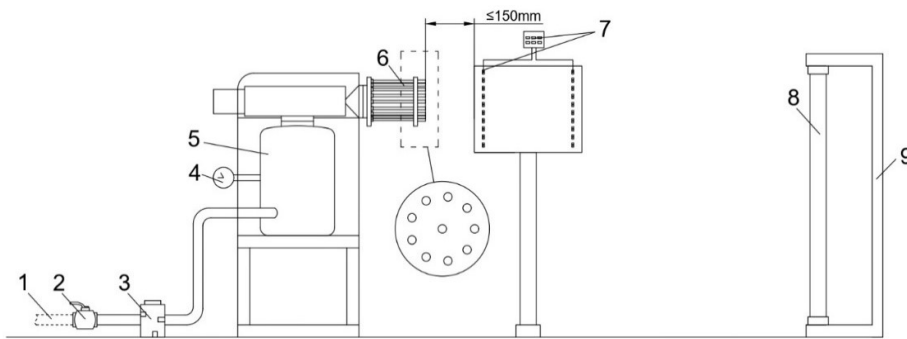
Figure 18 - Schematic diagram of steel ball testing apparatus configuration (based on ASTM 2019).

Key

1	air pipe
2	valve
3	solenoid valve
4	pressure gage
5	pressure vessel
6	launching tube
7	velometer
8	specimen
9	pressure chamber

2.3.2 Electronic system

It is used to monitor the flight and impact speed of the projectile. Furthermore, its main function includes maintaining the design air reservoir pressure, and controlling both the filling and the purging, to launch the projectile. It controls the electronic valve for projectile launch. It can communicate with the velometer to, finally, control the projectile's speed and with the pressure measuring apparatus, to control the pressure cycling phase after the impacts have been performed on the test specimen.

2.3.3 Mounting Frame

The mounting frame is supporting the outer specimen test frame(s) in a vertical position during testing. The mounting frame shall be either integral to the test chamber or capable of being installed into the test chamber before to or following projectile impact(s). The mounting frame shall be anchored so it does not move when the specimen is impacted. The specifications for the inner and the outer specimen-support frame shall be specified in the testing report.

2.3.4 Test Specimen

The test specimen shall consist of the entire fenestration or impact protective system assembly and contain all devices used to resist wind and wind-borne debris. Test specimens for large fenestration and curtain wall assemblies shall be one panel unless otherwise specified. All parts of the test specimen shall be full size, as specified for actual use, using identical materials, details, and methods of construction.

The test specimen to be tested shall have nominal dimensions representative of the commercial production. The size of the test specimen shall be determined by the building envelope designer. All components of each test specimen shall be full-size. Where it is impractical to test the entire fenestration assembly such as curtain walling and heavy commercial assemblies, usually the largest size of each type of panel is tested, to qualify the entire assembly.

These best practices are not considering the window/curtain wall panel stiffness and this is one of the ongoing improvements that the ISO Technical Committee 162, Working Group 4, and Working Group 5, are proposing in the new standard that is under development, based on the ASTM requirements (ASTM 2019,

2020). If the panel dimension decreases, its stiffness inversely increases, and it can somehow take to higher fragility behavior of the building component. It would be beneficial to consider a different test when it comes to a significant decrease in panel size (e.g. when smaller panels exceed a 50% reduction in their individual length size with reference to the panel that has been already tested for certification purposes). It should be checked, for certification purposes, that the higher stiffness of smaller building components is not influencing their impact performances when it comes to wind-borne debris simulation.

Individual building envelope components such as windows, doors, curtain walling, or windstorm protective systems should be tested separately. When these building envelope technologies are intended to be installed combined, they shall be tested by joining at least three lites into one mounting frame, separated only by the mullions. These mullions should be representative of the mullions of the building envelope to be tested. Windstorm protective systems should be tested also to verify their deflection after the testing, to verify what should be the minimum design distance of these building components installation from the internal building envelope to be protected and/or from the internal content.

2.3.5 Air Pressure Cycling Test Chamber

The air pressure cycling test chamber is an enclosure or box with an opening against which the test specimen is installed. It shall be capable of withstanding the specified cyclic static pressure differential. The chamber shall be deep enough to avoid contact with the test specimen during pressure cycling. Pressure taps shall be provided to facilitate the measurement of the cyclic-pressure differential. They shall be located such that the measurements are unaffected by the air supplied to or evacuated from the test chamber or by any other air movements.

2.3.6 Air Pressure System and Measuring Apparatus

The air pressure system is a controllable blower, a compressed air supply/vacuum system, or other suitable systems capable of providing the required maximum air pressure differential (inward and outward acting) across the test specimen. Specified pressure differentials across the test specimen shall be imposed and controlled through any system that subjects the test specimen to the prescribed test loading program.

Examples of suitable control systems include manually operated valves, electrically operated valves, or computer-controlled servo-operated valves.

Pressure differentials across the test specimen shall be measured by an air pressure measuring apparatus with an accuracy of ±2 % of its maximum rated capacity, or ±100 Pa, whichever is less, and with a response time of less than 50 ms. Examples of acceptable apparatus are mechanical pressure gages and electronic pressure transducers. The air pressure measuring apparatus communicates with the electronic system.

2.3.7 Testing Equipment Calibration: Velometer

This electronic device is capable of measuring roof tile projectile speeds calibrated to an accuracy of ±2% of the elapsed time required to measure the speed of the specified projectile. Calibration shall be performed at the manufacturer's recommended frequency, but in any event, not more than six months before the test date.

For those wishing to use speed-measuring devices that have already been developed, the following three systems are recommended:

- **Photoelectric Sensors** — Two photoelectric sensors shall be used. Both photoelectric sensors shall be the same model. An electronic timing device shall be activated when the reference point of the projectile passes the first sensor. The electronic timing device shall be stopped when the reference point of the projectile passes the second sensor. The electronic timing device shall have an operating frequency of no less than 10 kHz with a response time not to exceed 0.15 ms. The speed of the projectile shall be determined by dividing the distance between the two through-beam photoelectric sensors by the time interval counted by the electronic timing device. The photoelectric sensors can be mounted on an extension of the barrel or supported independently of the cannon. In either case, the projectile shall not be accelerating as its trailing edge passes between the photoelectric sensors.

- **High-Speed Video Camera** — A high-speed video camera and a single-frame viewing device with a frame rate exceeding 500 frames per second and capable of producing a clear image and a device that allows single frame viewing, may be used as the speed measuring system. The high-speed video camera shall be used in conjunction with an appropriate grid that may be a fixed background or on the projectile, and a reference line that may be the trailing edge of the projectile or a fixed background,

respectively. The video camera shall be used to record the relative distance traveled between the line and the grid. The speed of the projectile is computed as the product of the distance traveled in two consecutive frames and the frame rate of the high-speed video camera. For example, if the frame rate of the high-speed video camera is 500 frames per second and the recorded change in position is 27 mm, then the projectile speed is 500 × 0.027 = 13.5 m⁄s.

- **Standard Video Camera** — A standard video camera and a four-head videotape playback device with stop-action capabilities may be used. The time between consecutive images is 1/30 s.

2.3.8 Testing Equipment Calibration: Pressure transducers

Electronic pressure transducers shall be calibrated at six-month intervals using a standardized calibrating system or a manometer readable to 10 Pa (1 mm of water).

2.3.9 Testing Equipment Calibration: Manometers

The calibration of manometers is normally not required, provided that the instruments are used at a temperature near their design temperature.

2.3.10 Projectiles

Projectiles vary in their characteristics to currently certify products for various performances. These, therefore, vary in size, material, weight, and impact speeds, to reach various levels of performance of the tested building envelope component. Following ASTM standards (ASTM 2019, 2020), we have:

- the "small-ball projectile": a solid steel ball weighing 2 g ± 5 %, with an 8 mm nominal diameter, and an impact speed according to Table 1;

- the lumber projectile that shall be made of pine with a cross-section of 50-by-100 mm, a mass between 910 ± 100 g and 4100 ± 100 g, and an impact speed according to Table 1.

ASTM standard leaves the possibility open to identify (ASTM 2019, 2020) any other representative projectiles with different mass, size, shape, and impact speed determined by engineering analysis to conduct tests on the building envelope components, considering the design reference wind speed of the wind zone

location. Standard projectiles (Table 1), depending on the wind zone of the building and the elevation of the assembly, follow precise tests, depending on the design level of protection (Table 2).

Table 1 - Projectiles according to ASTM testing procedure for wind-borne debris (ASTM 2019)

Projectile type	Projectile	Impact speed (m/s)
A	(2 ± 0,1) g (small steel ball)	39.62
B	(0.91 ± 0,1) kg (small lumber)	15.25
C	(2.05 ± 0,1) kg (small lumber)	12.19
D	(4.1 ± 0,1) kg (medium lumber)	15.25
E	(4.1 ± 0,1) kg (medium lumber)	24.38

Table 2 - Required projectiles for testing classification according to ASTM (2019, 2020) requirements

Level of protection	Essential facilities		Basic protection		Unprotected	
H (m)	≤9.1m	>9.1m	≤9.1m	>9.1m	≤9.1m	>9.1m
Wind zone 1	D	D	C	A	None	None
Wind zone 2	D	D	C	A	None	None
Wind zone 3	E	D	D	A	None	None

2.4 Testing Equipment to Conduct Alternative Wind-Borne Debris Impact Tests

The thesis explores a design framework to enable façade designers to consider alternative projectiles, regarding the ones mentioned (Table 1), which are widely adopted. Wind-borne debris impact tests aim to verify façade solution effectiveness in withstanding the impact of identified exogenous debris that could fail under the effects of wind loads. The testing apparatus should have controlled accuracy, flight mode and speeds, and flexibility in considering widely adopted equipment, to allow the largest number of façade consultants to use the alternative design framework.

The possibility to conduct wind-borne debris impact tests with alternative projectiles has been already explored in contexts such as the previously mentioned Disaster Prevention Research Institute of Kyoto University. In this case, the debris element to conduct the impact tests is the typical Japanese roof tile (Figure 22, Figure 21). Another experiment has been conducted on typical U.S. roof tiles at the University of Florida (Fernandez et al. 2010). In both cases, the same calibration and verification stages that are set in place for the previously described equipment used to conduct the tests according to ASTM standards (ASTM 2019, 2020) were used to control the testing phase. The goal in both cases is to use the currently available air cannon platforms, with some additional launch decks, to contain the variation of the equipment modification both in terms of materials and costs.

Fernandez et al. (2010) simulated the impact of the typical U.S. concrete roof tile, a commercialized one. Every single test was performed using a new roof tile, avoiding the use of already damaged ones. Various components that are constituting the equipment to conduct the test are reported in Figure 19. The major difference from the standard testing equipment to conduct wind-borne debris impact testing, previously described, is the presence of a launch deck (guided track). This component is supported by extruded T-slot aluminum rails that extend from the exit of the barrel toward the target. The roof tile projectile sits upon this deck, and it is propelled toward the target via the pneumatic ram. The deck is lined with a polyoxymethylene sheet to reduce sliding friction. The pneumatic ram forward motion is arrested as the tile and ram approach the end of the deck, putting the roof tile in free flight toward the target.

2.4.1 Impact Orientation Control

When it comes to roofing tile impacts, it has been shown by Fernandez et al. (2010) that an important factor is related to the roof tile's orientation relative to the target specimen. This parameter can be controlled by a combination of launch deck length and free flight distance to the target. The edge impact and the flat impact and the consequences of two flight modes are imparted by controlling the length of the launch deck. When the pneumatic ram motion is arrested before the tile exits the deck, the tile travels toward the target normally to the tile plane vertical (edge impact). When the launch deck is shortened such that the front end of the tile exits, the launch deck before arresting the push ram motion, a forward rotation is imparted to the tile. The calibration of the free flight distance to the target specimen should be conducted to find out the two free flight distances to have "edge impact" either "flat impact".
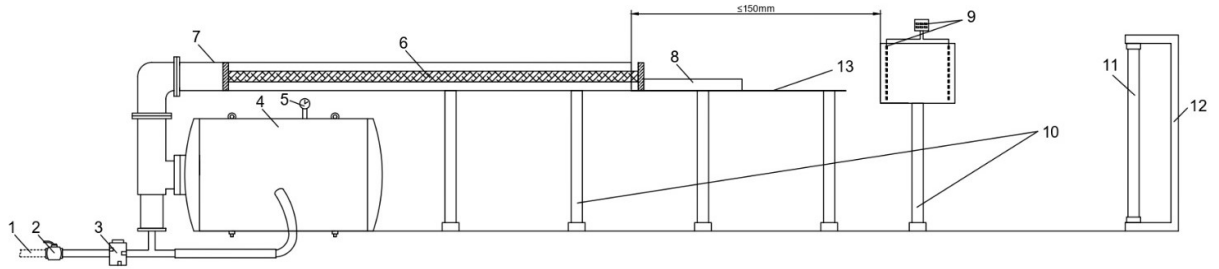
Figure 19 - Roof tile testing apparatus (based on Fernandez et al. 2010).

Key

1   air pipe
2   valve
3   solenoid valve
4   pressure gage
5   pressure vessel
6   pneumatic ram
7   launching tube
8   roof tile
9   velometer
10   support of the launching deck
11   test specimen
12   pressure chamber
13   guided track

Figure 20 - Air cannon for missile impact-testing of glazing according to ISO 16932, DPRI, Kyoto University.

Figure 21 - Typical Japanese roof tile used to test the wind-borne debris impact resistance of the building envelope at DPRI, Kyoto University.

Figure 22 - Typical Japanese roof tile and air cannon adaptor equipment to shoot the tile through a glass sheet, DPRI, Kyoto University.

2.5 Methods to Determine Failure Wind Speeds

Various methods can be used to estimate the failure wind speeds of an object. Regarding Figure 23, the failure of a building component is assumed to occur when the aerodynamic force (F_a) exceeds the total hold-down force on the debris element (F_H). The evaluations can be conducted through a deterministic or a stochastic approach, or through a combination of both. In this Section, various methods that have been explored in the literature are discussed, to provide information that is used to solve the problem, as examined in detail in Chapter 4. In Table 3 there is a synthesis of the main characteristics of the approaches that are presented in this Chapter.
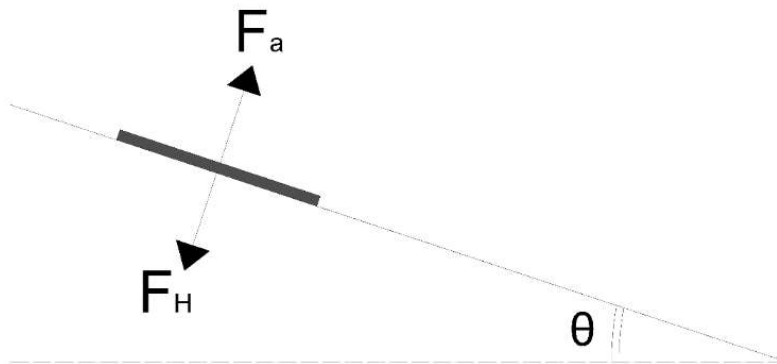
Figure 23 - Resultant hold-down force (F_H) and aerodynamic force acting on the roof tile (F_a).

Table 3 - Methods to Determine Failure Wind Speeds

	Failure Models	Fixture Strength Integrity	Fragility Analysis
Wind Loads	stochastic	deterministic	stochastic
Failure Capacity	deterministic	deterministic	stochastic
Section	2.5.1	2.5.2	2.5.3

2.5.1 Failure Models

Past research activities, such as Kordi et al. (2009) and Visscher and Kopp (2007), used the failure model approach developed by Surry et al. (2005), considering the effect of initial holding forces (Wills et al. 2002). They investigated how various roof building component failures from an initial source position influence the consequential debris flight. They studied the failure and flight trajectories of typical roof tiles, asphalt

shingles, and plywood sheathing panels through numerical simulation and wind tunnel testing. In the tests, the hold-down forces of these building components, according to the best practices of the building technology, have been scaled and realized using magnets on scaled building and building components' models. The capacity and the failure mechanism of the objects should be known prior to testing. Through an experimental approach, the gust wind speed causing the failure of the object can be measured. Accordingly, the capacity is deterministic, but the load is stochastic.

2.5.2 Fixture Strength Integrity

In the approach proposed by Wills et al. (2002), the concept of "fixture strength integrity" has been introduced. It is the wind force required to break loose objects divided by the object's weight. For significant hold-down forces, the effect on the debris element is an acceleration in the wind field, that causes the debris to fly consistently further than the loose-laid ones, staying airborne for a significantly longer distance. When the debris does not have any hold-down force and is loose-laid, after the failure occurs, it immediately starts lowering the relative velocity, and tends to fall back to the ground if the wind speed is reasonably uniform. As a result, the fixture strength integrity has a direct impact on the distance that debris travels from a given point, even though the connection is visibly affected by local flow field effects.

According to the definition of "fixing strength" (FS), which is a coefficient dependent on the fixing conditions of the debris on the source building envelope, the debris flight initialization could be calculated based on the force balance of Figure 23. The fixing strength plays an important role in the debris flight, since it ensures that the initiation of flight is not occurring until the wind speed is sufficient to maintain the flight for greater distances:

- FS =1 when the debris could be associated with a loose object, and it is happening when no fixing systems are adopted for a such component to secure it to the main structure of the source building;

- FS > 1 when the debris is a restrained object, and this coefficient is therefore calculated based on the minimum wind speed to have the failure of both the loose and the restrained configurations of the debris element. FS > 1 when there is a hold-down force applied on the object (F_H) and usually this force is related to the fixing mechanism used to install the object.

It is possible to relate the two wind speeds that would cause the failure of the same debris element in the "loose object" and "restrained object" scenarios, through the following formula:

$$V_r = V_u \sqrt{FS} \tag{2.1}$$

where:

V_r = flight initialization wind speed for the restrained debris element

V_s = flight initialization wind speed for the unrestrained debris element

The fixing strength (FS) of various fixing combinations, with reference to Figure 23, is, therefore:

$$FS = (F_H) / F_m \tag{2.2}$$

with:

$F_H = F_{HoldDown} + F_m$ = total hold-down force on the debris element

$F_m = m * g * \cos(\theta)$ = hold-down force given by the weight of the debris element

$F_{HoldDown}$ = hold-down force of the restraint system type

The resultant hold-down force (F_H) is acting against the aerodynamic force (F_a) caused by the wind pressure on the debris element. When it comes to building components' failure in extreme winds, their failure mechanism, is based on Newton's 2nd Law. Based on Newton's 2nd law, for loose debris elements, the aerodynamic force:

$$F_a = m \, a \tag{2.3}$$

The aerodynamic force, F_a, considers the fluid in which the debris is immersed, which is air in the examined scenarios, and the influence area of the debris itself. Regrading code provisions, incorporating all the coefficients that are characterizing the building component behavior (ASCE 7-22 2022), the definition of F_a is:

$$F_a = 0.5 \, \rho_a \, V_b{}^2 \, A \, C_e \, C_g \, Cp_N \tag{2.4}$$

In the "fixture strength integrity" model, both the wind loads and the object's failure capacity are treated deterministically to go to a single analytical solution. The capacity is calculated from experimental tests, and the loads are yielded from building codes or wind tunnel experiments. Wind loads can vary spatially, based on the aerodynamics of the source building.

Consequently, following building code definitions (with reference to ASCE 7-22 2022), flight initialization occurs if:

$$0.5 \, \rho_a \, (V_b)^2 \, A \, C_e \, C_g \, Cp_N > m \, g \, FS \qquad\qquad (2.5)$$

and, therefore, the minimum basic wind speed to have debris failure (V_{b_ini}) is:

$$V_{b\_ini} = \sqrt{\frac{2 \, m \, g \, FS}{A \, \rho_a \, C_e \, C_g \, Cp_N}} \qquad\qquad (2.6)$$

The resulting 3-s gust failure wind velocity could be calculated once the 3-s gust net pressure coefficient $C_g \, Cp_N$ (= GCp) acting on the building component is known (and it is defined in ASCE 7-22 2022, Section 30.3). These net pressure coefficients (ASCE 7-22 2022) are reported in the design building code for various building geometries, heights, roof types, and roof slopes. The 3-s gust net pressure coefficients (ASCE 7-22 2022) have been developed through wind tunnel tests of different building geometries, terrain conditions, and directions. The code requirements, therefore, have been maximized, considering the worst case in terms of negative/positive pressures acting on the building envelope. The design GCp are identified for various areas on the walls and on the roof slopes, for various building types. Even though this outcome is conservative when it comes to building envelope design (maximum and minimum pressure to test the façade element), it is underestimating design wind speeds to have the failure of a building component located on the building envelope itself. A more significant suction (more negative) on the roof corresponds to a lower wind speed to have the building component failure. Accordingly, if the failure occurs at a lower than the design wind speed, in some scenarios the designer can underestimate the problem of wind-borne debris, considering the surrounding area and objects that can fail and be wind-borne.

2.5.3   Fragility Analysis

Another possibility, when it comes to the determination of failure wind speed for debris elements, is to develop a fragility analysis. In the literature, impact risk assessments and vulnerability models (Grayson et al. 2012; Zhang et al. 2014) have been implemented. A probabilistic approach has been adopted also for studies such as Abdelhady et al. (2022), to determine again a risk assessment for the building envelope, related to wind-borne debris impacts in hurricane events. These models considered wind-borne debris impacts on target windows, and the probability of failure estimation starts from Equation 2.5, but the solution is not deterministic. The solution is instead stochastically analyzed to yield probabilistic curves. The process can consider analytical solutions where simulations such as Monte Carlo lead to come out with a probability of failure (Figure 24) and, finally, a probability of impact on a target building.

Smith (2014) presented probability of failure curves, to relate the basic wind speed (ASCE 7-22 2022) to the probability of failure of different roof tile types and various restraint technologies for roof tiles. His study is the consensus when it comes to roofing technology failure analysis, and it is one reference of this thesis. This thesis aims to propose fragility analysis to evaluate alternative design impact performances of the building envelope.

Equation 2.5 can, therefore, be the expression of the limit state function for an object (with S ≥ 1) subjected to an uplifting wind load. Failure is intended to occur when wind speed is equal to or larger than V_{b_ini} (Equation 2.6), for the single debris element, considering variation both in the wind pressure time histories and on the failure capacity of the debris element.

The variation in the pressure distribution on a debris element should be considered to conduct a fragility analysis. For building design, the net pressure coefficient (GCp) is the parameter that should be defined to conduct the fragility analysis. Existing databases such as Gavanski et al. (2013) recorded the external pressure coefficient time histories, through wind tunnel testing, for low-rise building models. The information regards various roof slopes, heights, and terrain features, and formed the basis of the current version of ASCE 7-22 (2022). Therefore, the variation in the GCp values can be studied, for terrain categories, based on various wind directions.

The failure capacity (F_H) of an object, to conduct a fragility analysis, should be expressed stochastically, based on statistical data distributions coming from experiments and on engineering assumptions. This approach has been used by Smith (2014), defining roof tile failure as the lift of this building component for at least 5 cm. He defined roof tile failure for different attachment methods through an

experimental campaign, obtaining a value distribution depending on roof tile type and fixing method. Mean and coefficient of variation describe probabilistically the failure capacity of building components, to conduct a fragility analysis. According to this approach, both the $F_{HoldDown}$ of the restraint system and the hold-down force given by the weight of the debris element (F_m) can be described by a mean value and a coefficient of variation. The combination of the two components describes stochastically the failure capacity ($F_H = F_{HoldDown} + F_m$).
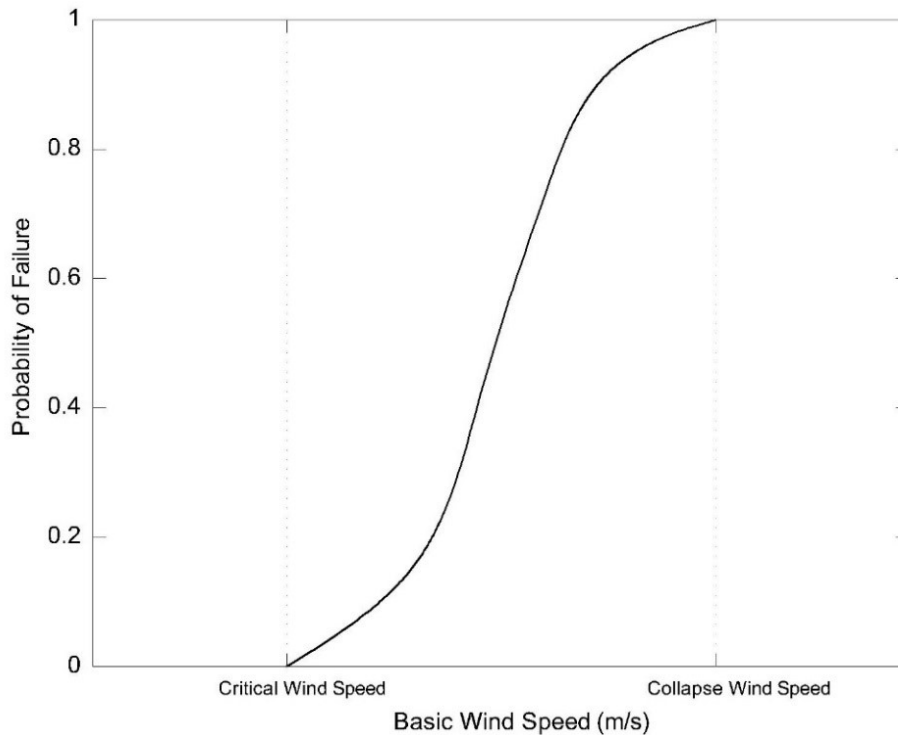
Figure 24 - Probability of failure curve based on basic wind speed. Critical and collapse wind speeds can be identified by the curve. Collapse wind speed corresponds to a 100% probability of failure.

2.6 Limit States and Capacities of Roof Components

When it comes to building components that can fail in extreme winds, roof shingles and roof tiles should be discussed. Roof tiles' uplift resistance depends on the restraint system and the installation interaction between the various elements of the roofing. The failure mechanism of the roof tiles installed on a building at various inclines and pitch configurations has been examined in the existing literature to assess capacities and failure mechanisms.

Testing procedures to determine the uplift resistance of roof tiles have been developed worldwide in the 1990s, starting from the studies conducted in the United Kingdom by the company Redland Technology

(Smith & Morrison 2019). This research lead to the definition of British Standard BS 5534 (BSI 2015) and the U.S. SSTD-11 (SBCCI 1999), based on wind loading mechanisms of roofing elements pioneer studies that have been discussed in detail by Smith et al. (2016). For roof tile capacity definition, in Australia, Standards Australia (2002) published Australian Standard AS 2050. In Europe, there is the European Standard EN 14437 (CEN 2004, Figure 25), and the Dutch Standard NEN 6707 (Netherlands Standardization Institute 2011). It should be underlined, again, the complexity of the problem, that takes to cases and certification programs that cannot be currently addressed following the available standard protocols. It is this the case of the over-and-under roof tiles (UNI 9460 2008), a roof tile type widely adopted in Italy (Figure 26). It is explicitly specified in EN 14437 (2004) that this testing protocol cannot be used for this roof tile-type testing.
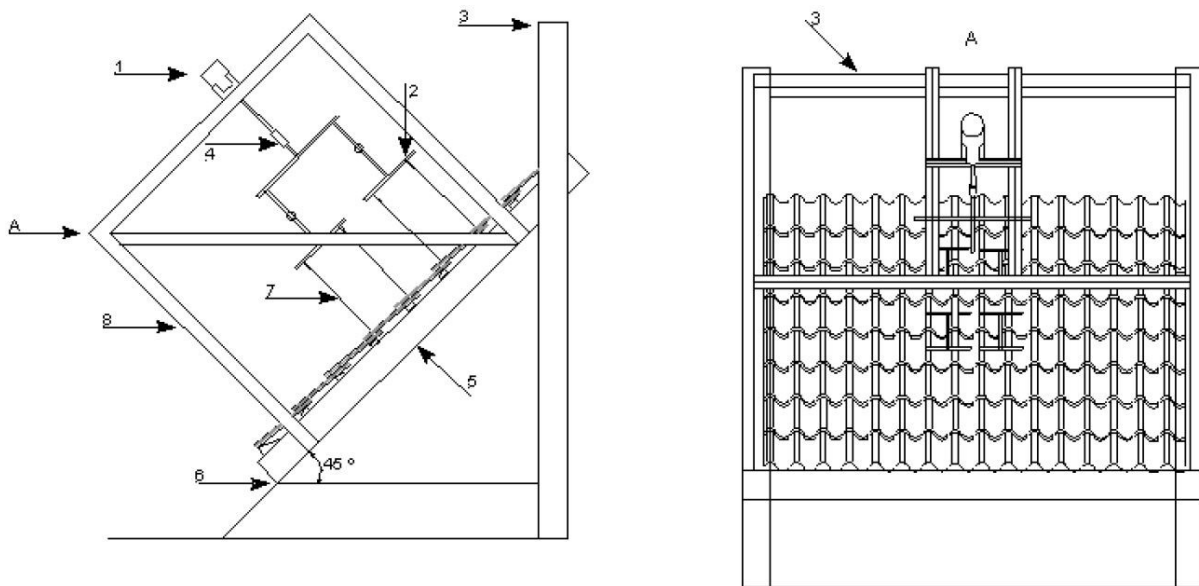
Figure 25 - Example of test rig (EN 144437 2004).

Key
1   Hydraulic pull / push provision
2   Force application
3   Frame
4   Force measuring
5   Rafter
6   Joint
7   Cable
8   Frame

Figure 26 - Terracotta over-and-under roof tile. The geometric and material characteristics of this roof tile type follows UNI 9460 (2008). The international standard EN 14437 (CEN 2004) cannot be used to calculate the uplift capacity of this building technology. The framework to estimate debris element failure and flight in wind events, presented in the thesis, can be used to calculate the uplift capacity of these building components (Wikimedia Commons).

The failing building elements can be therefore characterized through standard procedures and wind engineering considerations. The studies consider debris' geometric features, configuration, wind velocity, direction, and duration, as well as shielding effects, among other parameters. Existing research (Gavanski et al. 2013) investigated the pressure equalization acting on the building envelope and the pressure distribution. Based on these data, Gavanski & Kopp (2017) assessed roof-to-wall connection failures for wood-frame houses. Smith (2014) focused, through the numerical and experimental campaign, on the wind resistance of clay and concrete roofing tile systems, providing a scientific consensus on the topic. These studies can be used as a reference to develop a fragility analysis of building components.

The studies on the roof tiles' failure capacity (Smith 2014) demonstrated that various roof tile types have different failure capacities, and these depend also on the uplift test locations used to fix the cables (Figure 25). He studied the variation in terms of uplift capacity of various roof tile types (high-[17], medium-[18], low-profile[19] tiles) with different installation techniques (battened[20], direct to deck[21], foam adhesive[22]), and different uplift test locations. Smith (2014), furthermore, developed a design model to convert the uplift capacity of roof tiles that are analyzed through uplift testing to the failure wind speed, for a specific roof tile type and installation technique. Considering building components that are available in the market, however, the uplift capacities, for different attachment configurations, follow precise uplift test locations. According to the standard, the uplift test is conducted at 0.76 L_t, where L_t is the maximum overall dimension of the tile measured parallel to the watercourse (ASTM 2022).

2.7 Wind-Borne Debris Aerodynamics

In this section, the aerodynamics of wind-borne debris is analyzed, based on existing literature. The aim is to explain how the complex problem of wind-borne debris has been investigated so far. The differences in numerical and experimental models that have been developed to estimate debris trajectory are analyzed.

In extreme wind, various building components have been identified as being wind-prone and, therefore, as the most common sources of wind-borne debris. These are roofing materials such as gravel, shingles, roof tiles (Figure 6), sheathing, and wooden structural members (Kordi 2009). The current testing protocols to simulate wind-borne debris impacts consider the complete failure of typical balloon frame construction: the flight of structural members (large missiles, representative of the 2x4 inches section wood frame construction),

---

[17] High-profile roof tile - tile with a rise-to-width ratio greater than 1:5 (ASTM 2022).

[18] Medium-profile roof tile - tile with a rise greater than 1⁄2 in (1.27 cm) and a rise-to-width ratio of less than or equal to 1:5 (ASTM 2022).

[19] Low-profile roof tile - tile with a rise equal to or less than 1⁄2 in (1.27 cm) (ASTM 2022).

[20] Battens are fastening strips installed to the underlayment or sub-roof to which roof tiles are then installed (FRSA–TRI 2020).

[21] Deck is the surface installed over the structural framing members to which roofing is applied. May be of wood boards, plywood, or other approved material (FRSA–TRI 2020).

[22] Foam adhesive technology uses a bonding agent to join two surfaces for permanent attachment as approved by local regulations. Roof slopes greater than 6:12 require the use of mechanical fasteners in addition to foam adhesive (FRSA–TRI 2020).

and the roof gravel (small missiles) to conduct impact tests on façade products (Mejorin et al. 2019). The current testing protocols, therefore, assume that, somehow, the wind-borne objects have these two characteristics. In Japan, at the Disaster Prevention Research Institute of the Kyoto University for a research project in conjunction with the Building Research Institute in Tsukuba (which is a national research and development agency in Japan), various local building and urban components have been studied in the typhoon and tornadic winds (Maruyama 2011), among which the typical Japanese roof tiles were utilized (Mejorin et al. 2009). Roof tiles have been deeply investigated to implement the existing testing equipment developed for the ASTM testing procedures (ASTM 2019, 2020) for the local Japanese context.

Regarding wind-borne debris, several studies have been performed, focusing on flight initialization and trajectory. It is a complex problem, difficult to be generalized because of the range of wind-borne object characteristics (e.g., shape, mass per unit area, source building shape, etc.) that play a key role. Wind-borne debris has been consequently discussed in its behavior related to different shapes. Wills et al. (2002) defined three groups of debris, based on their aerodynamic properties (Figure 27):

- compact (e.g., roof gravel);

- plate-like (e.g., roof tiles);

- rod-like (e.g., 2 by 4 in. lumber structure).
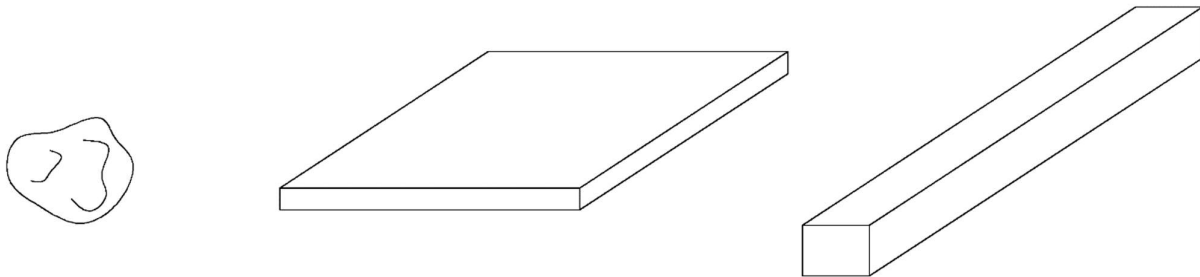
Figure 27 – From left to right: compact, plate-like, rod-like debris, according to Wills et al. (2002).

2.7.1   Wind-Borne Debris Flight Analysis

The first wind-borne debris studies to assess flight and trajectory were developed by Tachikawa (1983, 1988). Tachikawa demonstrated that plate-like debris, in a smooth, uniform flow, depending on the initial angle of attack (β), varies in flight trajectory, with autorotational, translational, and intermediate modes of flight. His output is two-dimensional as it tracks plane flight trajectories to estimate the variability of flight in real storms.

For plates, the model considers a sum of a static and an autorotational component, using the quasi-steady method. For rods and compact debris, the model is entirely quasi-steady. The static component is related to the angle of attack of the relative velocity with reference to the instantaneous rotation. In contrast, the autorotational (or Magnus) component is proportional to the rotational speed (Figure 28, Figure 29). For plate-like debris, the autorotational component is an influential parameter on the flight.

Tachikawa (1983) defined the equations of motion for a general debris object, in uniform flow:

$$\frac{d^2x}{dt^2} = \frac{\rho_a\,(C_D\,\cos\beta - C_L\,\sin\beta\,)\,[(U-u)^2 + (-w)^2]}{2\,\rho_m h} \tag{2.7}$$

$$\frac{d^2z}{dt^2} = \frac{\rho_a\,(C_D\,\sin\beta + C_L\,\cos\beta\,)\,[(U-u)^2 + (-w)^2]}{2\,\rho_m h} - g \tag{2.8}$$

$$\frac{d^2\theta}{dt^2} = \frac{\rho_a\,C_M\,A\,l\,[(U-u)^2 + (-w)^2]}{2\,I} \tag{2.9}$$
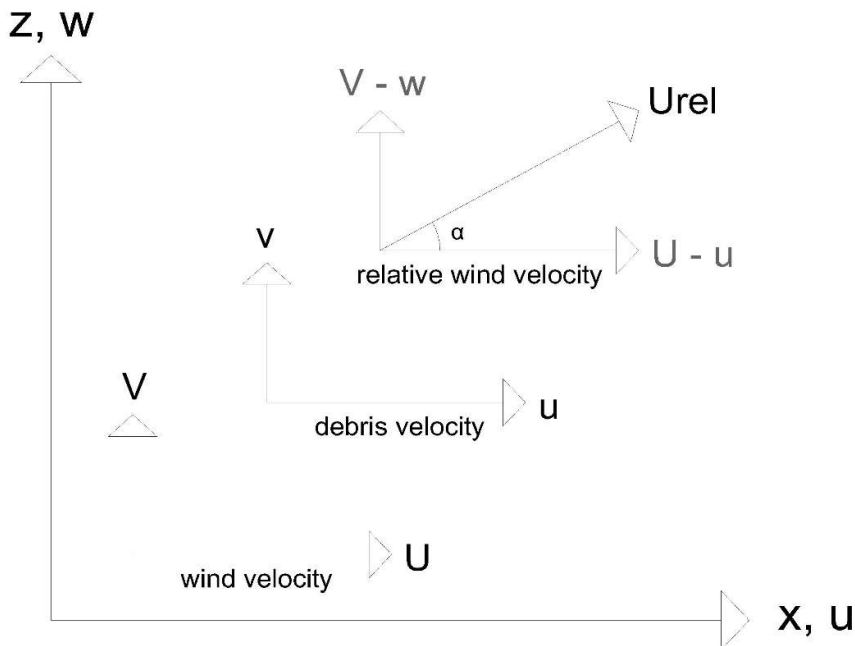
Figure 28 - Horizontal and vertical components of wind velocity and debris velocity. Relative wind velocity.
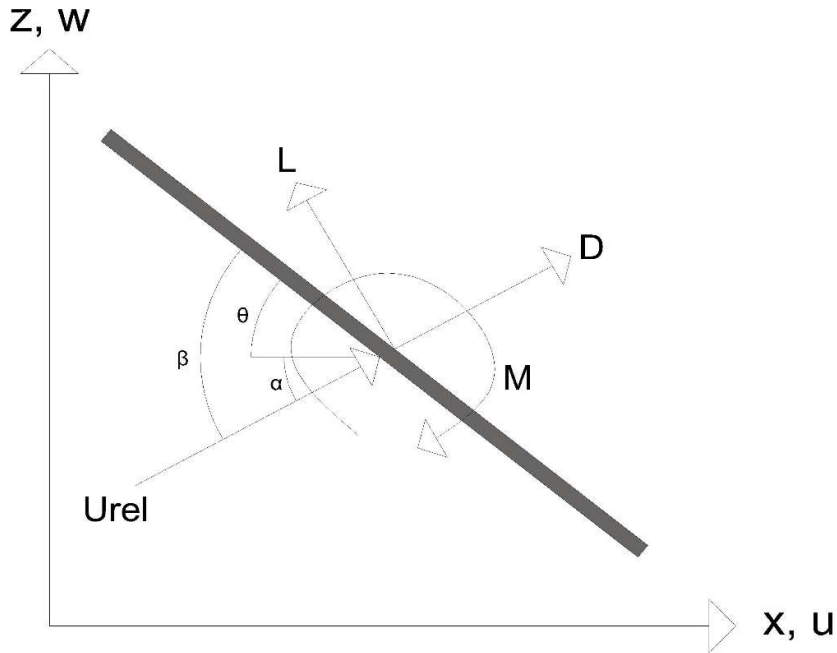
Figure 29 - Forces and moments on a plate-like debris element.

Considering m (mass of the debris), V (vertical wind velocity), and $U_{rel} = ((U - u)^2 + (V - v)^2)^{05}$, Baker (2007) proposed a non-dimensional form for the variables:

$\bar{x} = \left(\frac{x}{l}\right)\varphi$ = non-dimensional horizontal displacement of the debris element

$\bar{z} = \left(\frac{z}{l}\right)\varphi$ = non-dimensional vertical displacement of the debris element

$\bar{\theta} = \theta\,\varphi$ = non-dimensional angular rotation of the debris element

$\bar{t} = \left(\frac{t\,U}{l}\right)\varphi$ = non-dimensional time

$\bar{u} = \left(\frac{u}{U}\right)$ = non-dimensional horizontal velocity of the plate

$\bar{w} = \left(\frac{w}{U}\right)$ = non-dimensional vertical velocity of the plate

$\bar{V} = \left(\frac{V}{U}\right)$ = non-dimensional vertical wind velocity

$\bar{U}_{rel} = \frac{U_{rel}}{U}$ = non-dimensional relative wind velocity

$\Delta = \left(\frac{m\,l^2}{I}\right)$ = non-dimensional plate inertia

$\varphi = \left(\frac{0.5\,\rho_a\,A\,U^2}{M}\right)$ = buoyancy parameter

$\Omega = \left(\frac{M\,g}{0.5\,\rho_a\,A\,U^2}\right)$ = dimensionless parameter

Accordingly, the non-dimensional form of the equations of motions:

$$\frac{d^2 \bar{x}}{d\,t^2} = (C_D\,(1 - \bar{u}) - C_L\,(\bar{V} - \bar{w})\,)\,\bar{U}_{rel}$$

(2. 10)

$$\frac{d^2 \bar{z}}{d\,t^2} = (C_D\,(\bar{V} - \bar{w}) + C_L\,(1 - \bar{u})\,)\,\bar{U}_{rel} - \left(1 - \frac{\rho_a}{\rho_m}\right)\,\Omega$$

(2. 11)

$$\frac{d^2 \bar{\theta}}{d\,t^2} = \Delta\,C_M\,\bar{U}_{rel}^{\,2}$$

(2. 12)

Tachikawa (1983) offered, as well, non-dimensional versions of the equations of motion and identified the dimensionless parameter that has since been named in his honor (Holmes et al. 2006): the Tachikawa number $T_a = \left(\frac{0.5\,\rho_a\,A\,U^2}{M\,g}\right)$. This parameter ($T_a = 1/\Omega$) is the ratio of the aerodynamic force to the gravitational force. Low-mass objects with a large surface area have high T_a; these debris types tend to fly faster and for longer distances if compared to ones with lower T_a. Tachikawa produced graphs showing the variation of T_a as a function of debris properties and wind speed (Holmes et al. 2006), to show how T_a is the main non-dimensional parameter determining the trajectories of debris objects of all types.

Lin et al. (2006), Holmes et al. (2006), Holmes (2015), Richards et al. (2008), and Kordi (2009) conducted flight analyses for different wind-borne debris typologies, in uniform wind flow, using the quasi-steady theory. Following Tachikawa's work, Kordi & Kopp (2009) developed the aerodynamic drag, lift, and moment coefficients both for the static (C_{DS}, C_{LS}, C_{MS}) and the rotational (C_{DR}, C_{LR}, C_{MR}) components, to solve the equations of motion for a square plate-like debris.

$$C_{DR} = \begin{cases} 0.66\,\left|\frac{S}{S_0}\right| & \left|\frac{S}{S_0}\right| \leq 0.4 \\ 0.12 + 0.36\,\left|\frac{S}{S_0}\right| & 0.4 < \left|\frac{S}{S_0}\right| < 1 \\ 0.48 & \left|\frac{S}{S_0}\right| \geq 1 \end{cases}$$

(2. 13)

$$C_{LR} = \begin{cases} 0.1575 + 0.2625\,\frac{S}{S_0} & \frac{S}{S_0} \geq 0.2 \\ 0.15\,\frac{S}{S_0} & -0.2 < \frac{S}{S_0} < 0.2 \\ -0.1575 + 0.2625\,\frac{S}{S_0} & \frac{S}{S_0} \leq 0.2 \end{cases}$$

(2. 14)

$$C_{MR} = \begin{cases} 0.12 \left(1 - \frac{S}{S_0}\right) & \frac{S}{S_0} > 1 \\ 0.12 \left(1 - \left|\frac{S}{S_0}\right|\right) \frac{S}{S_0} & -1 \leq \frac{S}{S_0} \leq 1 \\ -0.12 \left(1 + \frac{S}{S_0}\right) & \frac{S}{S_0} < -1 \end{cases}$$ (2. 15)

where:

$S = \omega\, \ell\, /\, (2\, U_{rel})$ = spin parameter of the plate

$S_0 = \omega_0 \ell\, /\, (2\, U_{rel})$ = spin parameter of the plate at the point of stable autorotation

ω = angular velocity of the plate

ω_0 = angular velocity of the plate at the point of stable autorotation

Following Kordi & Kopp (2009) and based on Iversen (1979), if the non-dimensional moment of inertia of a plate (I^*):

$I^* = (\,32\,I\,)\,/\,(\,\pi\,\rho_a\ell^4\,B^{23}\,) > 1$ (2. 16)

with:

$\tau = \frac{h}{l}$ = thickness ratio of the plate

AR = $B\,/\,\ell$ = aspect ratio of the plate

$$S_0 = (0.329 \ln \tau^{-1} - 0.0246(\ln \tau^{-1})^2) \times \left\{\left[\frac{AR}{2+(4+AR^2)^{1/2}}\right]\left[2 - \left(\frac{AR}{AR+0.595}\right)^{0.76}\right]\right\}^{2/3}$$ (2. 17)

To define the static components of drag, lift, and moment coefficients, the definition (Kordi & Kopp 2009; Hoerner 1965) of the static normal coefficient on the plate (C_N) is:

---

[23] B is the maximum overall dimension of the roof tile measured perpendicular to the length or water channel (ASTM 2022).

$$
C_N = \begin{cases} 0.7\,\dfrac{\beta}{7°} & \beta \le 7° \\[2mm] 0.7 + 0.15\,\dfrac{\beta - 7°}{13°} & 7° < \beta \le 20° \\[2mm] 0.253 + 1.747\sin\beta & 20° < \beta < 160° \\[2mm] 0.7 + 0.15\,\dfrac{173° - \beta}{13°} & 160° \le \beta \le 173° \\[2mm] 0.7\,\dfrac{180° - \beta}{7°} & 173° \le \beta \le 180° \end{cases}
$$

(2. 18)

Accordingly:

$$
C_{DS} = 0.15 + C_N \sin\beta
$$

(2. 19)

$$
C_{LS} = C_N \cos\beta
$$

(2. 20)

$$
C_{MS} = \frac{c}{l} C_N
$$

(2. 21)

with:

c = center of pressure, which, for plates with AR = 4, follows the formula:

$$
\frac{c}{l} = 0.25 - \frac{\beta}{2\pi}
$$

(2. 22)

Based on Kordi et al. (2011), through analytical and experimental simulations, the flight of the case study wind-borne debris has been analyzed, assuming $S_0 = 0.47$ (Skews 1990). The initial conditions have been highlighted in their significant influence on flight characteristics. Through wind tunnel experiments at Western University, Kordi (2009) studied how the flight of roof tiles and asphalt shingles is affected by the source building aerodynamics, the wind field around the building, the turbulence, and the peak wind gusts causing failure (Kordi et al. 2010). These observations were possible because, instead of simulating the debris flight in a uniform flow from an initial wind angle of attack, Kordi (2009) included both the failure from a building and the debris flight. The debris elements were located on a gable roof with a slope of 4:12, plan dimensions of 10.38 x 9.14 m, and an eave height of 6.8 m (Kordi & Kopp 2008). This model is representative of a typical North American 2-storey house. Kordi (2009) analyzed the typical U.S. shingles and concrete roof tile flight

behavior through a 1:20 scale model placed in a boundary layer wind tunnel (Kordi & Kopp 2008). The concrete roof tiles had equivalent full-scale dimensions of 41.9 x 34.3 cm, with the thickness of 3.17 cm, and a mass of 4.86 kg, following the characteristics of commercial low-profile concrete roof tiles. From the wind tunnel experiments, in some locations on the building roof, roof tiles and shingles, for some tested wind directions, did not fail or did fail but did not fly, even for extreme wind simulations (Kordi et al. 2010).

2.7.2   Wind-Borne Debris Trajectories

Kordi et al. (2010) highlighted that the resultant distributions and maximum values in the debris flight and the flight distances depend on the mode of flight of the debris element. Considering debris trajectories, Grayson et al. (2012) developed a model that can provide relevant debris trajectory information (e.g., linear and rotational position, velocity, and acceleration) needed to track wind-borne debris and assess any impacts on the building envelope that may occur due to the debris flight. Previously conducted wind-borne debris trajectory analyses (Tachikawa 1983; Holmes et al. 2006; Nin et al. 2006) considered debris elements that are free to fly in a uniform flow, thus, Kordi (2009) developed a better understanding of the real-world problem by bringing in correct boundary and initial conditions. The experimental database that has been developed at Western University represents a unique example of data collection on the specific research topic of wind-borne roof tiles' flight analysis.

Based on the wind tunnel experiments, Kordi et al. (2010) defined a numerical model to estimate debris trajectories and velocities with sufficient accuracy, to capture the effects of initial conditions in terms of turbulence and the building wake. Kordi et al. (2010) found that the 3-s gust failure wind speed (V_{b_ini}) represents a practical and reasonable upper-bound wind speed to estimate the upper-bound flight trajectory, but that it is overestimated the mean trajectory. Somehow, debris elements can miss the wind gust and, consequently, when the failure occurs, they accelerate and fly in "lower wind speeds environments" (Kordi & Kopp 2011). This has been explained by the effect of a negative vertical component of the wind velocity, which is not considered in the numerical calculations (Kordi et al. 2010). This vertical component is linked to the wake region behind the building, which reduces the maximum below the uniform, smooth flow trajectory results for debris. For plate-like debris (Wills et al. 2002), it has been found (Kordi et al. 2010; Kordi & Kopp 2011) that the lower bound wind speed to estimate debris' trajectories, is the average 10-min wind speed at source building roof height (V_{mean_ini}). Additionally, Kordi & Kopp (2011) noticed that the introduction of a negative

vertical component of the wind velocity of 20% of the horizontal wind speed can increase the accuracy of the numerical results for trajectory calculation. This additional vertical component can reproduce the local effects of the separation zones of the wind flow around the building.
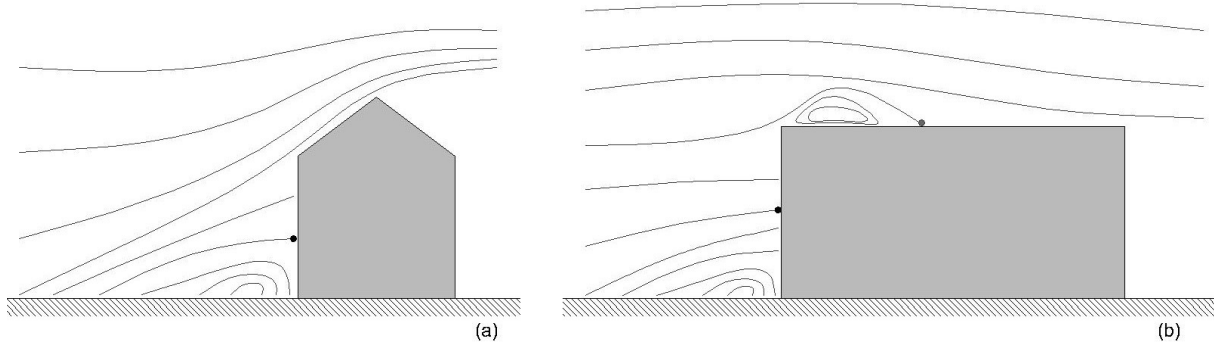
Figure 30 - Schematic sketches of flow fields for low-rise buildings: (a) 9:12 hip roof (9/12), and (b) flat roof. The black dots indicate the stagnation points on the windward walls. Flow separation occurs at the leading edge of the roof for (b), and the grey dot indicates the reattachment point for the flat roof. If the roof pitch is low enough, the flow can reattach downwind. In both (a) and (b) there is a sheltered region behind the leeward wall with relatively low wind speeds. The air flow around buildings in wind flows characteristic of extreme windstorm events are quite complex and, accordingly, also debris failure and trajectory analyses are. When it comes to target buildings, the most vulnerable area to wind-borne debris impact is the windward wall region. However, impacts can also occur in the reattachment region on the roof and side walls. As the air approaches the windward wall, its horizontal velocity reduces rapidly. Heavier debris elements have higher inertia and, in the wind flow, will probably continue with their velocity slightly changes until they impact the target façade. Lighter and smaller debris elements may lose velocity in this region or even be swept around the building with the flow if they are not directed to the stagnation point.

Roof gravel is another building component used to protect waterproof membranes on roofs that can fail and fly, becoming wind-borne debris and impacting surrounding constructions. Roof gravel behavior has been investigated especially in the North American context, where it is widely used (Doddipatla & Kopp 2019; Kopp 2009). It has experimentally proved its weakness also in conditions that, from a design perspective, lead to safe design solutions for the roof covering. It has been noticed that parapets cannot prevent roof gravel

failure when it comes to sustained winds, not even for parapets heights of 1.37 m on buildings with a flat roof height of 45 m. These findings mean that the wind field created by the building aerodynamics is an influential parameter to consider. Accordingly, when it comes to flat roofs where roof gravel is positioned on the top, a vertical component of the wind velocity should be included for numerical calculation, to match the experimental results described by Doddipatla & Kopp (2019). In Figure 30 two schematic sketches are represented for the flow fields for a hip roof (9/12) and a flat roof. From the flat roof representation, it is possible to understand the phenomena of the roof gravel uplift, caused by the wake region in the proximity of the separation of the flow. The vertical component of the wind velocity should be, therefore, used to justify roof gravel uplift and the subsequential flight. For the upper bound, on average for plate-like debris, the 3-s gust wind speed at the source building roof height is a good estimation, so that the dispersion of debris can be estimated by these two bonds.

Kordi's (2009) observations of the high-speed video recorded plate-like debris flight trajectories, which have been categorized for the different identified debris patterns: auto-rotational, 3D spinning, translational, falling, and "no flight". These trajectories usually followed complex paths, as a result of the combination of the categorized patterns. The most common (Kordi 2009) has been found to be the 3D spinning mode, in which there is a rotation in any direction but the one which identifies the "auto-rotational" mode, which is perpendicular to the axes that theoretically contain the 2D motion. The results highlighted that the model building and the debris elements, are 3D scenarios and, accordingly, experimental results yield 3D recorded motions.

2.7.3   Wind-Borne Debris Speeds

Wind-borne debris flight speeds are complex to assess through real-world observations. From video and photographic observations of windstorm events, it is not possible to develop an understanding of wind-borne objects' speeds. Data cannot be achieved because it is difficult to record a single element since usually failure occurs simultaneously for multiple ones. Through numerical calculations, using Tachikawa's equations of motion (Equations 2.7, 2.8, 2.9), wind-borne debris flight trajectory can be calculated. Accordingly, information about the flight speeds can be evaluated when there is enough information about the debris characteristics and failure wind velocity.

Experimental results for plate-like debris showed that, considering numerical results to estimate flight speeds, these ranges are:

- between 40 and 120% 3-s gust wind speed at failure for roof shingles (Kordi & Kopp 2011);

- between 20 and 95% 3-s gust wind speed at failure for roof sheathing panels (Kordi et al. 2010);

- between 30 and 60% 3-s gust wind speed at failure for roof tiles (Kordi & Kopp 2011).

The variation in the estimated range for the three debris elements that have been investigated through wind tunnel experiments is due to the different T_a numbers and, accordingly, to the different aerodynamic behavior of these objects. T_a number depends on the wind field for the debris element flight and, therefore, on the failure wind velocity. V_{b_ini} can be calculated through Equation 2.6, knowing the failure uplift capacity of the debris element, which is based on the intrinsic characteristics of the object, and on its attachment configuration.

In Section 2.6 the failure capacities of low-profile concrete roof tiles have been discussed. For various restraint systems, their mean uplift capacities according to ASTM (2008) standard testing procedure can be obtained. For analytical calculation, it can be assumed that the failure wind velocity is the 3-s gust wind velocity that caused the debris element failure. Therefore, following Baker (2007) and the non-dimensional form of the equations of motions (Equations 2.10, 2.11, 2.12), the speed ranges that have been experimentally observed by Kordi (2009), can be estimated for wind-borne debris. Using the numerical approach validated in Appendix A - Wind-Borne Debris Trajectory Calculation, for the typical concrete low-profile roof tiles characteristics the non-dimensional debris velocity can be estimated.

Figure 31 – Tampa, Florida. Extreme winds caused roof tile to fly and hit the neighbour's house (photo courtesy of Tim Reinhold).

2.8 Summary

Codes and standards development for wind-borne debris impact requirements have been presented. The best practices, identified in the ASTM standard method (ASTM 2019, 2020), are going to be compared against the numerical results in Chapter 4, for a specific example. The focus of the comparison regards the façade design impact energies calculated for an essential facility following the current standardization framework (Section 2.2), and an alternative one (**Error! Reference source not found.**). Furthermore, the test equipment to conduct wind-borne debris impact tests has been analyzed in Section 2.3, together with the experimentations that have been developed to use alternative projectiles (Section 2.4). The testing equipment in Figure 19 is going to be the reference one for the example of Chapter 4. The introduction of the impact orientation control (Section 2.4.1) is proposed to be calibrated, based on the example results in Chapter 4, based on wind-borne debris trajectory analytical results (Section 4.7.3).

In Section 2.5, the methods to determine debris failure wind speeds are presented. These methods can have a stochastics (fragility analysis), or a deterministic approach (fixture strength integrity), or a combination of the two (failure models). For the example presented in the thesis in Chapter 4, a fragility analysis is conducted, to determine the probability of impact on the façade for an essential facility. In Section 2.6, the methods to evaluate the uplift capacities of roof components have been presented, to understand the dataset used to present the numerical calculations in Chapter 4.

Finally, this Chapter provided an overview of the state of the art for wind-borne debris aerodynamics. Existing literature has been analyzed, to present available numerical models to conduct wind-borne debris flight analysis. The equations of motion and the aerodynamic coefficients have been explained, based on the literature. Past wind-borne debris experimental campaigns, conducted to analyze debris flight trajectory paths, have been examined. These experimental outcomes give variability to the analytical model used for the calculations, which is going to be presented in Chapter 4. In Section 2.7.2, considerations about the wind field and about building aerodynamics showed the complexity of the problem for wind-borne debris flight assessment.

Chapter 3. Design Tool to Identify Alternative Façade Impact Tests

3.1 Objectives

The thesis proposes a design framework to fill the gap in façade impact test requirements related to local wind-borne debris' types and based on wind engineering assumptions. The projectiles and impact energies to perform performance-based impact tests are evaluated by estimating the trajectory and the velocity of specific debris, based on the surrounding buildings and considerations of the aerodynamics of wind-borne debris. The existing test procedures for wind-borne resistance of façades *"have largely been developed from post-damage investigations, with little research on the aerodynamics of flying debris. Knowledge of debris aerodynamics and proper estimation of debris trajectory is necessary to establish rational impact criteria and risk assessment models"* (Lin et al. 2006).

The best practices in terms of impact testing to simulate wind-borne debris in windstorm events are the ASTM standard procedures (ASTM 2019; ASTM 2020) and these consider standardized projectiles. However, the specification requirements already give façade designers the chance to go through engineering assumptions to develop ad-hoc wind-borne debris impact tests for their projects. In ASTM E 1886 (2019) is mentioned the possibility to have an "other projectile" to test the building envelope, to guarantee wind-borne debris resilience in windstorms. This could be considered for *"any other representative projectile with mass, size, shape, and impact speed as a function of basic wind speed determined by engineering analysis"* (ASTM 2019). Façade designers' expertise differs from a wind engineer's skills. The objective of this thesis is to develop a design framework to explore failure and flight assessments of wind-borne debris considering the immediate surroundings. In the building envelope design process, wind experts are usually involved in major projects, and this entails that usually, when it comes to wind-borne debris resilience, a standard procedure (ASTM 2019, 2020) is most adopted. The façade impact tests are accordingly not based on the aerodynamics of wind-borne debris in local environments, also because there is no available database about wind-borne debris speeds in windstorms (Kordi 2009). This research aims to highlight and propose a design framework to identify an alternative wind-borne debris impact-resistance of façades, to mitigate wind-induced damage to buildings considering case-specific contexts.

The thesis describes the step-by-step application of the design method, using the U.S. typical concrete roof tile as a case study, examining their failure and flight. The final output aims to evaluate the kinetic energy to be absorbed by building envelope solutions when hit by this specific wind-borne building component. The

presented design tool is therefore intended to improve technological efficiency and to support decision-making strategies, providing, eventually, a risk analysis of the occurrence of wind-borne debris-related damages. This alternative design framework considers first of all essential facilities as target buildings since these should guarantee their service, especially in the post-disaster event scenarios. Hospitals, for example, belong to this building category.
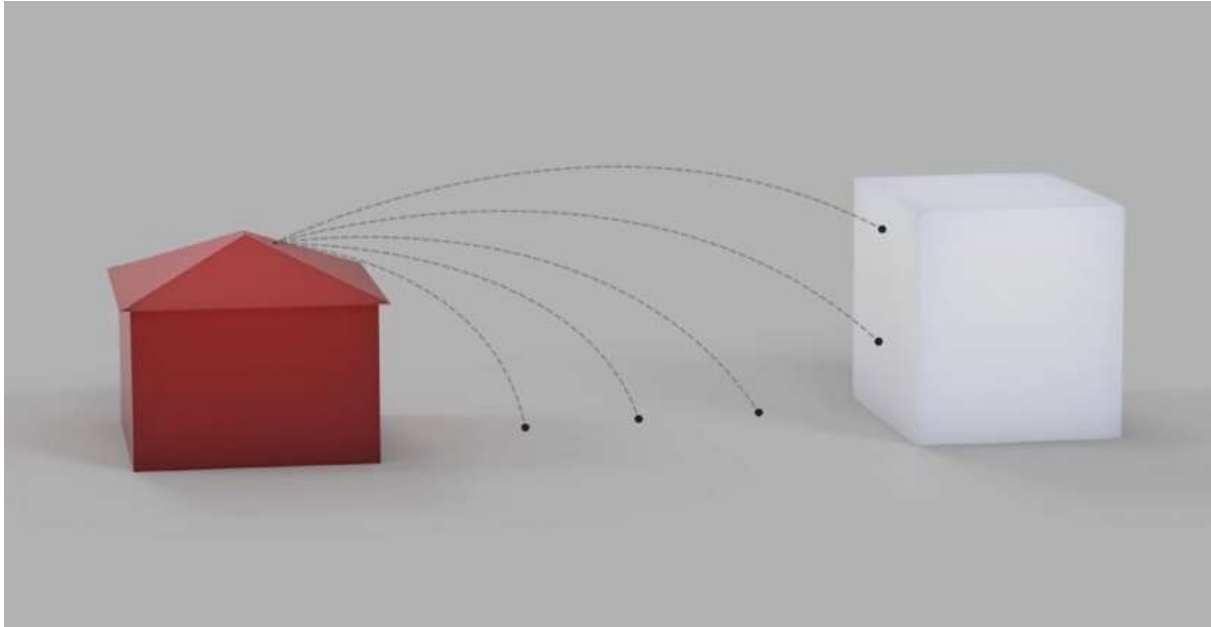
Figure 32 - Sketch for "source building" (red), "target building" (white), and roof tile trajectories (dashed). The wind direction can vary in a windstorm event, but the position of source and target buildings remains the same. Accordingly, three of the four façades on a rectangular target building have the potential to be hit by wind-borne debris in windstorm events, for a given debris source. This can happen if the debris element is light enough to possibly being swept around the target building with the flow, to finally hit the side façades. For heavier debris elements such as roof tiles, for the configuration on the figure, just the windward façade and the roof of the target building can be hit by roof tiles originated from the source building. This is related to the high inertia of the debris element, which influence the debris trajectory. Therefore, wind-borne debris impact performance can be diversified, based on source building and target façade location. Consideration should be based on the case-specific wind fields, on the leeward, windward, and side target building walls locations, on debris characteristics.

3.2   Methodology

The approach to this research is to utilize and synthesize the existing literature on wind-borne debris impact performances of façades. It uses analysis of failures, debris flight trajectories, and flight speeds. The final goal is to estimate the consequent projectiles and impact energy to be absorbed by a target building envelope in wind events. Through the review of past disasters and building envelope damage assessments, the problem of wind-borne debris impact on façades is presented. The current code and standard requirements that have been identified and adopted as the best practices when it comes to building envelope design in the extreme wind-prone area are analyzed.

The extensive review of wind engineering studies regarding wind-borne debris behavior is the basis to formulate the research question that this thesis aims to answer. The current necessity to consider the aerodynamics of wind-borne debris in wind events and specific environments, to provide impact resistance to the building envelopes is underlined through the critical review of the current best practices that are adopted worldwide. Through a probabilistic approach, the research presents a tool for façade designers.
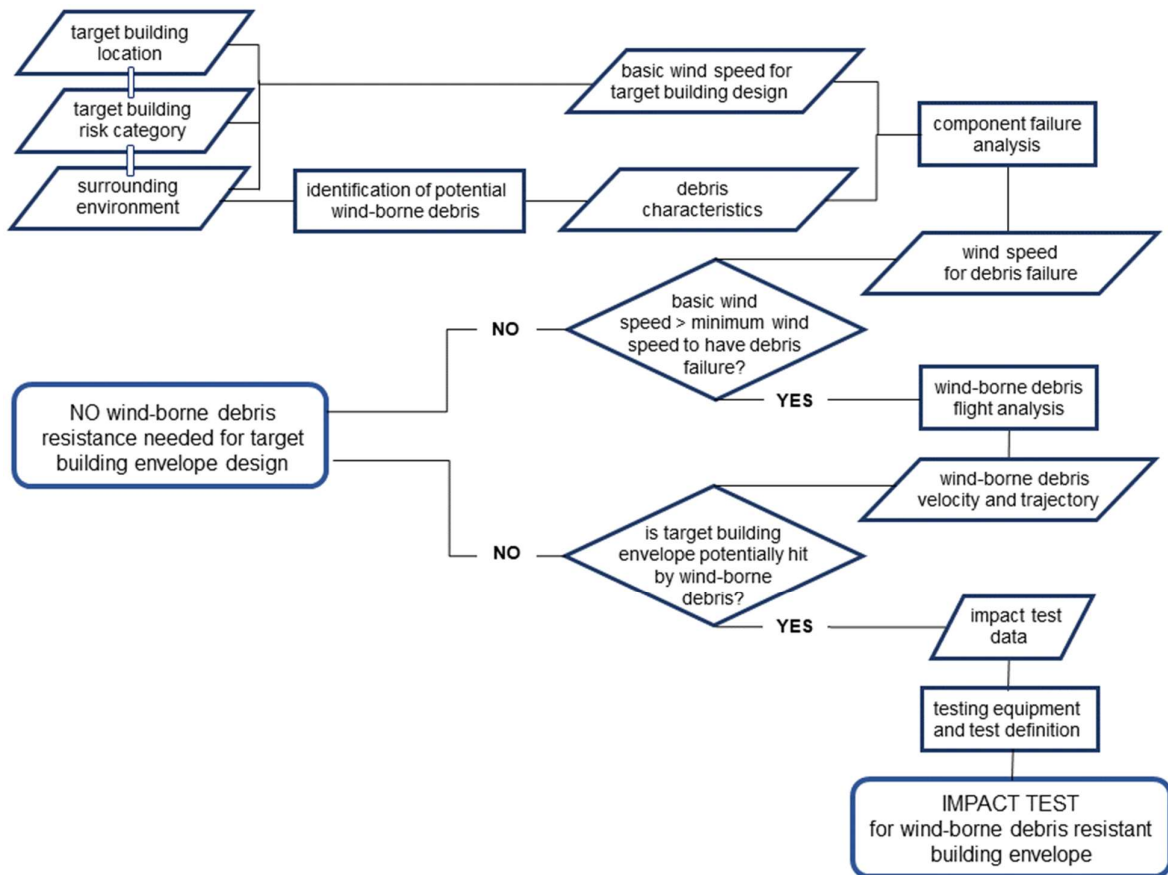
Figure 33 - Flowchart of the proposed design tool.

Two main investigation areas are identified for the building technology and wind engineering studies on wind-borne debris: the failure mechanism, and the flight assessment, to ultimately have the impact energy on the final target. The failure mechanism considers the "source building", where the wind-borne debris could originate from, and the technical installation of the object, and therefore a probability of failure (Smith 2014). The "debris flight" does depend on the equations of motions that have been developed in the existing literature (Tachikawa 1983) and on experimental simulations that took to the estimation of the probability function (Kordi et al. 2010), depending on various aerodynamic parameters such as the Tachikawa number (T_a). Through a Monte Carlo simulation, it is possible to estimate the impacts to be conducted on the building envelope of a "target building" (Figure 32).

Based on failure and trajectory analysis of the wind-borne debris, the speed reached by the object (Willis et al. 2002; Kopp 2018), and the Debris Impact Module *"to determine if any of the wind-borne debris released from a building during a particular time step has impacted either itself or another building downstream"* (Grayson et al. 2012) can be assessed. Obtaining the failure wind speed of the case study building component, the flight features, and the velocities of the case study wind-borne debris type for the range of wind speeds is the object of the analysis. The probability that a building component detaches from the source building and hit the target building envelope to be designed can be calculated (Grayson et al. 2012). The analysis, following Zhang et al. (2014), can focus on the hazard feature and the vulnerability of the target façade, by considering a binary level of damage if the wind-borne debris hit the target building or not area. This analysis considers the probability that the case study wind-borne debris leaves the source building and reaches the target façade to be designed. The number of impacts and the wind-borne debris impact speeds over the life of the building, depending on the return period, and the level of importance of the building.

Considering the urban setting, the distribution of source and target buildings, the wind field, and the case study wind-borne debris typology, wind-borne debris impacts that can damage target building envelopes in extreme winds have been identified in various studies such as Cui & Caracoglia (2020). Hitting constructions, wind-borne objects could break the building envelope, creating consequently air infiltration, water penetration, internal pressurization, and finally the failure of roofs and exterior walls and windows (Henderson et al. 2018). Building envelope design, basing its impact performances on the kinetic energies evaluated through risk assessments that consider wind-borne debris and the impact characteristics such as the impact angle on the façade element (Moghim & Caracoglia 2012), lead to the increase of urban resilience.

The wind-borne debris impacts could be assessed throughout the analytical analysis:

- of the minimum wind speed to have the failure of the identified potential wind-borne debris (e.g., typical U.S. roof tiles) from a source building;

- of the distance that various types of wind-borne debris could reach and of the speeds reached by them;

- of the position of the source building and the target building envelope.

Therefore, with these data, the standard impact test proposal for target building envelopes could be developed, based on specific wind-borne debris features and debris' flight simulated through numerical models. The impact performance is referred to existing and new building envelopes and refers to any typologies: windows, walls, curtain walls, double-skin façades, etc. Debris impact resistance for the considered construction cases can be implemented, considering the heterogeneity of debris types (Abdelhady et al. 2022).

Through the analysis of the existing commercial testing equipment to conduct impact tests to simulate wind-borne debris on façades, and the review of variations of this widely adopted testing equipment developed to consider different projectiles (Fernandez et al. 2010), the testing proposal can be formulated. In the case study, the impact testing requirements for an essential facility are presented.

3.3   The Design Tool

This Section aims to present the design tool to identify alternative impact tests when it comes to wind-borne debris resistance of façades (Figure 33), the outcome of the critical literature review. The impact energies are evaluated by estimating the building component capacity, the failure wind speed velocity, the trajectory, and the impact velocity of the debris. The design method discards the widely adopted empirically developed impact performances for façade design, based on standardized projectiles. The ASTM standard requirements (ASTM 2019) already give façade designers the chance to go through engineering assumptions to develop ad-hoc wind-borne debris impact tests for their projects.

Façade designers could eventually manage case-specific circumstances, to realize adequate impact safety for buildings exposed to wind-borne debris in extreme winds. This approach is significant, especially for primary importance buildings in the urban environment. In such contexts, due to climate change effects, building components that traditionally didn't fail during windstorms, are currently experiencing higher strains, and this is causing them to fail. When they become wind-borne debris, they can impact target buildings that

can be adequately designed according to the proposed alternative design methodology. Based therefore on available data and literature in the field of wind-borne debris failure in extreme winds and the analytical investigation of specific building component failure mechanisms, the design tool is defined to set down laboratory testing procedures, representative of various wind-borne debris features.

The methodology to set wind-borne debris-resistance test requirements is discussed with specific examples in Chapter 4, but the proposed design tool could be implemented for any object that could fail in extreme winds. The case study analysis practically weighs impact energies to be absorbed in wind-borne debris resistant-façade design. Analyzing a specific building component in its failure mechanism, this design method opens a discussion about other building materials such as gravel that can fly and hit the surrounding façades in extreme winds.

3.3.1 Target Building Risk Category

The first step to go for, in the design procedure proposed in this thesis (Figure 33) is to identify the target building risk category. Currently, there are building codes such as the International Building Code (2021, Table 4) that support designers to identify it. Following international or local building codes, the risk category that can be identified is not just linked to the definition of the building function and the average amount of occupants in the building. It is especially important to target the design performances of the building, with a specific focus on façade breakage consequences, to understand if this is a risk the building can go for. The development of weighed impact resistance of the façade is the final scope of this design framework.

Essential facilities such as hospitals have usually a higher risk associated with design load estimation when it comes to building design. However, there are other structures such as nuclear reactors, hurricane shelters, and tornado shelters, that should have the highest resistance to extreme events than risk category IV buildings (IBC 2021). This is especially related to their façade impact resilience since the building envelope should remain intact to guarantee contaminating chemicals protection. The identification of the risk category of the target building to be designed is therefore a starting point, for further considerations that lead to the performance-based impact-resistance of the building envelope design, according to the alternative design framework.

Table 4 - Risk Category of Buildings and Other Structures (Table 1604.5, IBC 2021)

RISK CATEGORY	NATURE OF OCCUPANCY
I	Buildings and other structures that represent a low hazard to human life in the event of failure, including but not limited to: • Agricultural facilities. • Certain temporary facilities. • Minor storage facilities.
II	Buildings and other structures except those listed in Risk Categories I, III and IV.

III	Buildings and other structures that represent a substantial hazard to human life in the event of failure, including but not limited to:
	• Buildings and other structures whose primary occupancy is public assembly with an occupant load greater than 300.
	• Buildings and other structures containing Group E occupancies or Group I-4 occupancies or combination thereof, with an occupant load greater than 250.
	• Buildings and other structures containing educational occupancies for students above the 12th grade with an occupant load greater than 500.
	• Group I-2, Condition 1 occupancies with 50 or more care recipients.
	• Group I-2, Condition 2 occupancies not having emergency surgery or emergency treatment facilities.
	• Group I-3 occupancies.
	• Any other occupancy with an occupant load greater than 5,000. (a)
	• Power-generating stations, water treatment facilities for potable water, wastewater treatment facilities and other public utility facilities not included in Risk Category IV.
	• Buildings and other structures not included in Risk Category IV containing quantities of toxic or explosive materials that:
	   • Exceed maximum allowable quantities per control area as given in Table 307.1(1) or 307.1(2) or per outdoor control area in accordance with the *International Fire Code*; and
	    • Are sufficient to pose a threat to the public if released. (b)

IV	Buildings and other structures designated as essential facilities, including but not limited to:
	• Group I-2 occupancies having surgery or emergency treatment facilities.
	• Fire, rescue, ambulance and police stations and emergency vehicle garages.
	• Designated earthquake, hurricane or other emergency shelters.
	• Designated emergency preparedness, communications and operations centers and other facilities required for emergency response.
	• Power-generating stations and other public utility facilities required as emergency backup facilities for *Risk Category IV* structures.
	• Buildings and other structures containing quantities of highly toxic materials that:
	   • Exceed maximum allowable quantities per control area as given in Table 307.1(2) or per outdoor control area in accordance with the *International Fire Code*; and
	    • Are sufficient to pose a threat to the public if released. (b)
	• Aviation control towers, air traffic control centers and emergency aircraft hangars.
	• Buildings and other structures having critical national defense functions.
	• Water storage facilities and pump structures required to maintain water pressure for fire suppression.

(a) For purposes of occupant load calculation, occupancies required by Table 1004.1.2 to use gross floor area calculations shall be permitted to use net floor areas to determine the total occupant load. (b) Where approved by the building official, the classification of buildings and other structures as Risk Category III or IV based on their quantities of toxic, highly toxic or explosive materials is permitted to be reduced to Risk Category II, provided it can be demonstrated by a hazard assessment in accordance with Section 1.5.3 of ASCE 7 that a release of the toxic, highly toxic or explosive materials is not sufficient to pose a threat to the public.

3.3.2 Building Location Analysis

Related to various risk categories of buildings (0), designers can find associated wind load requirements based on the target building location (Figure 34). Currently, just in very few contexts, wind-borne debris requirements are already set in place, to guide designers in the verification of impact test performances related to wind-borne debris in extreme wind events (ASCE 7-22 2022; AS/NZS 1170.2 2021; NSCP 2015). The requirements are, therefore, addressed to hurricane and tornadic regions and in some cases, there are local regulations that are more stringent than the ones set in place at a national level.
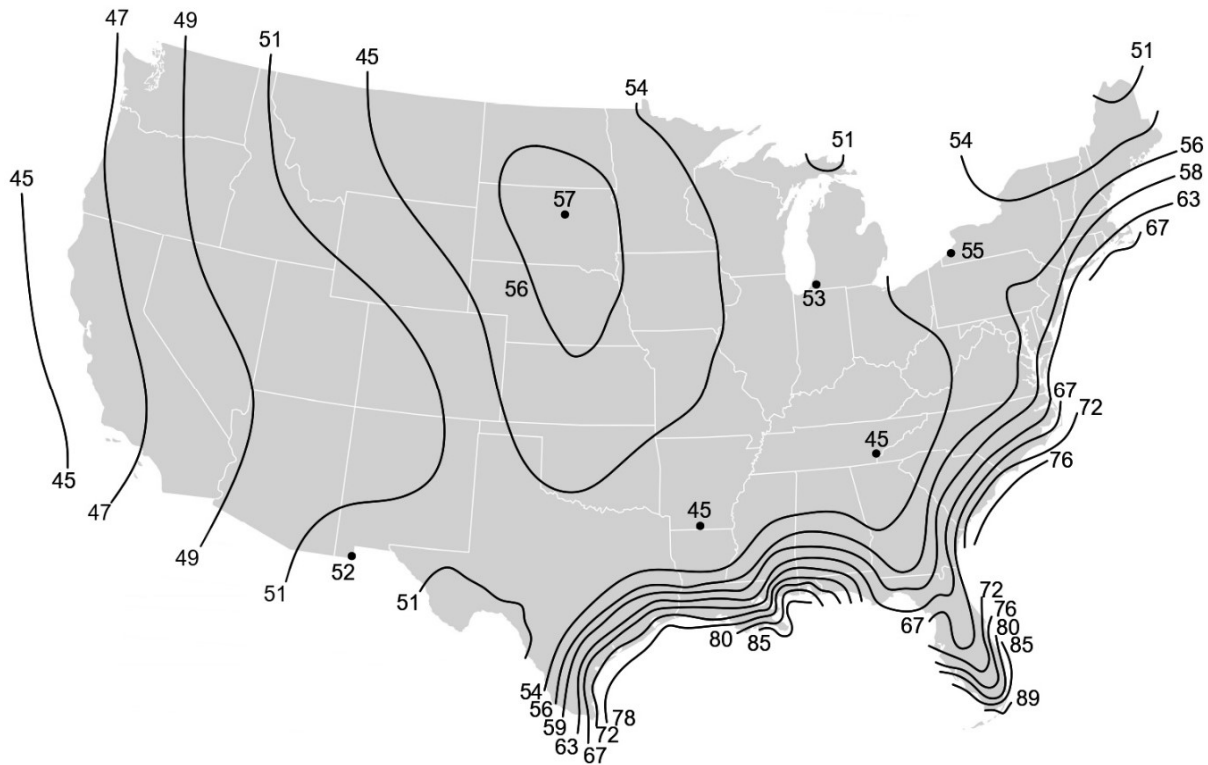
Figure 34 - Basic design wind speeds for Risk Category IV (Table 4) buildings (based on Figure 1609.3(3), IBC 2021).

3.3.3 Reference Wind Speed for Target Building Design

Considering the risk category (Section 3.3.1) and the location (Section 3.3.2) of the target building, the designer can calculate the minimum requirements in terms of design wind speeds to be considered for the design wind loads of the building. The design framework that is presented in this thesis aims, however, to

provide to façade designers a tool to go beyond the code requirements. Considering this assumption, the reference wind speed to estimate wind-borne debris impact performances of façades should also consider the upward trend of extreme winds events that have been recorded. This analysis should be conducted also in other than the already formally classified hurricane and tornadic regions. If we refer to the European contest, for example, we don't find any test requirements, but in the area has been recorded extreme wind gusts. These types of assumptions can be linked to the precise and case-specific necessity of the project.

This stage of the design process implies that the façade designer should conduct a preliminary assessment in the target building location area, to study the wind low behavior, related to the effective terrain roughness. The analysis of the surrounding environment, therefore, considers the terrain features, following code requirements.

Therefore, in general, the outcome of the analysis for target building design should consider:

- Wind-borne debris impact requirements for façades if already set in place (building code requirement);
- Building design wind speeds, for the design return periods (building code requirement);
- Extreme wind events' recorded wind speeds (alternative impact design analysis);
- Information about the upward trends in local extreme events (alternative impact design analysis).

Conducting this analysis, the façade design wind speed can eventually consider wind velocities that are extremely ahead of the building code minimum requirements. This phase should be conducted to address the design to specific technological, environmental, and further constraints, depending on design goals. GIS technology, using databases about past extreme wind events, can be a useful help in looking at the highest wind record and its occurrence in the target building location.

3.3.4   Analysis of the Surrounding Environment

The surrounding environment analysis is a core part in the alternative design framework for wind-borne debris façade design (Figure 33). As already mentioned, the aim of the design framework presented goes beyond code requirements. Therefore, through in-person assessments and/or with the use of web mapping platforms where high-resolution satellite images and aerial photography is provided (checking on the update), deeper investigation into the target building location's surroundings should be conducted. The report should be developed following the designer's expertise, and the lesson learned from previous extreme wind events' post-damage assessments. The main elements that are going to be articulated in the report are:

- The list of surrounding buildings and distance from the target façade to be designed;

- Information about the building technologies adopted in the surrounding constructions;

- The list of surrounding urban objects and distance from the target façade to be designed;

- Information about urban objects' characteristics;

- Collection of images, aerial photos, and videos.

Considering surrounding buildings implies a mapping of the building technologies adopted, especially considering elements that are attached to the main structure. A conjunct engineering and building technology preliminary assessment in the surrounding environment should be, therefore, conducted. This evaluation can take the designer to consider also temporary structures such as events and market stalls, depending on the risk category of the building to be designed (Section 3.3.1). The façade designer can include all the information considered important to proceed to the identification of potential wind-borne debris (Section 3.3.5).

3.3.5   Identification of Potential Wind-Borne Debris

The design wind speed identification for the wind-borne debris impact assessment of the target building envelope is conducted (Section 3.3.3). Façade designers, according to the surrounding environment analysis (Section 3.3.4), can highlight what are the objects that can fly due to the design winds and, becoming wind-borne debris, hit the target façade. The assessment is based on professional experience, and existing damage indicators (DI). These are 28 in the United States (Table 6; WSEC 2006), 31 in Canada, and 30 in Japan (Gavanski & Kopp 2017). For each DI there are various associated degrees of damage (DOD), for windstorms of various intensities that can be classified following the Enhanced Fujita Scale (Table 5; Mehta 2013). In the design environment, an assessment should be conducted, to highlight the building components or and these are the buildings identified to potentially produce wind-borne debris when their building components would eventually fail due to specific failure wind loads.

This step considers various source buildings, and the objects present in the urban environment (such as trash bins, signs, etc.) to verify in the next steps if, for the design wind speed (Section 3.3.3), failure of these elements can occur. This step is fundamental to identify how many wind engineering studies (Section 3.3.6) should be conducted to estimate the behavior of wind loads on various objects identified as potentially wind-borne.

Table 5 - Enhanced Fujita Scale (WSEC 2004)

EF-scale	Class	Wind speed (km/h)	Description
EF-0	weak	105-137	Gale
EF-1	weak	138-177	Moderate
EF-2	strong	178-217	Significant
EF-3	strong	218-266	Severe
EF-4	violent	267-322	Devastating
EF-5	violent	> 322	Incredible

Table 6 - Enhanced Fujita Scale Damage Indicators (WSEC 2004)

Number	Damage Indicator	Abbreviation
1	Small barns, farm outbuildings	SBO
2	One- or two-family residences	FR12
3	Single-wide mobile home (MHSW)	MHSW
4	Double-wide mobile home	MHDW
5	Apt, condo, townhouse (3 stories or less)	ACT
6	Motel	M
7	Masonry apt. or motel	MAM
8	Small retail bldg. (fast food)	SRB
9	Small professional (doctor office, branch bank)	SPB
10	Strip mall	SM
11	Large shopping mall	LSM
12	Large, isolated ("big box") retail bldg.	LIRB
13	Automobile showroom	ASR
14	Automotive service building	ASB
15	School - 1-story elementary (interior or exterior halls)	ES
16	School - jr. or sr. high school	JHSH
17	Low-rise (1-4 story) bldg.	LRB
18	Mid-rise (5-20 story) bldg.	MRB
19	High-rise (over 20 stories)	HRB
20	Institutional bldg. (hospital, govt. or university)	IB
21	Metal building system	MBS
22	Service station canopy	SSC
23	Warehouse (tilt-up walls or heavy timber)	WHB
24	Transmission line tower	TLT
25	Free-standing tower	FST
26	Free standing pole (light, flag, luminary)	FSP
27	Tree - hardwood	TH
28	Tree - softwood	TS

3.3.6   Wind-Borne Debris Characteristics

Through the previous step (Section 3.3.5), the various wind-borne debris typologies to be verified are identified, for the design purposes object of the alternative design framework (Figure 33). These objects should be analyzed in their characteristics: geometric features, weight, constituent material density, restraint systems, and position on the source building/in the urban environment.

The identified object should be investigated in its uplift resistance. According to technical specifications, for building components such as roofing systems, there are typical failure capacities, depending on the features of the element and the fixing system. It is therefore significant the identification, when it is possible through on-site investigations, of the fixing mechanism of the objects that should be verified. When it is not possible, a range of uplift capacities can be used, considering a probabilistic distribution.

According to Wills et al. (2002), various wind-borne debris typologies should be classified into three classes (compact, plate-like, and rod-like). The identification of the debris characteristic is a fundamental step to discuss its technological failure and its aerodynamic behavior in the wind field. It can happen that the object identified is loose and free to fly and, in this case, its weight and position are the only parameters to consider to understand the uplift resistance.

3.3.7   Debris Failure Analysis: Wind Speeds at the Initiation of Flight

Through the information collected in the design steps in Sections 3.3.6 and 3.3.3, Newton's 2nd law (Equation 2.3), and the aerodynamic force definition (Equation 2.4) that follows from ASCE 7-22 (2022), the failure analysis of the object can be conducted. Failure occurs when the condition defined in Equation 2.5 is verified and, accordingly, the failure 3-s gust wind speed is defined in Equation 2.6. If instead of a precise failure capacity of the debris we have a range of values, through Monte Carlo simulation, it is possible to find a range of failure wind speeds.

It is more likely to obtain through the previous analysis (Section 3.3.6) a range of values since the objects in the surrounding environment are not objectives of the design. Therefore, the façade designer does not have enough information about the technologies adopted. And, even if the information and technical specification of uplift capacity of various objects has been achieved, there is uncertainty in the correct

installation, following the technical specification. The necessity for a probabilistic approach arises from these variabilities.

If for building design purposes, the design wind speed is not the 3-s gust wind speed, the failure wind velocity can be converted to 10-minute mean wind speed using conversion coefficients (Appendix B).

Through the debris failure assessment described in this design step, the façade designer can verify if the wind speed to have debris failure is larger than the reference wind speed for the target building design (Section 3.3.3), which can be different from the code basic wind speed (V_b). If the failure of the object does not verify, the façade designer should not proceed with the following design steps because there is no risk for the object to be wind-borne. Whereas, if the failure occurs for wind speeds smaller than the reference wind speed for the target building design (Section 3.3.3), the flight analysis should follow (Section 3.3.8).

3.3.8   Debris Flight Analysis: Wind-Borne Debris Velocity and Trajectory

The definition of the wind speed for the target building design (Section 3.3.3) gives the range of wind speeds to analyze the debris failure (Section 3.3.7) and to evaluate its flight (Section 3.3.8). The flight analysis is based on numerical calculation. Therefore, using a 4th-order Runge-Kutta scheme, dimensional (Equation 2.7, 2.8, 2.9) and non-dimensional (Equation 2.10, 2.11, 2.12) equations of motion can be solved. Based on Wills et al. (2002), the debris element has been classified in (Section 3.3.6). The rotational aerodynamic coefficients for lift, drag, and momentum, to calculate the debris trajectory are defined in Equations 2.13, 2.14, 2.15, based on the spin parameter (Equation 2.17). The static aerodynamic coefficients for lift, drag, and momentum, are based on the definition of the normal coefficient (Equation 2.18), and defined in Equations 2.19, 2.20, 2.21. Further details about the numerical calculations can be found in Appendix A - Wind-Borne Debris Trajectory Calculation.

The debris flight analysis is a probabilistic distribution of results. Various initial conditions for the velocity and trajectory analyses of the object should be defined:
-    Range of wind speeds to assess the flight;
-    Height of the debris element above the ground level (Figure 7);
-    Probability density function for flight wind speed, depending on the T_a of the debris element.

This analysis should be conducted using Monte Carlo simulation, to find out a range of trajectories and terminal velocities. The debris' terminal velocity is the velocity at the impact with the ground level.

Based on step (Section 3.3.4), the location between the debris element and the target façade has been recorded. Crossing data related to trajectory analysis and source and target building location, a probability distribution is given. Through this design step, it is also possible to estimate the maximum height to have debris impact on the target façade, besides the impact velocity.

3.3.9   Synthesis of Result to Set Wind-Borne Debris Impact Test Requirements

Through the debris flight analysis (Section   3.3.8), the presented alternative design framework to determine the performance-based impact performance of façades (Figure 33) and engineering assumptions are a core part of the design performance estimation. In the proposed design approach, the impact resistance of façades is based on local considerations. Projectile impact velocity and characteristics (material properties, geometry, etc.) are, therefore, representative of the case-specific target building location, including the distance from source buildings in the surrounding environment. The surrounding buildings are, in this method, seen as the debris source when building components fail due to specific wind loads.

The proposed building envelope impact performance is, therefore, based on:

- target building location;

- location of target and source buildings;

- wind-borne debris characteristics;

- debris element failure capacities and failure wind speeds;

- design wind speed;

- debris flight trajectories;

- height and face of the target building envelope;

- probabilistic assessment of debris impact on façade.

The information about impact features is achieved through a wind engineering analysis of the wind-borne debris that has been identified as a vulnerable element in specific wind loads. The achievement of these data about specific debris trajectories and speeds leads designers to weigh façade performances, encouraging site-specific solutions. A Monte Carlo simulation (Section 3.3.10) is used to determine impact speeds and locations (heights) for the probabilistic design of the façade. Through this information, it is possible to define the necessary equipment (Section 3.3.11) to be arranged for the verification of the building envelope's effectiveness in its flying debris protection.

71

Building code requirements (ASCE 2016; AS 1170.2 2016) are currently required to test the façade based on the target building location and height of the target building envelope, with reference to the ground (Figure 7). The alternative impact performances can, accordingly, identify:

- design impact velocity for the debris element;

- maximum height to consider façade impacts.

3.3.10 Calculation of Fragility Curves for Target Façade Impact Performance

A Monte Carlo simulation can be used to estimate the probability of impact of a debris element on a target façade, as a function of the design reference wind speed. The steps of this analysis, in a general formulation that can be applied to multiple cases, follow:

1. Identification of reference wind speed for target building design (Section 3.3.3);

2. Identification of distance between the source of debris and the target building (Sections 3.3.4 and 3.3.5);

3. Identification of debris element geometric and weight characteristics (Section 3.3.6);

4. Classification of the debris element according to Wills et al. (2002) and identification of rotational and static aerodynamic coefficients for lift, drag, and momentum (Section 3.3.8);

5. Identification of GCp distribution on the assessed debris element;

6. Sample debris element failure capacity probabilistic distribution (Section 3.3.7);

7. Calculation of failure wind velocities based on Steps 3 and 6 and Equation 2.6;

8. If debris failure wind velocity (Step 5) is smaller than reference wind speed (Step 1) failure occurs, and debris trajectory is calculated by solving Equations 2.7, 2.8, 2.9 through a 4th-order Runge-Kutta scheme;

9. Step 7 is repeated with the trajectory calculation for the equivalent 10-min mean wind speed instead of the previously used 3-s gust failure wind speed (Step 6), using Equation B.1 (Annex B);

10. Calculate impact characteristics (speed, angle, height) distribution on target façade and probability of impact;

11. Repeat steps 5 to 10 for N_{total} times and count the number of times façade impact occurs ($N_{impacts}$). The probability of façade impact (P_{impact}) for the selected case is equal to N_{impact} / N_{total}. For debris impact

on target façade, the largest N_{impact} / N_{total} among all the debris elements restraint systems for selected wind speed for target building design is the estimator of P_{impact}.

12. Repeat Steps 5 – 11 for all selected GCp and debris failure capacities.

3.3.11 Impact Test Equipment and Test Definition

The goal of the design framework is to adapt the existing and widely adopted testing equipment to conduct impact tests to simulate wind-borne debris (Figure 17, Figure 18). This strategy aims to guide an easier introduction of the design framework proposed in the thesis façades (Figure 33) to improve building envelope resilience in case-specific environments. The projectile used to evaluate façade resistance is accordingly the object that has been assessed in previous design steps. The testing equipment modification has already been explored (Figure 20, Figure 19), to shut projectiles different from the ones adopted in the ASTM (2019, 2020) standard testing procedures. Therefore, the test equipment can be defined according to the projectile's characteristics, with the construction of launching decks or other devices.

The test aims to follow the best practices for wind-borne debris impact testing (ASTM 2019, 2020; AS/NZS 1170.2) when it comes to impact location on the façade (Figure 10, Figure 12). The impact areas defined (ASTM 2019, 2020) are both considering the elasticity and the stiffness of the infill panels, and, therefore, they are considered adequate to conduct the alternative impact tests. According to the alternative design framework, the impact tests can turn out to be very demanding, depending on engineering assumptions, and on how beyond the code the wind speed for the target building design (3.3.3) has been pushed. The kinetic energy to be absorbed by the façade, depending on the projectile characteristics and its impact speed, tests its resilience to case-specific wind-borne debris impacts.

Chapter 4. Wind-Borne Roof Tiles Impact-Resistance of Façades

4.1   Premise

Post-disaster event assessments have shown that in the same wind event, in neighborhoods where the roofing is predominantly roof tiles, the damage to the building envelope is more severe if compared to the neighborhoods where asphalt shingles have been adopted (Gurley et al. 2010). It has been frequently observed that these building components fly during windstorms (Kordi 2009) or that, when the storm is over, they are no longer in their original position (Figure 6). Roof tiles are vulnerable building components that can detach from roofs and hit surrounding structures causing building envelope breakage, especially when it comes to glazed components such as windows and curtain walls (Mejorin et al. 2020).

In the literature, Fernandez et al. (2010) conducted impact tests using roof tiles as projectiles, with the same mass and impact speed of missile type D (Table 1) but impacting flat (the tile and target are in parallel planes upon impact, with the long edge of the tile vertical) or on their edge (the plane of the tile is perpendicular to the plane of the target, the normal to the tile plane is vertical, and the short edge of the tile impacts the target) the target specimen. Fernandez et al. (2010) highlighted that the impact energy input alone cannot be representative of failure caused by different objects with same weight and impact speed, but different material and geometric characteristics.   The results of these tests (Fernandez et al. 2010) showed significant differences in the plastic and total deflection of tested metal panels, when these were subject to either lumber or roof tile impacts.

In this Chapter, alternative impact tests are proposed, which consider roof tile failure capacities, the aerodynamics and location of the source building, and the flight trajectory. These alternative tests consider, therefore, alternative impact velocities and projectiles using the approach described in Section 3.2. Here we consider a detailed numerical example utilizing a low-profile roof tile. The uplift capacity is considered, following Smith (2014) findings. This yields values of the 3-s gust failure wind velocities which are used to model the flight trajectories considering the effect of source building aerodynamics. Though Monte Carlo simulation, the fragility analysis to obtain the impact performances of façades is presented. Finally, the implication of the results is discussed.

4.2 Design Building for Case Study

The example reported in this Chapter considers the façade resistance for an essential facility, with risk category IV (Table 4), in which "enhanced protection" is required (IBC 2021; ASCE 2016; ASTM E 1996; ISO 16932). The design focus is on the target façade of a hospital located in Exposure category C, according to ASCE 7-22 (2022). The design example is located in an area with a basic wind speed of 80 m/s.

The return period of ASCE 7-22 (2022) for the wind map of the essential facilities is 3,000 years (ASCE 2022). Furthermore, currently, the code does not give any load factor to be used as a multiplier for building structural design, and, therefore, for a conservative approach, the load factor has been included in the wind maps. The load factor (LF) basic wind speed maps of this example, for wind map definition, is equal to 1.6. Therefore, the reference wind speed for the target building design is assumed to be equal to the V_b divided by $\sqrt{1.6}$, to obtain the design basic wind (without the load factor). Accordingly, to calculate the reference wind speed for the target building façade design:

$$V_{b\_ref} = V_b / \sqrt{LF} \qquad\qquad\qquad (4.1)$$

$V_{b\_ref,}$ for the example shown in this Section, is equal to 63 m/s.

In the hospital design location, there are wind-borne debris impact requirements for façades (hurricane regions, ASCE 7-22 2022). The building is in Wind Zone 3, where the basic wind speed (V_b) is larger than 67 m/s, and the building location is within 1.6 km from the coastline. For essential facilities in this area, the wind-borne debris impact performances to be guaranteed by the hospital's façade are (Table 1, Table 2, Figure 7):

- missile level D above 9.1 m on the ground level;
- missile level E up to 9.1 m on the ground level.

In the hospital location, extreme wind record events did reach 3-s wind gusts of 63 m/s. The recorded wind gusts are considered in line with future trends, and, accordingly, the maximum reference wind speed, for alternative wind-borne debris impact tests requirement definition is assumed to be 63 m/s. This 3-s gust wind speed is beyond the code specifications, to provide façade resilience also in future scenarios that account for climate change increasing in intensity of windstorm events.

4.3 Analysis of Surroundings of the Design Building

Following the methodology described in Figure 33 and Section 3.3.4, an assessment of the local environment in the surroundings of the design building is conducted, for façade wind-borne debris impact design purposes. This analysis reports information regarding the construction in the surroundings, locations of these, and the design building. Depending on the design goals, also urban objects can be identified as vulnerable elements in windstorm events, related to target façade distance and position. Accordingly, photos and schematic drawings are collected to proceed with the analysis.

To illustrate the process, one building has been identified in the surroundings, 2-storey building with concrete tiles on a hip roof. The distance between this building and the design building façade is 75 m, as shown in the plan (Figure 36) and elevation (Figure 35) views. The low-rise building is labeled as the "source building" for wind-borne debris generation.

The roof tiles on the building are typical, but from the on-site and aerial photo assessments, it is not possible to identify the adopted restraint techniques. The plan dimension of the source building is 9 x 10 m, with a mean roof height[24] of 10 m and a slope of 9/12 (36°).
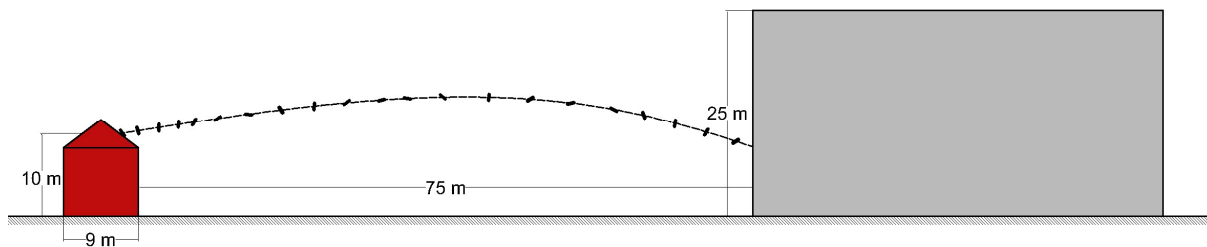
Figure 35 - Elevation of the "source building" (red), and "target façade" (grey) that is to be designed. Mean roof height is 10 m and one roof tile trajectory is reported with the dashed line.

---

[24] The mean roof height is the average elevation above grade height measured between the eave and ridge of a roof area where; the ridge is the uppermost horizontal external angle formed by the intersection of two sloping planes of the roof (FRSA–TRI 2020).

4.4   Wind-Borne Debris Identification

Section 3.3.5 discussed, in general, how to proceed to the identification of vulnerable building components and urban objects that can be wind-borne in windstorms, turning into projectiles. This assessment is linked to the analysis of surroundings (Section 4.3), focusing on single elements, to evaluate their relevance for building design purposes.

The source building identified above has low-profile concrete roof tiles. Table 7 provides the geometric characteristics of these roof tiles, with a photograph provided in Figure 37. These building components lay on the roof to provide water tightness and natural ventilation, and they have restraint systems to avoid failure due to wind load, according to local requirements for Wind Zone 3 (ASCE 7-22 2022). Different restraint system combinations are analyzed in this case study section, because of the uncertainty after the investigation campaign (Section 4.3). These tiles can be classified as plate-like debris (Wills et al. 2002) in terms of aerodynamic behavior and debris flight trajectory calculations.
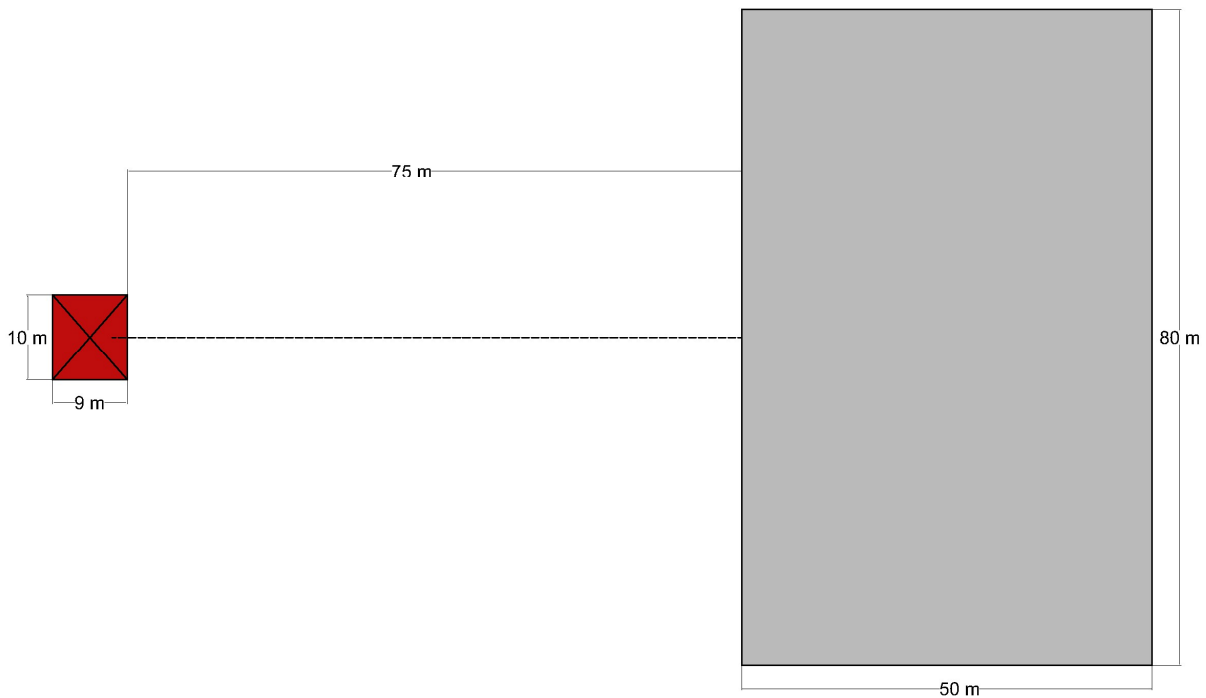
Figure 36 - Plan of the "source building" (red), and "target façade" (grey) that is to be designed. Mean roof height is 10 m and one roof tile trajectory is reported with the dashed line.

Table 7 - Typical U.S. concrete low-profile roof tile characteristics

Tile dimensions	41.9 x 34.3 cm
Tile thickness	3.0 cm
Tile weight	4.86 kg
n° tiles / m^2	7
ρ_m	1,120 kg/m^3

Figure 37 - Concrete low-profile roof tiles.

4.5 Failure Analysis of Low-Profile Roof Tiles

The failure analysis is the first step in the analytical calculations. The engineering assumptions to consider can vary, based on the local design requirements and construction practices. In this example, which considers low-profile concrete roof tiles, the work of Smith (2014) is utilized. In Figure 39, the failure probability of low-profile concrete roof tiles for ASCE 7-22 (2022) basic wind speeds, developed by Smith (2014), is illustrated. These curves consider direct to deck and battened attachment methods (Figure 38). The probability of failure of roof tiles has been, accordingly, developed to assess, based on the design Wind Zone (ASCE 2022), if the building component can be considered vulnerable, depending on the basic wind speed (V_b).
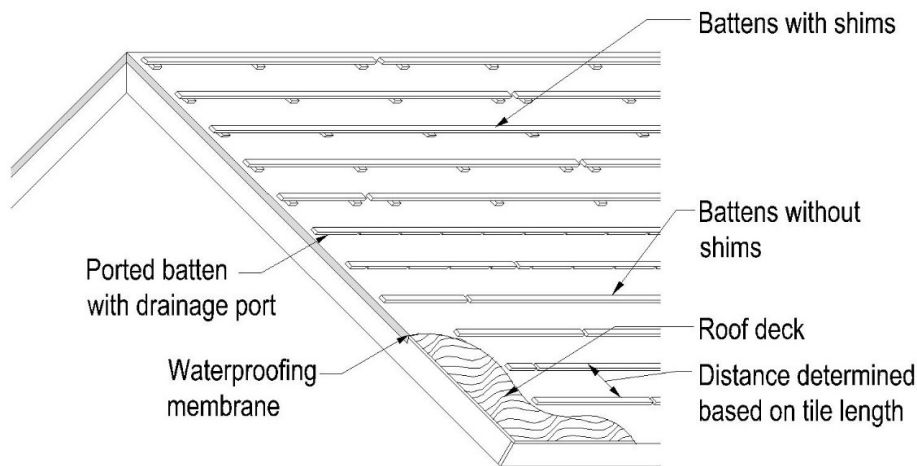
Figure 38 - Batten layout options for roof tile installation.

4.5.1 Uplift Capacity of Low-Profile Roof Tiles

In Section 2.6, the testing methods to calculate the uplift capacities of roof tiles have been presented. Smith (2014) investigated the aerodynamic behavior and the uplift capacity for concrete roof tiles in the U.S.. In the testing methods that are in place, the uplift capacity is calculated at a precise point on the roof tile and this position is chosen for the current analysis from Smith's (2014) results, to be consistent with code requirements and commercial products technical specifications. The uplift capacity of low-profile roof tiles (according to ASTM 2008) is therefore presented for the tests conducted at 0.76 L_t.

The uplift capacity depends on the attachment solution (Table 8). Since, from on-site investigation and aerial photograph analysis, it is not possible to know the technological solutions adopted to restrain the roof tiles on the source building, the uplift capacities of various restraint systems should be considered in the

analysis. Moreover, the loose-laid solution of the roof tile should also be accounted for because another parameter that cannot be known is the correctness of the roof tile installation itself. Accordingly, the loose-laid roof tile should be considered in case the attachment has not been applied properly on the roof of the source building.

Following Smith (2014), the mean uplift capacities of low-profile roof tiles for various attachment solutions (Table 8) are considered, assuming a normal distribution with a standard deviation of 20%, and uplift force application according to ASTM (2008). The same normal distribution and standard variation are considered for a the loose-laid roof tiles that have FS=1, $F_{HoldDown}$ = 0, and F_H = F_m. For low-profile roof tiles on a roof slope of 9/12 (36°), the uplift capacity for the loose-laid configuration follows the definition of F_m and is equal to 38 N.

Smith (2014) characterized the pressure field acting on the roof tiles and the roof tile attachment capacities. He analyzed how the uplift capacities of roofing systems depend on attachment type and roof tile profile, presenting a probability of failure which is based on 3-s gust basic wind speed according to ASCE-7 22 (2022). Figure 39 represents the probability of failure for low-profile concrete roof tiles, for the direct to deck and battened attachment methods. An initial number of 1,000 simulations have been run for each roof tile attachment configuration and, therefore, for each uplift capacity calculation (Table 8) in the Monte Carlo simulation. The sampled distributions in the simulation are provided in Figure 40 - Figure 43.
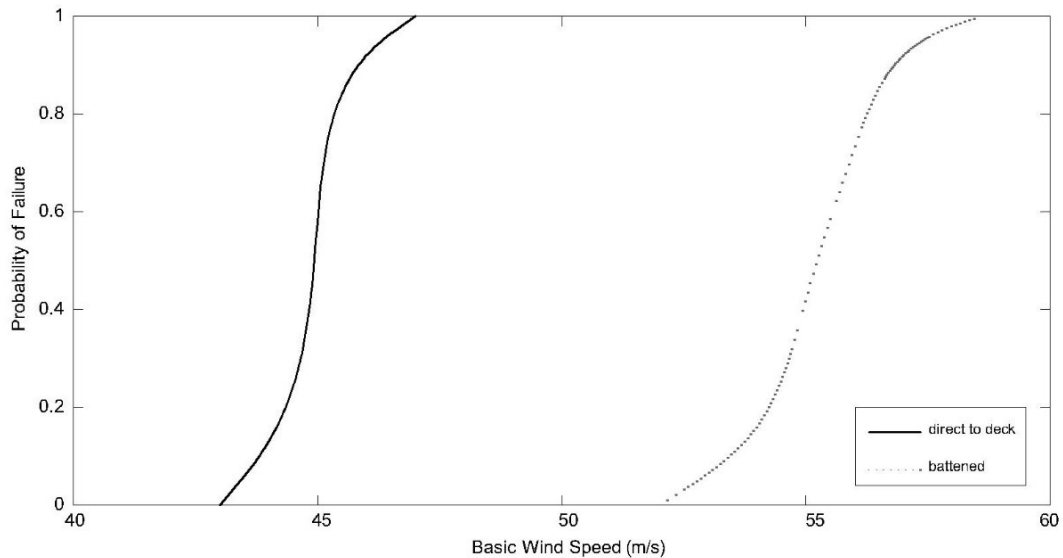
Figure 39 - Probability of failure curves for low-profile concrete roof tiles based on empirical data for wind-induced loads and attachment resistances of direct to deck and battened attachment methods (Smith 2014).

Table 8 - Uplift capacities of low-profile concrete roof tiles for different attachment configurations for each configuration to conduct the Monte Carlo simulation

Attachment Configuration	Mean Uplift Capacity (N) of Low-Profile Roof Tiles	Distribution	Variance
loose-laid	38	Gaussian	Figure 40
battened	92	Gaussian	Figure 41
direct to deck	184	Gaussian	Figure 42
foam adhesive	880	Gaussian	Figure 43
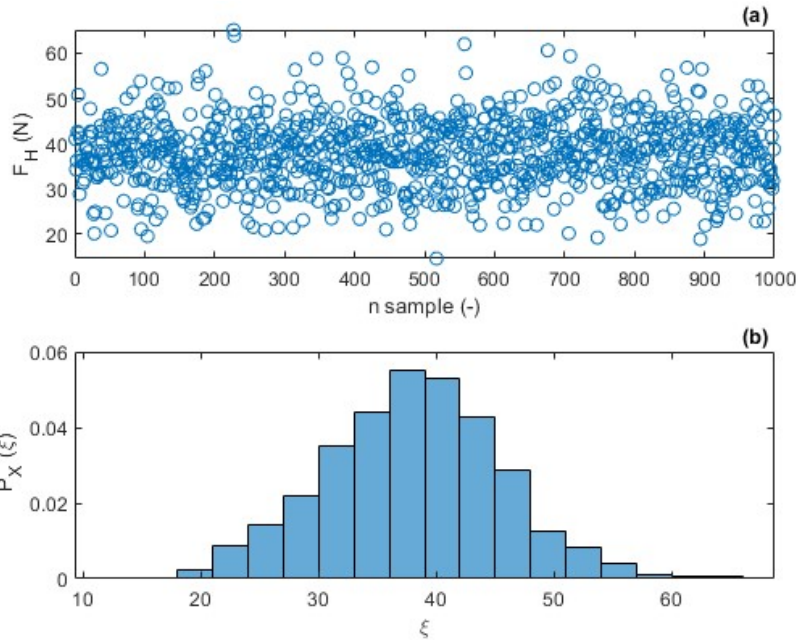
Figure 40 - (a) Sampled values of uplift capacity and (b) probability density function for loose-laid low-profile roof tiles.
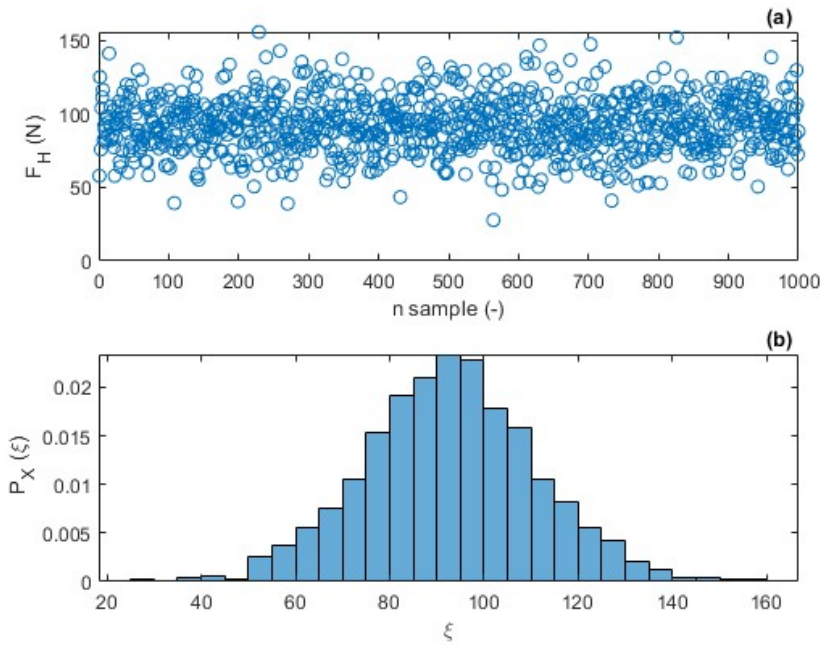
Figure 41 - (a) Sampled values of uplift capacity and (b) probability density function for battened low-profile roof tiles.
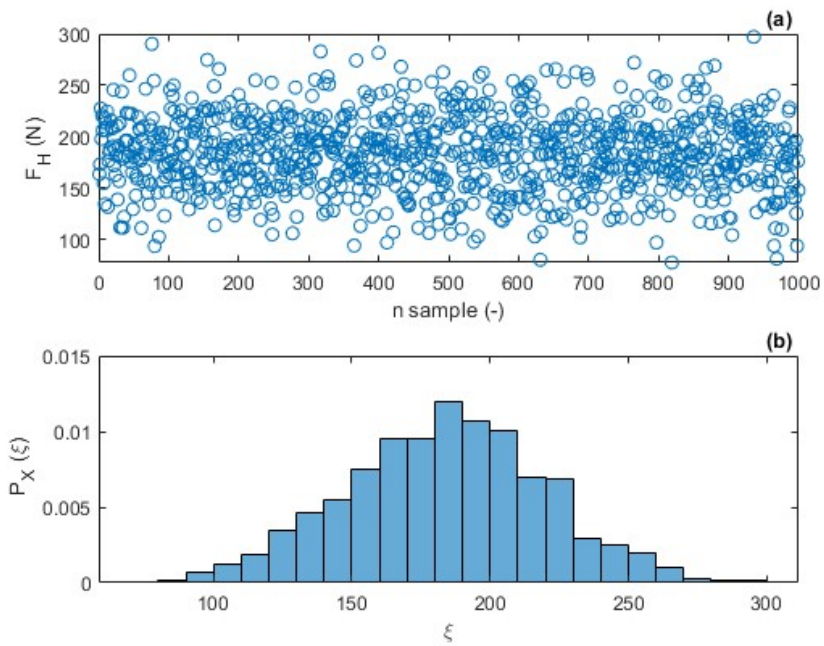
Figure 42 - (a) Sampled values of uplift capacity and (b) probability density function for direct to deck low-profile roof tiles.
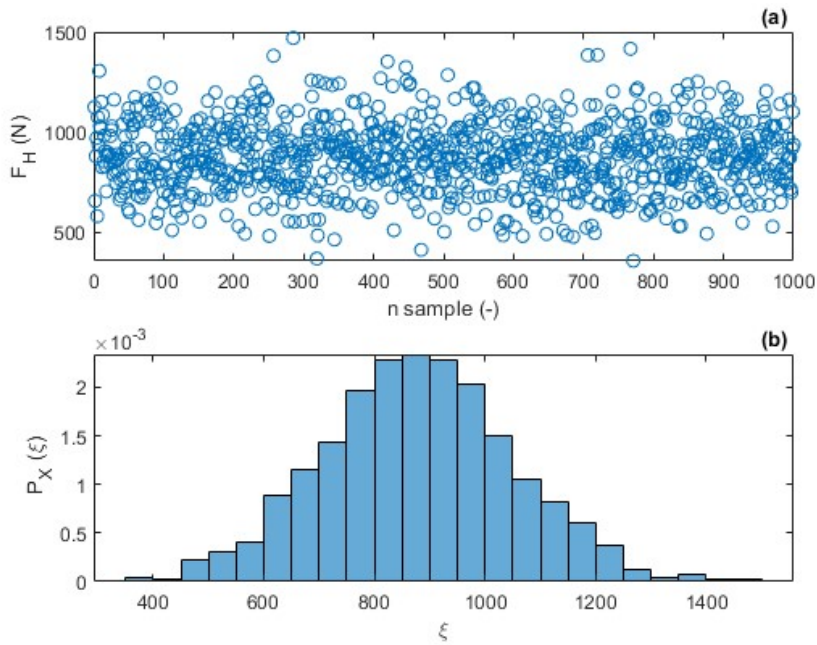
Figure 43 - (a) Sampled values of uplift capacity and (b) probability density function for foam adhesive low-profile roof tiles.

4.5.2   Wind Speeds for Roof Tiles' Flight Initialization

Roof tile failure occurs when the uplift capacity (Section 4.5.1) is exceeded by the aerodynamic force (F_a) acting on the element. With reference to IBC (Equation 16-18 in IBC 2021), the wind loads on rigid tile roof coverings are determined in accordance with Equation 4.1 which incorporates Bernoulli's equation, to predict near-roof surface flow velocity from external pressure values presented in ASCE 7-22 (2022; Smith 2014).

$$M_a = q_h\, C_{L\_IBC}\, b\, L_t\, L_{at}\, [1.0 - GCp] \qquad\qquad (4.2)$$

IBC (2021) expresses, therefore, the aerodynamic uplift moment acting to raise the tail of the roof tile as a function of L_{at}, the moment arm from the axis of rotation to the point of uplift on the roof tile: $M_a = F_H\, L_{at}$. The point of uplift estimation is taken at $0.76\, L_t$ from the head of the tile and the middle of the exposed width.

This is the same point considered in the previous step (4.5.1), to evaluate the uplift capacity of the low-profile roof tile (F_H), for various fixing technologies.

Based on the geometric features of the source building, in which the hip roof has a slope of 9/12 (36°), the speed-up factor (S_{up} = [1.0 - GCp]) must be calculated, based on the roof pressure coefficients (GCp) for each applicable roof zone, determined from Chapter 30 of ASCE 7-22 (2022). The pressure coefficients that should be evaluated are negative, that is representing the suction on the building roof that can cause roof tile uplift.

For hip roofs with H ≤ 18.3 m, and roof slopes 27° < θ < 45°, the GCp values can be determined, for each roof zone, by the interpolation of the coefficient values from Figures 30.3-2F and 30.3-2G (ASCE 7-22 2022). The two figures (ASCE 2022) are respectively presenting the GCp values for low-rise hip roofs with slopes 20° < θ ≤ 27° and θ = 45°. When the roof slope 27° < θ < 45°, the interpolation formula follows Equation 4.3, for the three roof zones represented in Figure 44.

In Table 9 the code (ASCE 2022) GCp values, for various roof slopes and roof zones are reported, together with the result of the interpolation for the roof slope example of 36°. Accordingly, S_{up} values can be estimated, for each roof zone, and for the example of this Section, these are reported in Table 9.

$$GCp(\theta) = \frac{[\ GCp(2G) - GCp(2F)]*(\ \theta - 27°)}{(45° - 27°)} + GCp(2F)$$

(4.3)

Table 9 - GCp pressure coefficients for hip roofs with effective wind area < 0.9 m^2, for different roof zones (1, 2, 3) and roof slopes (20° < θ ≤ 27°, θ = 45°, θ = 36°). S_{up} values for low-rise hip roofs (H ≤ 18.3 m) for roof zones 1, 2, 3 when roof slope θ = 36°

			GCp		S_{up}
		20° < θ ≤ 27°	θ = 45°	θ = 36°	θ = 36°
Roof Zone	1	-1.40	-1.50	-1.45	2.45
	2	-2.00	-1.80	-1.90	2.90
	3	-2.00	-2.40	-2.20	3.20
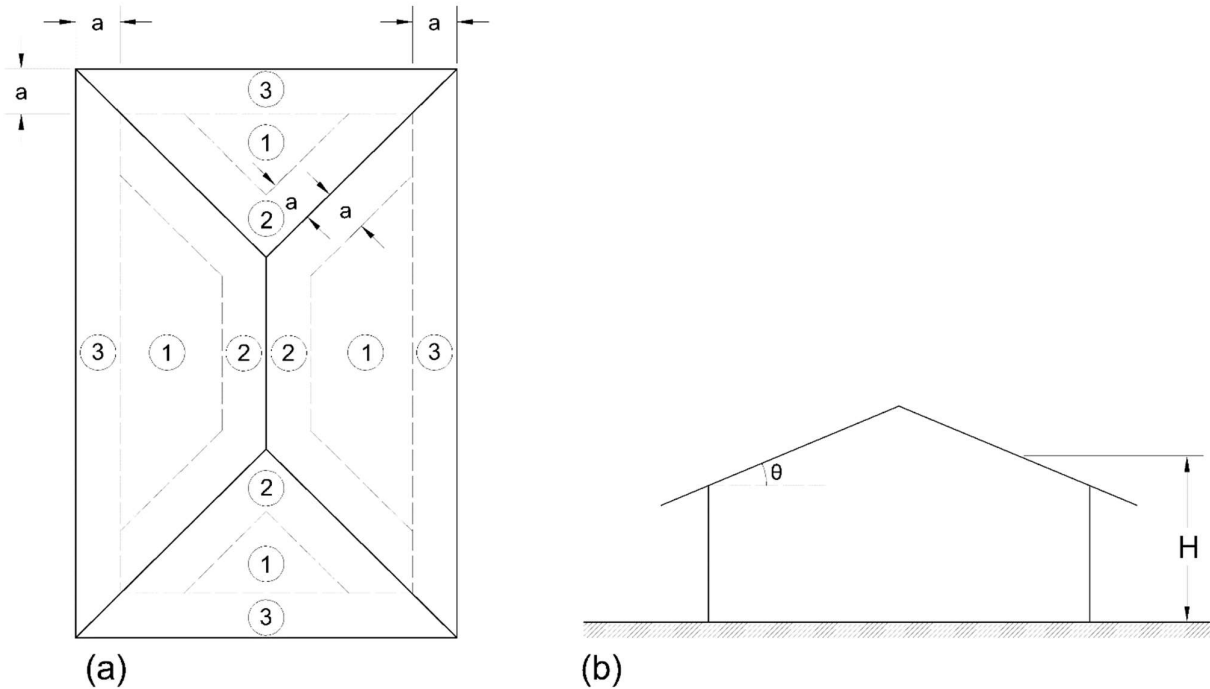
Figure 44 - Plan (a) and elevation (b) views of low-rise hip roofs (H ≤ 18.3 m) for roof zone identification according to Chapter 30 of ASCE 7-22 (2022). With reference to the plan view, a = 10% of least horizontal plan dimension or 0.4 * H, whichever is smaller, but not less than either 4% of least horizontal dimension or 0.9 m. if an overhang exists, the edge distance shall be measured from the outside edge of the overhang. The horizontal dimensions used to compute the edge distance shall not include any overhang dimensions.

For the Monte Carlo simulation, the probability of the three S_{up} reported in Table 9 to occur is assumed to be uniformly distributed. The speed-up factor accounts for the acceleration of the wind flow on the roof, which depends on roof geometric features, that can contribute to roof tile failure. According to the computation of F_H (Figure 40, Figure 41, Figure 42, Figure 43) and S_{up} (Table 9), following Code definitions (IBC 2021; ASCE 2022), through Equation 4.4 the failure basic wind speed (V_{b_ini}) of low-profile roof tiles can be estimated. In the calculations it is assumed, according to the source building location, $C_e = 0.85$, with $K_z = K_{zt} = K_e = 1$ and $K_d = 0.85$ (for components and cladding). To solve Equation 4.4, C_{L_IBC} is assumed 0.2, following Code definitions (IBC 2021).

$$V_{b\_ini} = \sqrt{\frac{2\,F_H}{\rho_a\,A\,C_e\,S_{up}\,C_{L\_IBC}}}$$

(4. 4)

Consequently, in Figure 45, Figure 46, Figure 47, and Figure 48 the failure wind speeds ($V_{failure}$) at mean roof height for low-profile roof tiles are shown, for respectively loose-laid, battened, direct to deck, and foam adhesive fixing systems, that are used in the analysis. The 3-s gust failure wind speeds (V_{b_ini}) are reported in red in the figures. These 3-s gust $V_{failure}$ have been converted in 10-min mean equivalent failure wind speeds (V_{mean_ini}), to find the lower bound of flight trajectories, according to Kordi et al. (2010). This second wind speed (in orange in the figures) can be calculated using standards such as ISO 4354 (2009) which is presented in Appendix B - 3-s Gust Design Wind Speed Conversions. With reference to ASCE 7-22 (2022) V_{b_ini} can be converted into V_{mean_ini} using the gust factors (Section 26, ASCE 2022). The 3-s gust and 10-min mean failure wind velocities ($V_{failure}$) are represented in the figures, respectively in red and orange colors.

We can notice that, when it comes to the foam adhesive roof tile fixing technology, the failure wind speeds are higher (Figure 48) than the reference design wind speed for the target building design (63 m/s) almost for all the sampled wind speed values. There are just very few cases in which the roof tile failure would occur, but these $V_{failure}$ cases are coming from the conversion of the 3-s gust wind speed into the 10-min mean equivalent wind speed. Flight initialization is, therefore, considered not to occur for foam adhesive fixed roof tiles in the design building location, for the example presented in this Section. For foam adhesive technology, the roof tiles are considered not to fail and, consequently, not to fly. Accordingly, for the Monte Carlo simulation, as initial conditions for flight trajectory analysis, the foam adhesive fixing technology has been discarded.
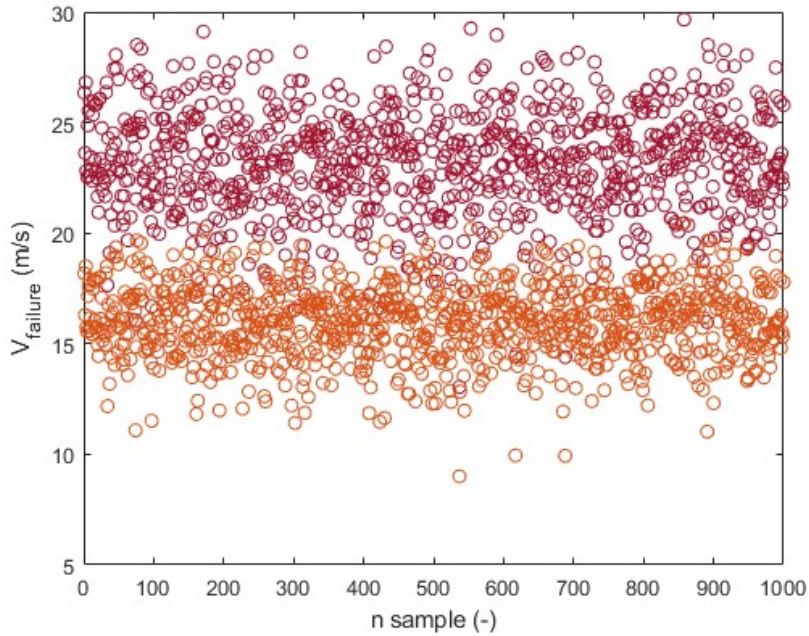
Figure 45 - Sampled values of 3-s gust (in red) and 10-min mean (in orange) failure wind speeds for loose-laid low-profile roof tiles. S_{up} factor of 2.90 is used for the representation of the dataset.
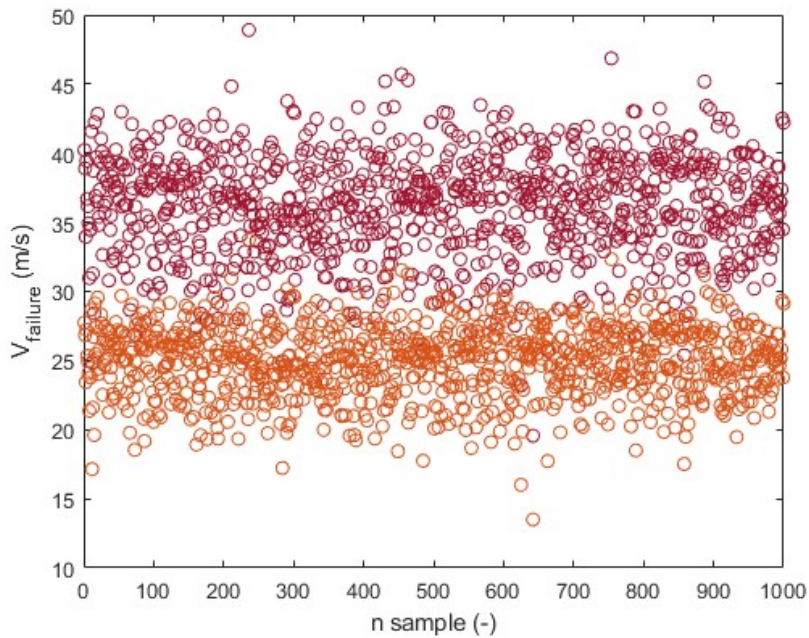
Figure 46 - Sampled values of 3-s gust (in red) and 10-min mean (in orange) failure wind speeds for battened low-profile roof tiles. S_{up} factor of 2.90 is used for the representation of the dataset.
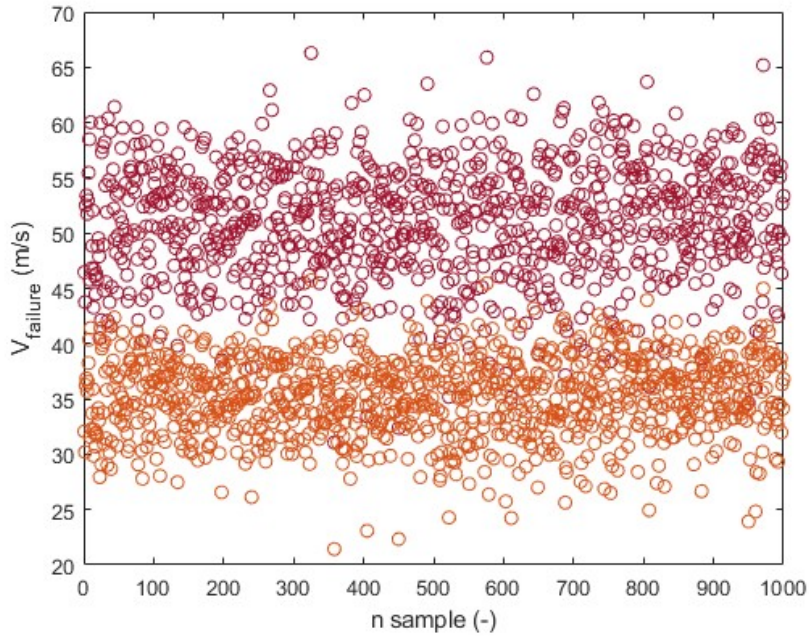
Figure 47 - Sampled values of 3-s gust (in red) and 10-min mean (in orange) failure wind speeds for direct to deck low-profile roof tiles. S_{up} factor of 2.90 is used for the representation of the dataset.
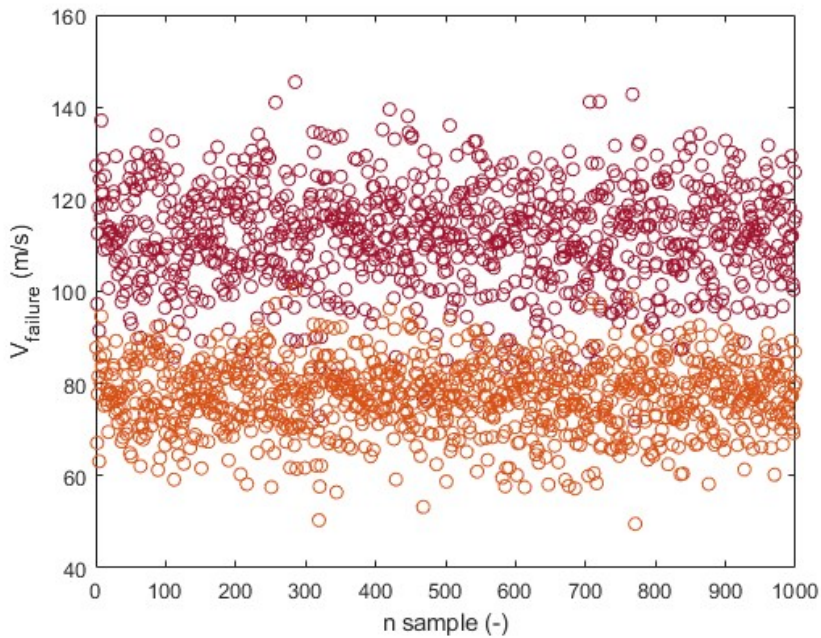
Figure 48 - Sampled values of 3-s gust (in red) and 10-min mean (in orange) failure wind speeds for foam adhesive low-profile roof tiles. S_{up} factor of 2.90 is used for the representation of the dataset.

4.6 Flight Trajectory Analysis of Low-Profile Roof Tiles

Based on the results of Section 4.5.2, the initial conditions for the roof tile flights are given in terms of failure wind speed ($V_{failure}$), which depend on the fixing characteristics and the related uplift capacities. For each basic failure wind speed, following Tachikawa (1983) and Kordi (2009), various initial angles of rotation of the debris element (θ) should be considered immediately after failure. In the calculation, the range of initial angles (θ) for the flight calculation is used, between 0° and 180°. This scattered initial flight condition accounts for the variability of flight results that are observed in real-world observation, where source building aerodynamics plays a key role in the trajectory definition (Kordi 2009). This range of θ accounts for the symmetry of plate-like debris (Wills et al. 2002) for angles between 0° and 180°, and angles between 180° and 360°. Various θ analyses provide the Monte Carlo simulation with better reliability on the probability of target façade impact. A uniform distribution of initial angles θ varying in 30° increments is considered in the analysis (Figure 49).
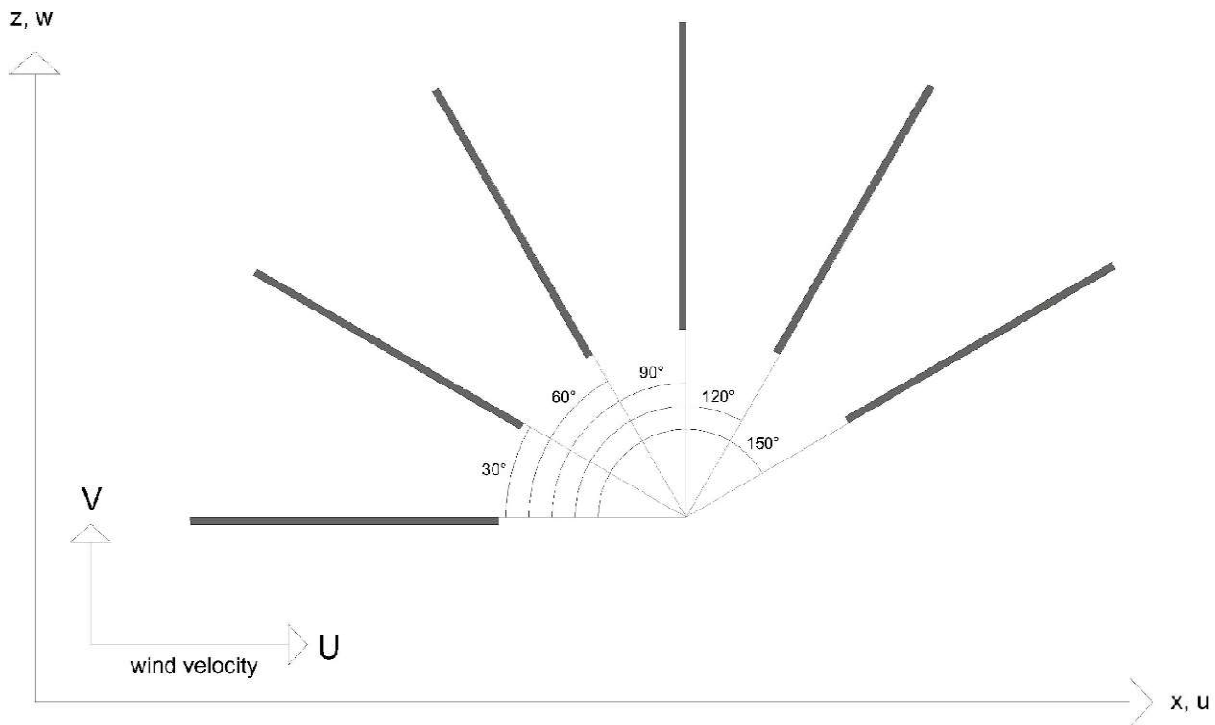
Figure 49 - Low-profile concrete roof tiles: the flight trajectories in the analysis are calculated for initial angles   θ = 0°, 30°, 60°, 90°, 120°, 150°.

The trajectory analysis is conducted by solving Tachikawa's (1983) dimensional equations (Equations 2.7, 2.8, 2.9) using a 4th-order Runge-Kutta scheme. In Equations 2.13, 2.14, and 2.15, the rotational aerodynamic coefficients for lift, drag, and momentum adopted in the calculations are defined. In Equation 2.18, the normal coefficient used for the calculation of the static aerodynamic coefficients for lift, drag, and momentum (Equations 2.19, 2.20, 2.21) is reported. Further details about the validation of the numerical calculations can be found in Appendix A - Wind-Borne Debris Trajectory Calculation. The aerodynamic coefficients used for the trajectory analysis are defined for a square-plate debris element, since the low-profile roof tile is close to AR=1.

4.6.1 Flight Distances

According to Kordi & Kopp (2011), to evaluate the effective range of roof tiles flight distances, accounting for the aerodynamic effects of the source building where the roof tile failure occurs, the trajectories have been calculated by varying the wind speed between the basic failure wind speed (V_{b_ini}) and the equivalent 10-min mean wind speed (V_{mean_ini}). Furthermore, Tachikawa's (1983) scattering for the initial angle θ has been adopted.

For the Monte Carlo simulation 108,000 trajectory analyses are supposed to be simulated considering:

- 3 restraint system technologies for low-profile concrete roof tiles;
- 1,000 F_H for each restraint technology;
- 3 S_{up} on the hip roof;
- 2 $V_{failure}$ (V_{b_ini} and V_{mean_ini});
- 6 initial angles (θ).

For $V_{failure}$ larger than the design reference wind speed (63 m/s), roof tile flight has not been calculated. According to this assumption, instead of 108,000, the calculated flight trajectories are 107,466 (= N_{total}). Flight initialization is analyzed at the mean source building height (10 m) and the simulated roof tile trajectories start for $V_{failure}$ of each particular case, for the scattered θ values. In Figure 50 the roof tiles' maximum flight distance distribution is reported, for the three fixing systems loose-laid, battened, and direct to deck, versus the number of simulations in which flight initialization occurs. These flight distances are reported without considering the impact on the target design façade, which is 75 m from the source building location (Figure 36, Figure 35) and indicated with a black line. Avoiding the introduction of the target façade in the trajectory analysis, we can

observe that flight distances reach more than 120 m from the source building location abscissa direction, even if the debris element is starting the trajectory at an H of 10 m.

The different fixing technology roof tile flights are shown in Figure 51 and, also in this figure, the distance of the target façade is reported with a black vertical line. From these trajectory analysis results, loose-laid roof tiles, starting their flight at lower wind velocities if compared to the same tiles with different fixing systems, end up not impacting the target façade. Loose-laid roof tiles reach a maximum distance of 23 m. The same thing happens, due to the distance between the source building and the target façade, for battened roof tiles. They reach a flight distance of 65 m (< 75 m). The only restraint technology analyzed in the Monte Carlo simulation that takes to the impact of the target façade is the direct to deck one.

The final flight distances of all the trajectory analyses, considering the target façade, are represented in Figure 52. At 75 m from the source location, 3,238 impact cases are reported in the histogram (N_{impact}). According to the calculation results, for the scenario in which there is an equally distributed combination of loose-laid, battened, and direct to deck roof tiles, the probability of impact (P_{impact}) is 3%.

In Figure 53 the distribution of impact heights is represented for loose-laid, battened, and direct to deck roof tiles. Loose-laid and battened roof tiles do not impact the target façade and this information is provided also by Figure 51. From Figure 53 direct to deck fixed roof tiles impact records go up to 7.8 m. None of the roof tiles are going to reach the roof of the hospital (25 m), and neither are recorded to fly over the building, impacting the leeward area of the target building.
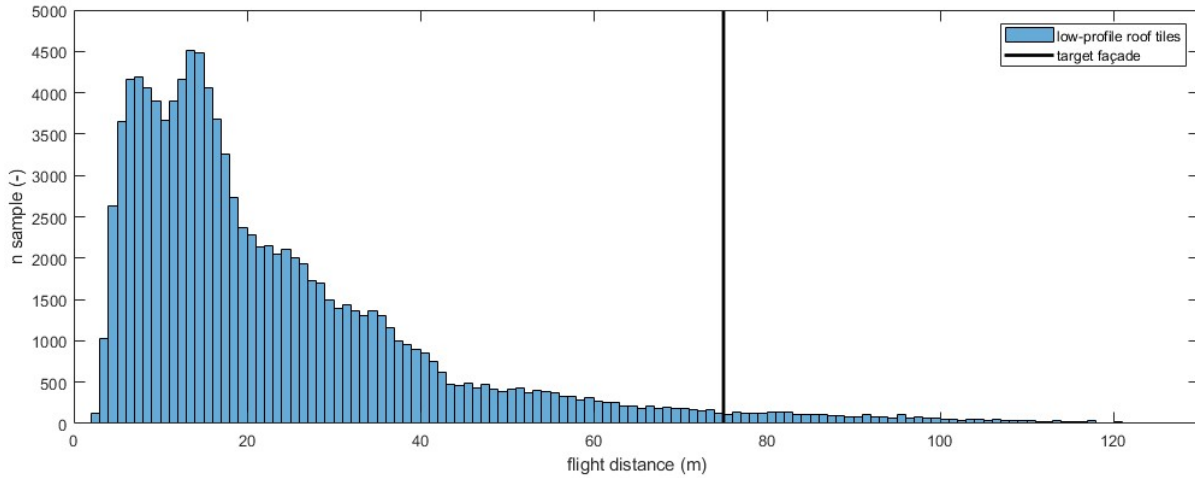
Figure 50 - Distribution of flight distances of loose-laid, battened, and direct to deck low-profile roof tiles. Roof tile failure occurs at an average roof height of 10 m and the design reference wind speed is 63 m/s. This analysis does not consider the target building. When failure wind speed for roof tile failure exceeds the reference wind speed for façade design, the trajectory analysis is not calculated. The black vertical line indicates the target façade location (75 m from flight initialization location) but the flights do not consider the presence of the target building.
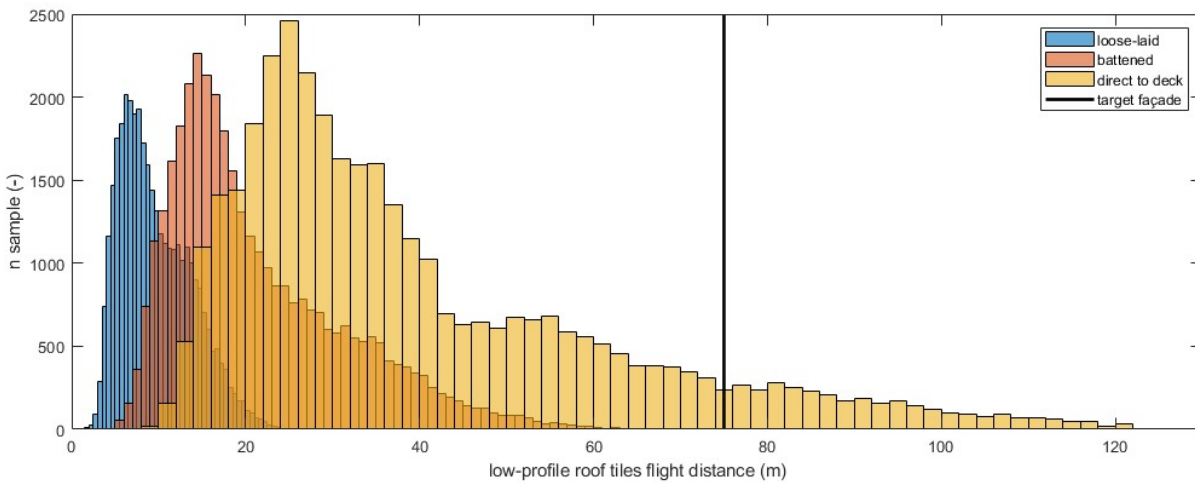
Figure 51 - Distribution of flight distances of loose-laid (blue), battened (orange), and direct to deck (yellow) low-profile roof tiles. Roof tile failure occurs at the average roof height of 10 m. The design reference wind speed is 63 m/s. The black vertical line indicates the target façade location (75 m from flight initialization location) but the flights do not consider the presence of the target building.
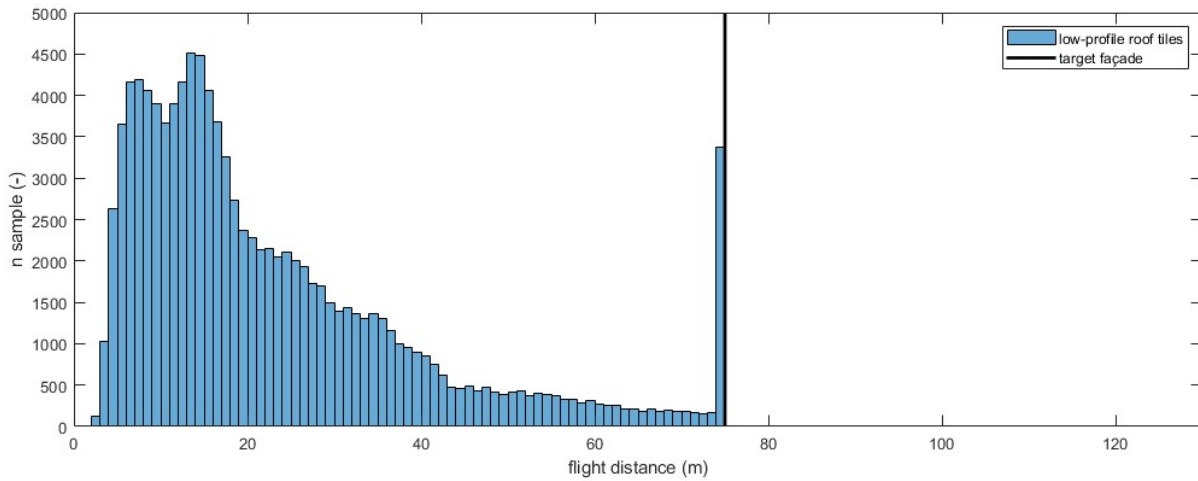
Figure 52 - Distribution of flight distances of loose-laid, battened, and direct to deck low-profile roof tiles. Roof tile failure occurs at an average roof height of 10 m and the design reference wind speed is 63 m/s. The flights do consider the target façade location (75 m from flight initialization location). 3,238 impacts are recorded on the target building façade. Roof tile maximum flight distance is equal to the distance between target façade and debris flight initialization. It means that none of the low-profile roof tiles are going to pass over target building or to impact the target building roof.
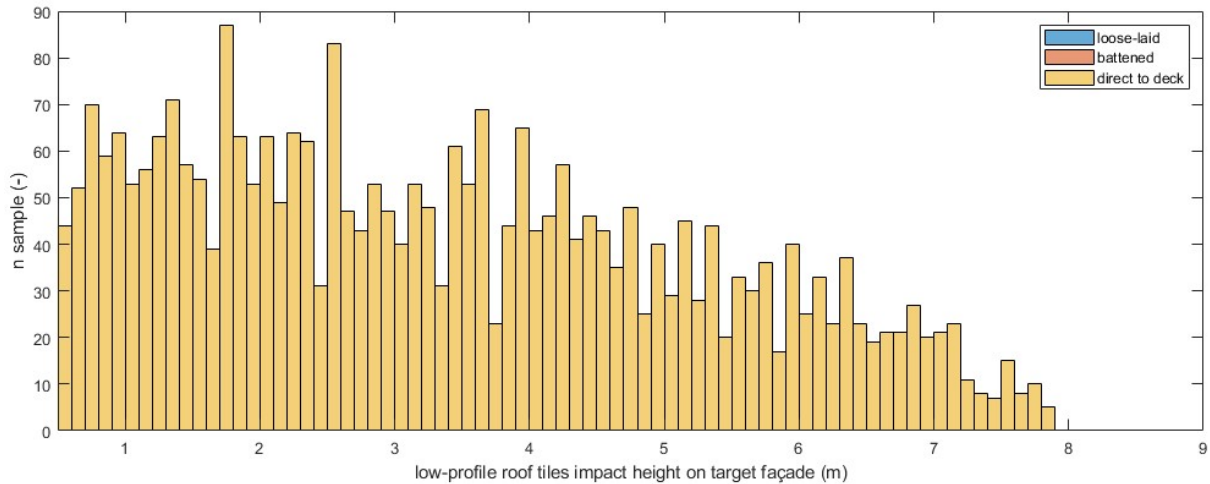
Figure 53 - Distribution of impact height of loose-laid low-profile roof tiles on target building façade. Loose-laid (blue), battened (orange), and direct to deck (yellow) attachment methods are reported. Roof tile failure occurs at an average roof height of 10 m and the design reference wind speed is 63 m/s. Target façade is at 75 m and it is never hit by loose-laid roof tiles. Target façade is 25 m high.

4.6.2   Impact Velocities

In this Section, with reference to the results of the Monte Carlo simulation that has been conducted, the range of impact velocities is analyzed, for the target façade and, in general, at the end of the flight, considering flight initialization at H = 10 m. The wind-borne debris velocity values are directly related to the failure capacities of the debris element analyzed, the wind velocity, and the angle of attack at flight initialization for the specific setting of the example presented in this Chapter. This analysis is based, therefore, on the results of the N_{total} simulations run to assess the flight of the low-profile roof tiles (Section 4.6.1), solving Tachikawa's (1983) equations of motion (Equation 2.7, 2.8, 2.9). Maximum, minimum, and median impact velocities on the building façade are reported in Table 10. These impact speed values follow the initial conditions of the simulation, such as the position for flight initiation at mean roof height.
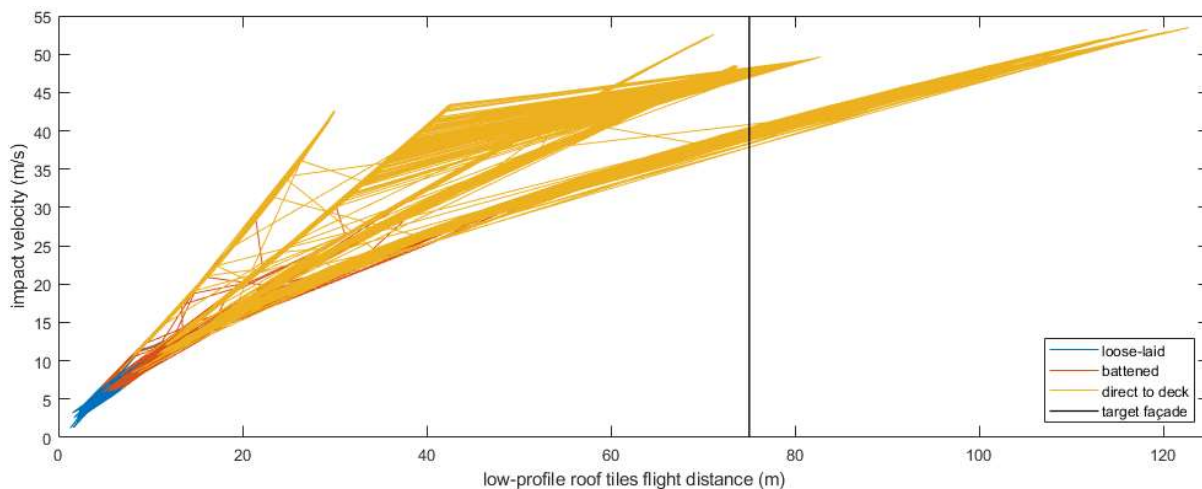
Figure 54 - Distribution of impact velocities as a function of maximum flight distances for loose-laid (blue), battened (orange), and direct to deck (yellow) low-profile roof tiles. Roof tile failure occurs at an average roof height of 10 m and the design reference wind speed is 63 m/s. The vertical line (black) indicates the target façade location, but the flights do not. The wind-borne debris alternative impact velocities for target building testing should be assessed considering the impact values for façade location (75 m from flight initialization).

Table 10 - Max impact speeds (m/s), impact energies (J), and maximum impact height on target façade (m) at the terminal trajectory for low-profile concrete roof tiles, from Monte Carlo simulation. Reported data consider different attachment configurations and flight initialization is assumed to occur at H= 10 m. No impact on target façade is indicated with (-)

Attachment Configuration	Max Impact Speed (m/s) and Impact Energy (J) of Low-Profile Roof Tiles		Max Impact Height (m) of Low-Profile Roof Tiles
loose-laid	26 m/s	1,643 J	(-)
battened	41 m/s	4,085 J	(-)
direct to deck	53 m/s	6,826 J	7.8 m

The maximum impact velocity that is recorded on the target façade of this example is equal to 53 m/s (Figure 54 and Table 10) and it is for the roof tiles with direct to deck connections. It has already been discussed in Chapter 2 how to preliminary assess debris impact speed when the failure mechanism and capacity of the element are known. Technical solutions that are acting against roof tile uplift, when uplift occurs, take the wind-borne debris to reach higher speeds and, therefore, also higher impact velocities. Figure 54 shows a range of impact wind speeds on the target façade 38 – 53 m/s.

4.7   Wind-Borne Low-Profile Roof Tiles' Impacts on Façades

The trajectories of low-profile roof tiles flights have been discussed in Section 4.6. With reference to the alternative design framework for wind-borne debris-resistance of façades (Figure 33) and the current standard requirements for façade design, performance-based impact energies for façade design are analyzed in this Section.

Debris element translational velocity indicates the energy it possesses. This is the final data to be achieved to set and perform alternative impact tests on building envelopes that are based on wind-borne debris aerodynamics, and on local environment analysis. The projectile impact speed is defined according to the target building location, location of the target façade and source building, target building envelope height, and level of importance of the target building. The design impact speed (Section 4.7) is a function of the basic wind

speed and the design reference wind speed (3-s gust in accordance with ASCE 7-22 2022; reference design wind speed according to Section 4.2).

From the roof tiles' failure assessment, V_{b_ini}, for the restraint systems considered to impact the target façade (direct to deck), reaches 53 m/s. The low-profile concrete roof tile failure analysis for foam adhesive fixing technology does not take the tile to fly, according to the assumptions of Section 4.5.2. Therefore, no impact speed is analyzed in these cases since the Monte Carlo analysis has the wind speed upper bound limit of the reference wind speed for façade design (63 m/s).

With reference to the solution of the trajectory analysis, the maximum impact speeds are reported in Table 10, per every fixing system that has been simulated (loose-laid, battened, direct to deck). However, based on the location between the target façade and the source building, no impacts are recorded for the loose-laid and the battened roof tiles. Therefore, the impact assessment on the target façade should be conducted exclusively for the direct to deck roof tile assessment.

The façade, to resist the impacts of wind-borne roof tiles, should be able to absorb their impact energy, which is also defined as the kinetic energy (K). The definition of K follows in Equation 4.3.

$$K = 0.5 \, m \, V_{imp}^{2}$$

$$(4.5)$$

with V_{imp} the impact velocity of the wind-borne debris.

4.7.1 Velocities and Locations for Low-Profile Roof Tiles Impact Test

Following Equation 4.5 and the design requirements in the example, the impact energies for façade design are respectively (ASCE 2022; ASTM 2019, 2020):
- 477 J (missile level D, Table 1) above 9.1 m on the ground level;
- 1,216 J (missile level E, Table 1) up to 9.1 m on the ground level.

In Table 10 are summarized the results of the low-profile trajectory analysis for the maximum impact speeds of roof tile at impact, the maximum impact height on the façade, the impact energies that the target façade would be required to withstand, based on the Monte Carlo simulation. Comparing the kinetic energy involved in the projectile impact, for direct to deck roof tile mean and max impact velocities, the kinetic energy is 5.6 times the impact test requirements of ASCE 7-22 (2022). This result is valid for the first three floors of

the target building (up to 9.1 m on the ground level). If we analyze the upper levels of the target building, these correlations change. From the Monte Carlo simulation, no impact is going to be recorded on the target building façade height larger than 7.8 m. Therefore, ASCE 7-22 (2022) impact test requirements are, for façade building heights larger than 9.1 m, overestimating the necessary impact performance of façades, when it comes to low-profile concrete roof tiles failure in the design set-up presented in the example. It is at a height of 7.8 m that the worst impact has been recorded in the simulation for façade design. An impact energy of more than 6,826 J can be required to be absorbed by an essential facility building envelope that avoids any interruptions when it comes to windstorm events.

The impact performances that can be proposed by façade designers based on the analysis presented in this Section and on kinetic energies in line with results summarized in Table 10, façade design would definitely be beyond the code when it comes to wind-borne debris resistance requirements. The aim of this example is to present a design solution that, if applied consistently with the local environment assessment, would take to technological solutions that avoid scenarios such as the St. John's Regional Medical Center (Kuligowski et al. 2014). Conducting the same analysis presented in this Chapter for the totality of the objects that are identified as a possible cause of damage due to failure and consequent flight, the impact performances of façades can be taken to a more resilient built environment.

The findings of this design framework are related to the impact inputs for façade impact testing. At this stage, the impact locations to conduct the test are intended to be the same as the current impact tests for wind-borne debris that follow ASTM (2019, 2020) requirements. In this testing protocol, the impact locations have been identified as the most representative of the window/curtain walling element performance. Fernandez et al. (2010) demonstrated the inadequacy of the current testing requirements for wind-borne roof tile impact testing. In their study, the same weight and impact velocities of the ASTM requirements have been used to perform impacts on metal panels, but roof tile projectiles have been used. They demonstrated a significant difference in deflection as a function of debris types with identical mass, speed, and impact location. They concluded that the kinetic energy itself is not enough to represent a specific debris element impact. The material, geometric characteristics, and impact orientation of the projectiles play a crucial role in the wind-borne debris resistance assessment. Accordingly, even if the kinetic energy involved in the roof tile impact would be the same as for lumber, based on standardized impact velocity (ASTM 2019, ASTM 2020), considering the roof tile projectile, the impact test outcome is expected to be considerably different, depending on building envelope features and on impact angle to conduct the impact test (Section 4.7.2).

4.7.2   Impact Angles for Low-Profile Roof Tiles Impact Test

From the trajectory analysis, it is possible to estimate the angle of impact (Figure 55), which is not always equal to the orthogonal position with respect to the vertical direction of the vertical façade ($\theta = 0°$, 180°, 360°). The orthogonal impact is the one performed with the standard projectiles (ASTM 2019, 2020). The major difference in impact test performance, together with the impact speed and the use of alternative projectiles, would be the execution of the test following impact angles θ calculated through trajectory analyses. Most of the low-profile roof tiles have an impact angle between 40° and 50°. The results have not been wrapped for the range between 0° or 180° because of the uncertainty in the symmetrical behavior of the upper and lower bounds of the concrete roof tile projectiles.

In Figure 56, the impact angle results have been divided, based on the fixing system. It is possible to highlight that the failure mechanism change, due to different failure capacities, influences a non-uniform distribution of the impact angles. Through the schematic representation of a glass panel which is intended to be representative of a cyclone-glass fenestration solution, in Figure 57 two different impact angles are reported. The impact angles are representative of the impact orthogonal to the building envelope (horizontal impact) and a different one indicated with θ. For fragile materials such as glass, there would be a considerable difference in the impact area, which is going to influence the mechanical performance of the panel.
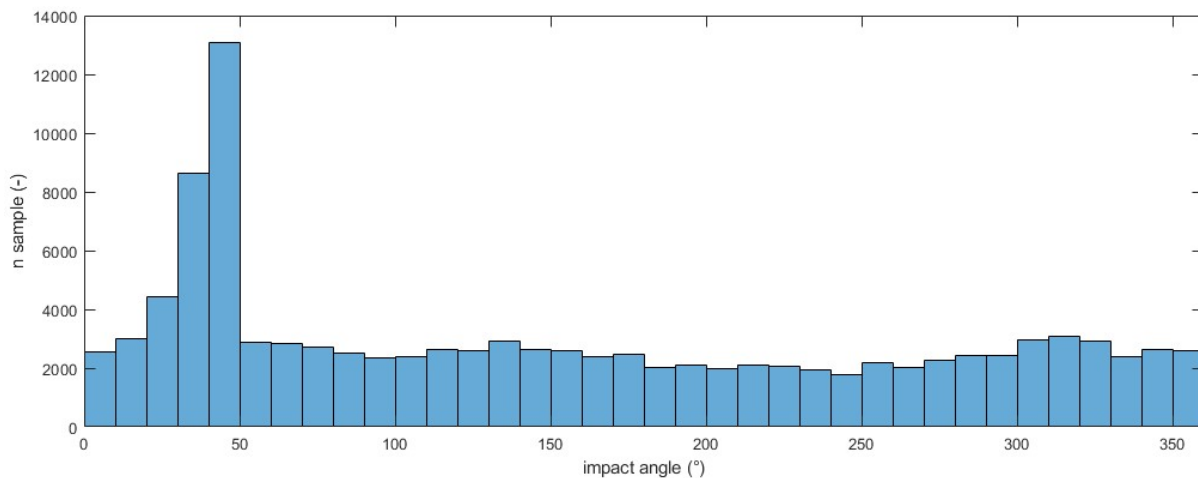
Figure 55 - Concrete low-profile roof tile impact angle distribution for loose-laid, battened, and direct to deck fixing systems. The impact angle θ is expressed between 0° and 360° since the geometric features of the upper bound of the concrete roof tiles are different from the lower one. Through a test campaign, it would be possible to understand if there is symmetry (0° - 180°) in the mechanical behaviour of the concrete roof tile at impact.
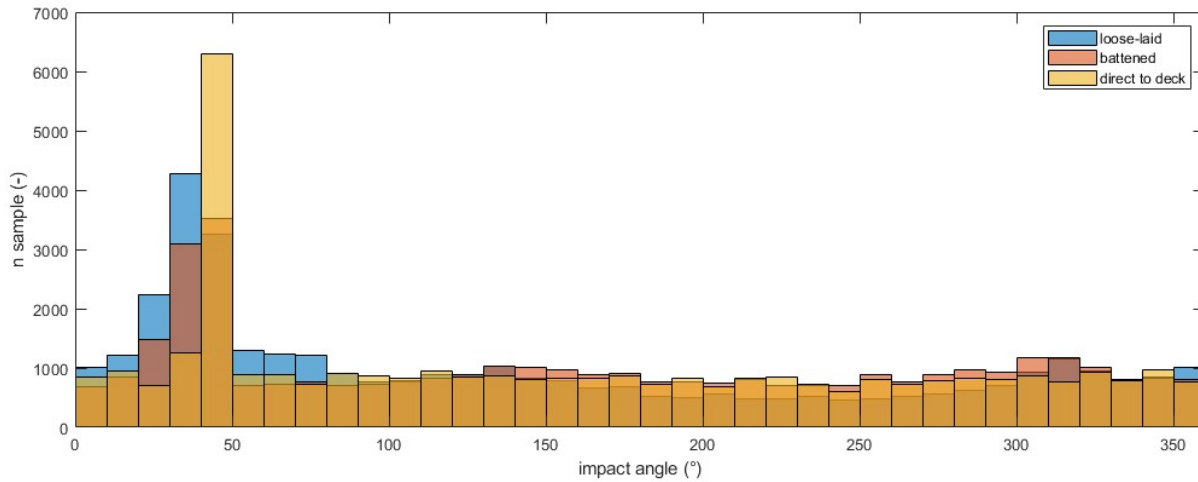
Figure 56 - Concrete low-profile roof tile impact angle distribution for loose-laid (blue), battened (orange), and direct to deck (yellow) low-profile roof tiles. There is no uniform distribution of impact angle results for the three different failure capacities and mechanisms.
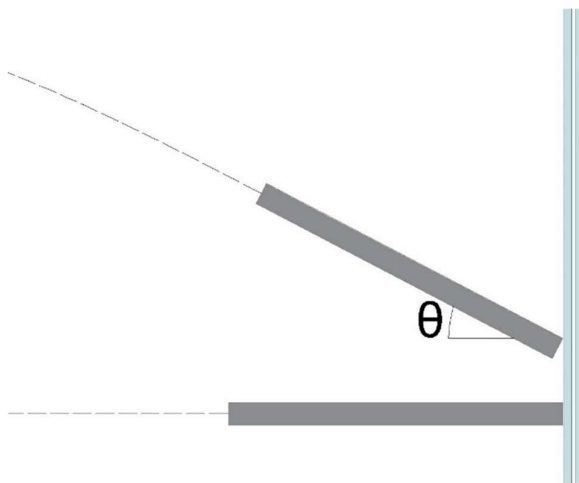
Figure 57 - Concrete low-profile roof tile impact on a laminated glass solution for impact angle θ and impact orthogonal to the panel. The impact area of the roof tile, for an orthogonal test, is equal to 11 mm^2. Depending on the impact angle, the impact area can reach more than one order of magnitude less than the orthogonal impact solution. Especially for fragile panels like glass lites, for the same impact kinetic energy, the impact area of the projectiles on the panel influences the mechanical performance of the test specimen.

4.7.3 Low-Profile Concrete Roof Tiles Impact Test Equipment

One of the goals of the presented alternative design framework for wind-borne debris impact performances of façades is to implement the currently adopted testing apparatus. This proposal avoids expensive solutions for test equipment implementation, to support designers in easy adoption of the design method to improve façade resilience. At the same time, this method aims to use the specific objects that are assessed in failure and flight behavior. This is important because the elastic and fragile behavior of the test specimen depends on projectile material and impact speeds. According to the testing equipment that has already been implemented (Section 2.4) and proposed by Fernandez et al. (2010), the impact test takes place with low-profile roof tiles as alternative impactors. In the testing methodology assessment, the impact should be conducted at the impact velocity that has been calculated in the debris trajectory analysis (Section 4.6).

The roof tile projectile shall have no defects, and it shall not have been used to conduct other tests before. The end of the projectile that impacts the target is denoted as the projectile impact end. The end of the missile opposite to the impact end is denoted as the projectile trailing edge. The projectile impact end should impact the test specimen with the design angle θ, with reference to the horizontal impact (which is orthogonal to the façade), according to trajectory estimation. Therefore, the air cannon should be inclined to follow design specifications for the alternative impact test requirements.

Chapter 5. Wind-Borne Debris-Resistant Façade Solutions

Façade breakage caused by wind-borne debris impacts could be avoided by understanding the potential impacts a building envelope solution has to withstand, based on existing debris in the local environment, on the level of importance of the building, on the design wind loads. Using the proposed design tool, new window, and façade design, as well as retrofit solutions could be developed, based on designer-chosen performance objectives. This research offers façade designers a solution to fill the gap in façade impact test requirements related to local wind-borne debris. The impact energies will be evaluated accordingly, by estimating the trajectory and the velocity of specific debris considering the immediate surroundings, enabling façade designers to investigate the possibilities given by the current best practices (ASTM 2019, 2020). The ASTM standard requirements allow façade designers the chance to go through engineering assumptions to develop ad hoc wind-borne debris impact tests for their projects, adopting an "other projectile" for the impact test. The result is site-specific designs for wind-borne debris impact-resistant façades. This will be of use for post-disaster buildings in an urban environment, such as hospitals, that are required to have "enhanced protection" (IBC 2021).

The design process begins by answering the minimum performance requirements related to local building codes and this also involves the energy performance requirements. After the basic design requirements are addressed, also extreme events are considered, to finally develop a system where various curtain wall components (the framing system and the glass installation within that system) must be designed to perform during these events. In Chapter 4, the methodology to set wind-borne debris-resistance test requirements is discussed with a specific example, but the proposed design tool could be implemented for any possible projectiles in windstorms. Analyzing a specific building component in its failure mechanism, this method opens a discussion about other materials such as gravel, shingles, sheathing, and structural members, the most common sources of wind-borne debris (Kordi 2009). This chapter discusses existing solutions and design methods to enhance façade resilience in disaster events and for debris-impact-resistant façades.

Patterson (2022) highlighted the urgency of setting down a strategy for "resilience planning". Regarding hurricane-prone regions, he set down goals and strategies to improve curtain wall resilience. His guideline is in line with the design framework proposed in this thesis (Figure 33) since the necessity to go beyond the code for a performance-based design of the building envelope is discussed, especially about windstorm events. Furthermore, he focused on the necessity of implementing strategies to minimize damage

from extreme events, treating the building envelope such as the structure of the construction, and considering loads that account for climate change-related scenarios. This approach would work to go towards a design approach that avoids post-event reports such as the St. John's Regional Medical Center, discussed in Chapter 1. It has already been underlined how the structural system of the Joplin hospital has not been affected by the tornadic winds, whereas almost the entirety of the building envelope experienced breakage, except for breakage-resistant window solutions (Kuligowski et al. 2014).

It takes more than just modifying the glazing system to create an impact-resistant façade that can endure the test required for product clearance. It is a difficult procedure that requires a lot of different elements to come together in order to provide the robustness the window system requires. To withstand the test protocols (ASTM 2019, 2020) and achieve performance goals in the real world, all the components must work together. The interlayer for glass lamination, the fastening technique, and the glass properties have an impact on how well the building glazing system performs. It is feasible to go forward with the design of glass thickness and strength characteristics, as well as the interlayer material qualities and thickness requirements, by concentrating on the size, geometry, and design pressure of the window or façade (Block et al. 2008).

Figure 58 - Tempered laminated glass with PVB interlayer.

For façade performance, both the curtain wall spandrel and glazed surfaces must remain in place to avoid breaches. If breakage occurs, the glass could injure people and, to avoid this, requirements for tempered glass should be introduced, even if there are still very few investigations related to the number of casualties by glass shards due to impacts on glass (Zhang & Hao 2013). During extreme wind events such as windstorms, usually, there is rain at the same time and, therefore, if the building envelope fails, the internal property loss could carry a significant recovery cost in terms of furniture, electronic devices, and documents. In 2017 Cyclone Debbie hit the Whitsunday Region in Australia and, even though there was no structural damage to the building, several residents of newer structures reported considerable damage from wind-driven rain entering via windows and doors (Boughton et al. 2017). In 2005, the MGM Mirage's Beau Rivage Hotel and Casino in Biloxi, after Hurricane Katrina had a lot of damage due to an internal mold problem, even if the window component didn't break (Mejorin et al. 2019). Therefore, one further area that should be further explored is the water-tightness performance of the building envelope, when it comes to extreme wind events that are associated with significant rains, such as hurricanes. To increase the performance of building envelopes during extreme wind events, more resilience is, therefore, needed also to avoid water infiltration in the system.

For impact resistance of façades, the framing system design and the installation of the spandrel and glass sheets in the framing system are two important components that need to be analyzed, properly designed, and finally tested to verify the minimum required performances. The façade framing is commonly designed to avoid the panels (glazed or opaque) from being ejected from this retaining system when subjected to high pressures. In this perspective, the curtain wall frame is more robust, compared to a façade not exposed to the analyzed extreme events. Furthermore, the glass/panel bite is usually deeper, to let the façade system work as a unit (consisting of glass/panel, sealant, and frame), for a glazing system is effective in mitigating damage from wind-borne debris, the entire system needs to be designed properly to resist such impact event.

Laminated glass could be defined as "cyclone glass" when it guarantees a precise level of impact performance in standard frame conditions, based on international standards (ISO 2007; ASTM 2019, 2020; AS/NZS 2021). This glass has been invented and developed for architectural use after Cyclone Tracy (Figure 5) occurred in Australia (Mason & Haynes 2010). The composition used in cyclone-resistant glass must resist both the wind load and the projectile impact specified by codes. Laminated glass works by coupling two or more lites of glass with one or more interlayer elements and the thickness of the glass lites is determined by the wind load and the interlayer type (Figure 58). A family of synthetic resin materials called interlayers is utilized in glass lamination, to connect with the surface of glass chemically strongly (Piscitelli 2018).

Figure 59 - Dallas, Nasher Sculpture Centre, designed by Arch. Renzo Piano, completed in 2003, interior view. The building roof has been designed to allow natural light to penetrate within the internal space of the museum. To reach the desired features, the building roof has been realized as a double-skin. To avoid glare, reflections in the exhibition area and to a porous external aluminium skin.
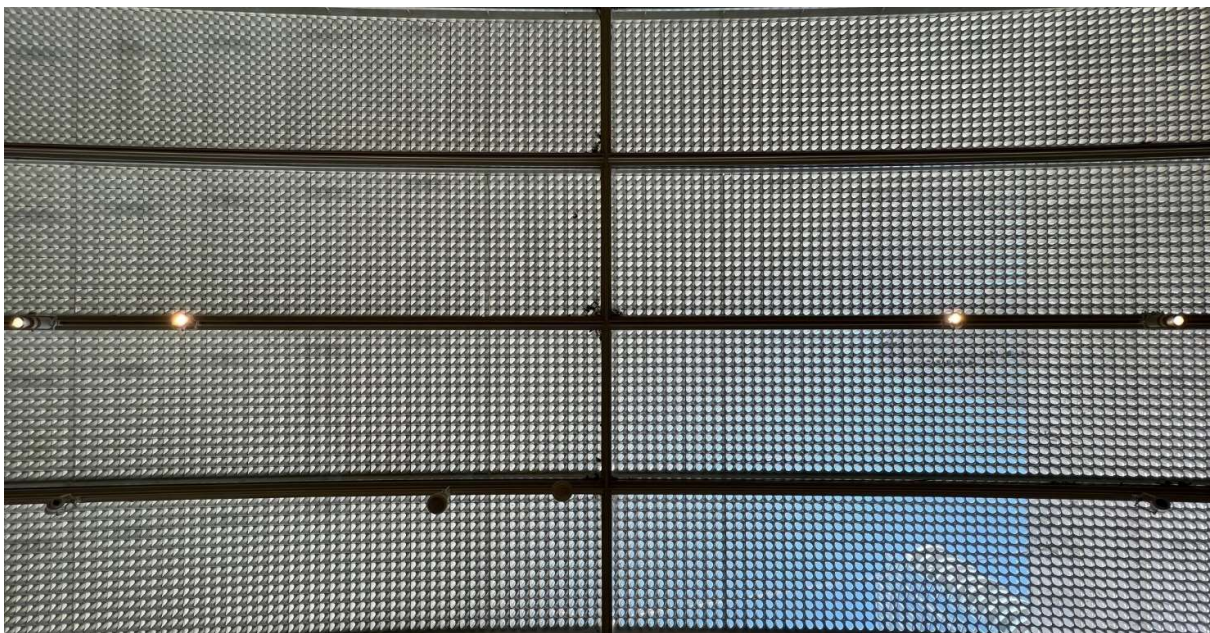
Figure 60 - Dallas, Nasher Sculpture Centre. View of the roof solution of the main floor.
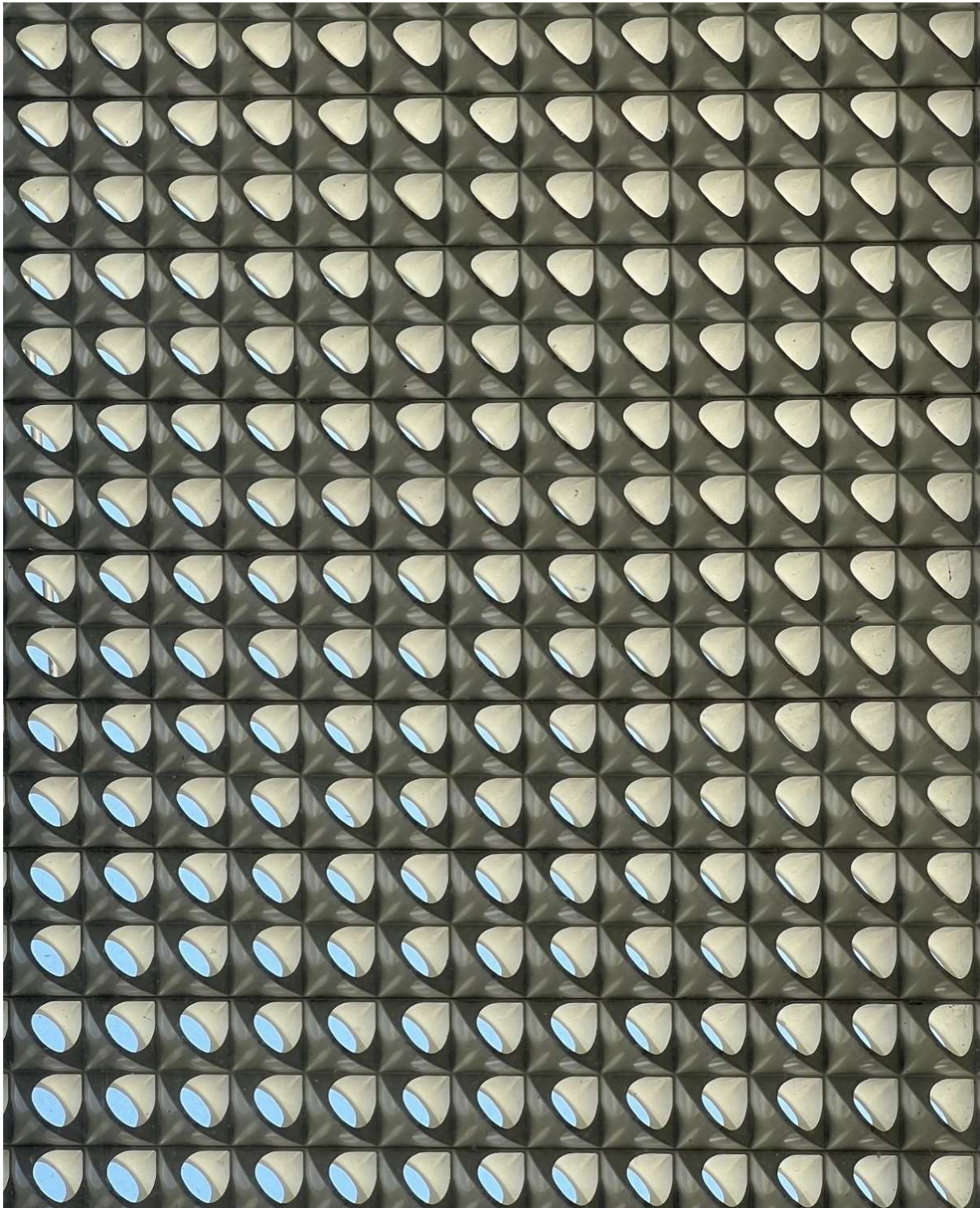
Figure 61 - Dallas, Nasher Sculpture Centre. Detailed photo of the outer skin of the double-skin roofing solution. The orientation of the panel holes filters natural light and allows just diffused light penetration, allowing just northern light penetration. This solution is an example of porous double-skin that can be further implemented to guarantee impact resistance against wind-borne debris.

These chemical connections may often be formed in an autoclave at a predetermined pressure and temperature levels. Typically, relatively thick polymer sheets, such as those based on poly(vinyl butyral), poly(urethane), and ethylene vinyl acetate (EVA), or ionoplast polymers (IP), are employed as the interlayers in safety laminates. Poly(vinyl butyral), also called PVB, has controlled the interlayer business for over eighty years (Piscitelli 2018), but the development of new products has been pushed by the rising demand for high-performance architectural glass. Countless plasticizers, fillers, and additives are often combined with pure polymeric matrixes in amounts that are protected by business secrets. Any commercial blend is therefore susceptible to significant changes brought about by technological advancements and chemical discoveries. However, resistance to penetration by the projectile impact is determined by the interlayer type and the thickness of the interlayer itself. The interlayer thickness relates to projectile impact speed, not to design wind load (Block et al. 2008). The interlayer guarantees glass retention if breakage occurs, and the main interlayer types are PVB and IP. Both these interlayers have been used successfully in laminated glass for hurricane glazing systems.

PVB is a soft interlayer and works well when the design pressure is lower, and the projectile size is smaller. Because of the low stiffness, laminates using PVB tend to not perform well when the design pressure is high. The high wind pressures can cause the laminated glass to pull out of the frame during the cycling portion of the test, and therefore it typically will need a better frame design or a thicker interlayer and/or glass. The PVB laminated glass is at risk of becoming detached with high wind pressures during the final pressure cycling testing (ASTM 2020).

IP interlayer was introduced in 1998 in South Florida; it can meet the highest performance criteria required for impact resistance: large projectile D and E (ASTM 2019; ASTM 2020). Being a stiff interlayer, it provides added strength and rigidity and remains intact after the pressure cycling test. This could potentially allow a lower grade of glass to be used, saving costs. Another advantage of the IP interlayer is the possibility it gives to the glazing system to be dry-glazed, reducing installation costs and time, as compared to the traditional wet-glaze system installation.

In the testing for the product approval process, the aim is not just to test the components, but the whole system. In this way, the glass can be pre-dimensioned based on the size of the specimen and the impact velocity of the projectile, but it is necessary to verify that the system can withstand testing requirements. Impact testing and subsequent application of pressure cycles and depression must present positive results for approval of the window to be used. Wet- and dry-glazed systems are both logical options for wind-borne debris

resistant façade solutions. The most typical example of wet-glazing involves the application of a sealant over a tape or gasket that has already been made. The sealant, during the application, is wet but with the polymerization process it loose water and it does stabilize. For dry-glazing, extruded rubber gaskets are used. The waterproofing performance of the glazing is influenced by the glazing process and drainage characteristics of the frame system. The wet-glazed systems are often used for shop-glazed fenestration products, and they are commonly used in high-velocity hurricane zones where large-projectile impact applications must be wet-glazed to pass the required cycling test. Dry-glazed systems are especially suitable for glazed fenestration systems that need to be assembled on the job site. These systems eliminate the use of wet sealants and more closely replicate the "as-tested" conditions. The large projectile impact systems have been certified up to ±6.2 kPa. The dry-glazed systems represent cost savings in terms of labor and materials, and further potential savings from replacing broken glass (such as after a hurricane event).

For existing buildings, building envelope solutions could be upgraded, for relatively small hazard reduction, through the application of safety/security films (daylight application) on glazed lites (Lin et al. 2004). The main advantages of such solutions relate to relatively low cost, easy installation, and continuity of the building's operability. For other situations, depending on the façade framing stiffness adequacy, it would be possible to replace the glazing, for a higher level of hazard reduction. The result could lead to an upgraded façade visually identical to the previous one but with an improved solution also in terms of energy efficiency. In this second example of façade retrofitting, the cost of the upgrade solution is higher compared to the one of the first example, and the load transferred to mullions, frames, and walls increases, thus the glass clamp must be adequate as a general consequence (Lin et al. 2004). These are just two examples of possible intervention, but there are many options, including security film; installation of catch bars; enhanced mullions and frames; replacement of the entire window system; installation of a secondary window system.

Modern buildings often adopt porous double-skin (DS) façades. This façade solution consists of the combination of an external permeable layer, combined with an inner façade solution. This building envelope system presents multiple benefits. For the building energy consumption, it reduces the heat load on the building, letting the air naturally circulate between the external and inner panels and acting as a shading system against solar radiation (Shahrzad & Berardi 2022; Zheng et al. 2012). Furthermore, performance-based DS façades can answer other internal comfort requirements such as noise insulation, which depends on the size of the ventilation opening of the external porous layer (Hu et al. 2021). DS porous façades can also reduce wind loads on the inner façade (Lo et al. 2020), by up to a 40% reduction (Pomaranzi et al. 2020). The porous

façade damping mechanism for wind load reduction has been studied and there has been difficulty in the understanding in the scaling of porous façades to conduct wind tunnel tests. For this reason, Allori et al. (2013) conducted an extensive campaign on confined and unconfined flows of different-shaped perforated plates. They found out that the porosity parameter should be kept consistent to correctly scale the porous façade external layer [25].

Figure 62 - Miami, Florida. The tallest building in the picture is the Porsche Design Tower, in which IP interlayer has been extensively used.

---

[25] This parameter is the ratio of the thickness of the screen to the hydraulic diameter of the holes, and Reynolds number (Allori et al. 2013).

Double-skin façade solutions can increase the performance of the façade, based on design goals, and this can be also related to wind-borne debris resistance. With reference to the example discussed in Chapter 4, based on the debris element analyzed and on its geometric features, an outer skin can be beneficial to avoid inner façade panel breakage. Usually, the inner façade panel is a glazed insulated glass unit (IGU) that provides natural lightening and thermal comfort to the interior. The outer permeable layer of the façade can be an implementation of façade wind-borne debris impact performances. The external skin of the façade would benefit the impact resilience if realized in a ductile material that can keep the debris element away from the inner glazed layer. The porosity and the geometry of the external panel should avoid that, in the example case, a roof tile (with dimensions of 41.9 x 34.3 cm) can penetrate and hit the inner panel. Accordingly, the openings of the porous layer should not be more than 34 cm in diameter. Furthermore, it should be installed at a distance that, according to impact test results, would not realize any contact between the external and internal skins. Some projects are shown (Figure 59 - Figure 64), to consider the adoption of porous double-skin façade solutions to address the design goal of wind-borne debris impact resilience of façades.

Figure 63 - Dallas, Dee and Charles Wyly Theatre, designed by REX / OMA, at the AT&T Performing Arts Centre, completed in 2009. Façade detail.

Figure 64 - Dallas, Dee and Charles Wyly Theatre. The building skin presents acoustic performances to address the requirements of the theatre. Moreover, some of the panels can be opened to let the actors enter the stage from alternative building entrances. 466 extruded aluminium tubes form the external cladding of the building, and these were designed to meet deflection criteria without the need of a subframe. A motorized black-out system shades the interior when necessary. A similar solution can be designed to withstand the impact of projectiles without requiring all the impact resistance to be on the glazed surface.

Chapter 6. Conclusions and Recommendations

6.1 Conclusions

This thesis presents an alternative design framework for wind-borne debris-impact-resistance of façades. The current best practices in terms of impact testing to simulate wind-borne debris in windstorm events are based on the ASTM standard procedures (ASTM 2019, 2020). These adopt standard projectiles and impact velocities: the lumber projectile (large missile) and the steel ball projectile (small missile), representative, respectively, of a piece of the balloon frame structure, and roof gravel used on flat-roof constructions. The impact speeds used to conduct these tests have been developed through an empirical approach (Lin 2006).

The design method analyzed in this document sets a new approach to establishing façade impact testing performance, to provide site-specific wind-borne debris impact resistance of building envelopes, based on building aerodynamics, wind-borne debris trajectory analysis, and risk assessments. This research offers façade designers a solution to relate to local wind-borne debris types and specific design goals. The impact energies on target façades are, accordingly, evaluated by estimating the trajectory and the velocity of specific debris elements after the failure occurs. The ASTM standard requirements (ASTM 2019, 2020) already give façade designers the chance to go through engineering assumptions to develop ad-hoc wind-borne debris impact tests for their projects, adopting an "other missile" for the impact test.

This project analyzed major studies undergone to simulate various debris types (Wills et al. 2002) behavior and their failure in wind, to highlight the findings of recent wind engineering research. The available data are used to elaborate a façade design tool for wind-borne debris resilience of the building envelope. The alternative design strategy lays its foundations in the study of the aerodynamics of wind-borne debris, to guide designers in evaluating site-specific situations, and to achieve building envelope resilience to local exogenous objects. The overall result of this project is, accordingly, the development of a design tool for the identification of alternative testing requirements, which uses the impact design inputs achieved through aerodynamics and building technology considerations, to reach the objective of improving built environment resilience to wind-borne debris impact. The study resolves the identification of a suitable testing apparatus to conduct the alternative impact tests on façades, adopting widely commercialized equipment, to perform the alternative impact tests, with a specific example.

The findings aim to be primarily addressed to essential post-disaster facilities such as hospitals, that are required to have "enhanced protection" (IBC 2021). Through a case study, the methodology to set wind-borne debris-resistance test requirements is discussed for a particular debris element, but the proposed design tool could be implemented for any building component or object that could be wind-borne in windstorms. Analyzing a specific element in its failure mechanism, this method opens a discussion about other building materials that demonstrated their weakness in windstorm events becoming wind-borne debris.

In Chapter 4, the design framework (Figure 33) to design wind-borne debris impact façades is analyzed for the specific case of an essential facility (IBC 2021), an area with a basic wind speed of 80 m/s (ASCE 2022), for a design return period of 50 years. The debris element considered for the calculation is the concrete low-profile roof tile, which weighs 4.86 kg. The source roof tile location is 75 m from the target façade, the focus of the design, and the mean source roof height is 10 m. Various restraint roofing technologies have been considered for the roof tile presented in the example, based on current standard requirements, and building technologies' best practices. Accordingly, various failure capacities have been calculated based on the variation of the speed up parameter on the roof, based on roof geometric features (9/12 slope). After failure assessment, the flight trajectory has been calculated both with the 3-s gust failure wind speed and the equivalent 10-min mean wind speed, based on experimental observations available in the literature (Kordi 2009). Furthermore, the initial angle of attack of the wind on the roof tile has been scattered, based on Tachikawa's (1983) remarks. From the Monte Carlo, it has been found that the direct-to-deck-fixed roof tiles impact the target façade, with a maximum speed of 53 m/s, for a maximum height of 7.8 m on the essential facility. The impact has a probability of occurrence of 3% and, therefore, the building would be required to resist an impact of 6,826 J. It should be highlighted that this roof tile type, initiating its failure at a height of just 10 m, is going to reach distances of more than 120 m, even if most of these wind-borne elements are falling to the ground in the first 40 m.

Current façade products tested and certified as wind-borne debris resistant, for the same area and type of facility analyzed in Chapter 4, are required to withstand impact energy that is 5.6 times less than the outcome from the alternative impact test requirements proposed in this design framework, for concrete low-profile roof tiles. The example opens a discussion about the adequacy of current façade impact requirements, for wind-prone areas.

6.2   Contributions

The contribution of the thesis is to bring together in an organized design tool all the elements to estimate the impact performances of façades, in a case-specific environment, to enable building-envelope resilience. Through synthesis and analysis of the most advanced research in building technology and wind engineering fields, various design steps of the alternative performance-based design framework are presented.

In the building technology field, the research presents the failure capacities of case study building components. It discusses a probabilistic approach to estimate real-world failure capacities, based on existing data. Furthermore, it identifies alternative projectiles and testing procedures for façade impact testing, to verify façade wind-borne debris impact resistance. The thesis proposes modifications of both the existing testing apparatus, following experiments already explored by existing literature, and of testing procedures to verify wind-borne debris.

In the wind engineering field, the thesis analyzes and links various studies that have been undergone to estimate wind-borne debris failure and flight. The aim is to consider the real-world object, with precise features, and the effects of building aerodynamics. The model to assess the trajectory of debris in the wind field, thus, considers a probabilistic distribution, following the experimental results that have been collected in the last decades.

New buildings and retrofit projects that involve building envelope renovation, following the design framework presented in this research, can consider performance-based wind-borne debris impact tests, improving the resilience of the urban habitat when it comes to extreme winds. This necessity is particularly urgent for primary importance public buildings such as hospitals, police stations, and schools (Minor 2009; ASCE 2016) as they need to remain in operation also during and after extreme events.

The stakeholders interested in the research findings are professionals responsible for the various phases of planning, commissioning, design, production, installation, testing, and certification of façades. The fragility analysis for local wind-borne debris types, can engage specific owners/managers of the building compounds to make them aware of the threat their buildings can have, and of potential measures that they can adopt to reduce the risk. Furthermore, insurance companies can use the tool to assess the risk-related effects of wind-borne debris impacts on clients' buildings, considering site-specific conditions, and raising the accuracy of risk and building damage estimation.

The impact of the presented design framework to identify alternative wind-borne debris façade impact test requirements is significant in the development of new testing standards, to be introduced in the

standardization regulation framework, at the voluntary level and regulatory level such as National Building Code. At the voluntary level, the International Standard Organization is developing a standard 'Windows, Doors and Curtain Walling - Impacted by Wind-Borne Debris in Windstorms - Test Method', proving the interest for the introduction of testing requirements to consider wind-borne debris impacts on façade. Technical Committee 162 "Doors, Windows, and Curtain Walling" formed an ad hoc group between Working Group 4 (Windows and Doors) and Working Group 5 (Curtain Walling) to develop the standard. The design framework proposed in the thesis is going to be introduced in the document as an informative Annex, to guide in exploring alternative impact performances, based on building technology and wind engineering assumptions.

6.3 Limitations of the Research and Reccomendation for Future Research

The limitations of the research can be identified in both the building technology and the wind engineering parts of the problem analysis.

In the building technology area, the limitations are, above all, represented by the lack of information on the impact performance of façades for other than the currently standardized projectiles. It would be interesting to test façades, using the design framework and the case study results presented in the thesis, on commercial products that have been already certified for wind-borne debris resistance according to ASTM standards (2019, 2020). Another gap is in the limited information about tests that involve debris elements shot on façades at various angles of incidence. The performance of building components can be investigated, accordingly, with a wide campaign that considers different building envelope solutions and materials, varying the mechanical resistance of the system, and/or the mechanical properties of the constituent materials.

In the wind engineering field, the limitations of the research are, first, related to the database used for the validation of the analytical design tool used for the wind engineering analysis. Available datasets to validate the numerical calculations of debris trajectory analysis are limited, and most of the studies do not consider real-world scenarios where the debris element originates from a source building. It would be useful to develop a wider database on various debris types, based on various Tachikawa numbers, that can be associated with building components or objects of the urban environment identified as wind-prone for their failure in extreme winds.

Considering the source building, it would be useful to study the failure and trajectory of debris elements both from low-rises and from high-rise buildings, for various roofing solutions (roof tiles, shingles, roof gravel,

green roof technologies, etc.) and roofing shapes (gable/hip/flat roof types). Tall buildings have not yet been assessed through experimental campaigns for wind-borne debris generation, in wind tunnel experiments.

Furthermore, due to major building certifications for sustainable construction, new low- and high-rise buildings often adopt green roof solutions, and these are realized by the installation of many elements (both vegetation and building components) that are potential debris sources, depending on various parameters among which wind zone location and the element characteristics. Currently, there are no design requirements for wind-borne debris impact resistance of façades when there are green roof solutions in the surroundings.

The effects of turbulence, associated with instantaneous peaks of the wind velocity, in the wind field, play a significant role. These affect both the uplift loads and the debris flight after the failure occurs. The thesis presents a design framework where the turbulence effects are considered with a statistical approach that takes the impact design requirement to have a range of results instead of a deterministic output. The assumptions take the analysis to a lower level of complexity if compared to the real-world scenario. These simplifications are managed, by considering different wind speeds for the uniform flow, calculating the debris flight and the impact energy of these wind-borne objects on target buildings in the surrounding area. Regarding the specific example of Chapter 4, further research is needed to assess the near-roof surface flow to derive roof tile wind uplift load, in the same way that has been done for asphalt shingles by Peterka et al. (1997).

For debris flight assessment, the design framework presented in the thesis can be used to verify, based on the target building location, current requirements both for steel ball (representing roof gravel) and lumber (representing the structural member of the balloon frame construction) projectiles, in simplified problems. ASCE 7-22 (2022) requirements extend wind-borne debris impact testing up to 1.6 km from the coastline. It should be assessed if rod-like debris can reach bigger flight distances, based on the source location. Expanding the assessment to building components that have been recurrently recorded to fail and fly in extreme winds such as roof components, it should be extended to different roof tile types and asphalt shingles.

Regarding the trajectory calculation of wind-borne debris, there are limitations related to the analytical models, that are not considering the real wind field in the target building location, especially when it comes to complex urban environments. Currently, computational fluid dynamics (CFD) methods are widely used to assess various design parameters, both for the target building design and for required checks to be done in the urban environment. Among others, CFD software is used to evaluate flow-generated noise and thermal and ventilation analyses for both the exterior and interior of the building. In complex urban environments that

have been widely studied through experimental campaigns, CFD models have been validated. It would be interesting to link the current best practices for urban design and CFD modeling to wind-borne debris generation, flight, and impacts on urban building envelopes. Accordingly, the CFD software can be implemented for debris trajectory simulation, after a significant dataset has been studied, for the analytical validation of the software and to identify the correct boundary conditions for debris failure and flight analysis.

Finally, another limitation of the research is linked to the fact that extreme wind events can be both synoptic and non-synoptic. Wind-borne debris failure and flight mechanism are presented in the thesis in a 2D model. There is no available database of experimental results for failure from a source construction and consequent flight, for the three debris types identified by Wills et al. (2002).

References

AAMA 506-16. Voluntary Specifications for Impact and Cycle Testing of Fenestration Products. American Architectural Manufacturers Association, Schaumburg, IL, USA.

Abdelhady, A.U., Spence, S.M.J., McCormick, J., 2022. Exogenous windborne debris: Definition and required extent of surrounding buildings for modeling in hurricanes. In: Engineering Structures 254 (2022) 113798.

Allori, D., Bartoli, G., Mannini, C., 2013. Wind tunnel tests on macro-porous structural elements: A scaling procedure. In: Journal of Wind Engineering and Industrial Aerodynamics 123 (2013), pp. 291-299.

AS 1170.2:1971. Minimum design loads on structures, Part 2: Wind actions. Standards Australia.

AS 1170.2:1983. Minimum design loads on structures, Part 2: Wind actions. Standards Australia.

AS 1170.2:1989. Minimum design loads on structures, Part 2: Wind actions. Standards Australia.

AS/NZS 1170.2:2002. Structural design actions, Part 2: Wind actions. Standards Australia / Standards New Zealand.

AS/NZS 1170.2:2011. Structural design actions, Part 2: Wind actions. Standards Australia / Standards New Zealand.

AS/NZS 1170.2:2021. Structural design actions, Part 2: Wind actions. Standards Australia / Standards New Zealand.

ASCE, 2014. Engineering Damage Assessments Following Hurricanes.

ASCE, 2016. Wind Engineering for Natural Hazards.

ASCE/SEI 7-22, 2022. Minimum Design Loads and Associated Criteria for Buildings and Other Structures.

ASTM C 1492-22. Standard Specification for Concrete Roof Tile.

ASTM C 1568-08. Wind Resistance of Concrete and Clay Roof Tiles (Mechanical Uplift Resistance Method).

ASTM E 1886-19. Standard Test Method for Performance of Exterior Windows, etc. impacted by Missile(s) and Exposed to Cyclic Pressure Differentials.

ASTM E 1996-20. Standard Specification for Performance of Exterior Windows, Curtain Walls, Doors and Storm Shutters Impacted by Windborne Debris in Hurricanes.

Bedon, C., Honfi, D.,Machalická, K. V., Eliášová, M.,Vokáč, M.,Kozłowski, M.,Wüest, T., Santos, F., Williams Portal, N., 2019. Structural characterization of adaptive façades in Europe - Part II: Validity of conventional experimental testing methods and key issues. In: Journal of Building Engineering 25.

Bedon, C., Zhang, X., Santos, F., Honfi, D., Kozłowski, M.,Arrigoni, M., Figuli, L., Lange, D., 2018.Performance of structural glass façades under extreme loads – Design methods, existing research, current issues and trends. In: Construction and Building Materials 163, pp. 921-937.

Block, V., Kopec, T. and Rinehart, D., 2008. A Hurricane by Many Other Names. Accessed on November 1st, 2022. http://www.usglassmag.com/digital/2008/usglass200809-dl.pdf.

Boughton, G.N., Falck, D.J., Henderson, D.J., Smith, D.J., Parackal, K., Kloetzke, T., Mason, M., Krupar III, R., Humphreys, M., Navaratnam, S., Bodhinayake, G., Ingham, S., Ginger, J.D., 2017. Tropical Cyclone Debbie: Damage to buildings in the Whitsunday Region. Technical Report No. 63. Cyclone Testing Station, James Cook University.

Brody, S.D., Zahran, S., Vedlitz, A., Grover, H., 2008. Examining the relationship between physical vulnerability and public perceptions of global climate change in the United States. In: Environment and Behavior 40(1), pp. 72-95.

Brooks, H. E., Lee, J. W., & Craven, J. P., 2003. The spatial distribution of severe thunderstorm and tornado environments from global reanalysis data. In: Atmospheric Research, 67-68, pp. 73-94.

BSI 2015. BS 5534:2014+A1:2015 Slating and tiling for pitched roofs and vertical cladding - Code of practice. British Standards Institution (BSI) Standards Limited.

Butler, K., Kareem, A., 2012. Anatomy of Glass Damage in Urban Areas during Hurricanes. In: Advances in Hurricane Engineering: Learning from Our Past. ASCE.

Chmielewski, T., Nowak, H., & Walkowiak, K., 2013. Tornado in Poland of August 15, 2008: Results of post-disaster investigation. In: Journal of Wind Engineering and Industrial Aerodynamics 118, pp. 54-60.

Chronis, T., Papadopoulos, V., Nikolopoulos, E.I., 2011. QuickSCAT observations of extreme wind events over the Mediterranean and Black Seas during 2000-2008. In: International Journal od Climatology, 31, pp. 2068-2077.

Cochran, L., Levitan, M., 1994. Lessons from Hurricane Andrew. In. Architectural Science Review 37(3), pp. 115-121.

CPR 305-2011. Construction Products Regulation. In: Official Journal of the European Union, Luxembourg.

Cui, W., Caracoglia, L., 2020. Performance-Based Wind Engineering of Tall Buildings Examining Life-Cycle Downtime and Multisource Wind Damage. In: Journal of Structural Engineering 146(1): 04019179.

Cyclone Testing Station (CTS) 2017. Technical Report No. 63: Tropical Cyclone Debbie Damage to buildings.

Darwin Reconstruction Commission, 1975. Darwin Area Building Manual. Darwin Reconstruction Commission, Darwin.

De La Guardia, R., 2012. Hazard Mitigation of the Building Envelope, In: Advances in Hurricane Eng. ASCE.

Doddipatla, L.S, Kopp, G.A., 2019. A review of critical scouring velocity of compact roof aggregate. In: Journal of Wind Engineering & Industrial Aerodynamics 188, pp. 110-124.

Eckstein, D., Kunzel, V., Schafer, L., 2021. Global Climate Risk Index 2021: Who Suffers Most from Extreme Weather Events? Weather-Related Loss Events in 2019 and 200-2019. Germanwatch.

EN 1024:2012. Clay roofing tiles for discontinuous laying. Determination of geometric characteristics. European Committee for Standardisation (CEN), Brussels, Belgium.

EN 12600:2002. Glass in building – Pendulum test – Impact test method and classification for flat glass, European Committee for Standardisation (CEN), Brussels, Belgium.

EN 1304:2013. Clay roofing tiles and fittings. Product definitions and specifications. European Committee for Standardisation (CEN), Brussels, Belgium.

EN 13049:2004. Windows – Soft and heavy body impact – Test method, safety requirements and classification, European Committee for Standardisation (CEN), Brussels, Belgium.

EN 14019:2016. Curtain walling – Impact resistance – Performance requirements, European Committee for Standardisation (CEN), Brussels, Belgium.

EN 14437:2004. Determination of the uplift resistance of installed clay or concrete tiles for roofing - Roof system test method. European Committee for Standardisation (CEN), Brussels, Belgium.

ESSL, 2014. European Severe Storms Laboratory Annual Report 2013.

ESSL, 2018. European Severe Storms Laboratory Annual Report 2017.

ESSL, 2020. European Severe Storms Laboratory Annual Report 2019.

ETAG 004:2013 Guideline for European Technical Approval of ETICS with Rendering. EAD.

ETAG 034:2012. Guideline for European Technical Approval of Kits for External Wall Claddings.

Eurocode EN 1991-1-4:2005 Eurocode 1: Actions on structures.

European Commission, 2019. Building and Renovating.

Experimental Building Station (EBS), Department of Construction, 1978. Technical Record (TR) 440 Guidelines for the Testing and Evaluation of Products for Cyclone-Prone Areas. EBS, North Ryde.

Experimental Building Station (EBS), Department of Construction, 1978. Technical Record (TR) 440 Guidelines for the Testing and Evaluation of Products for Cyclone-Prone Areas. EBS, North Ryde.

Farquhar, S. W.A., Kopp, G.A., and Surry, D., 2005. Wind tunnel and uniform pressure tests of a standing seam metal roof model. In: ASCE Journal of Structural Engineering 131, pp. 650-659.

FEMA, 1993. Building Performances: Hurricane Andrew in Florida.

FEMA, 2015. Safe Rooms for Tornadoes and Hurricanes. Publication 361, FEMA P-361.

Fernandez, G., Masters, F.J., Gurley, K.R., 2010. Performance of hurricane shutters under impact by roof tiles. In: Engineering Structures 32, pp. 3384–3393.

Florida Building Code (FBC) 2001. Florida Building Code Building. International Code Council (ICC).

Florida Building Code (FBC) 2020. Florida Building Code Building. International Code Council (ICC).

FRSA-TRI 2020. Florida High Wind Concrete and Clay Tile Installation Manual. 6th edition.

Gavanski, E., et al., 2013. Wind loads on roof sheathing of houses. In: Journal of Wind Engineering and Industrial Aerodynamics 114, pp.106-121.

Gergis, J., 2019. The Terrible Truth of Climate Change. In: The Monthly, August 2019. Accessed on October 16th, 2022. https://www.themonthly.com.au/issue/2019/august/1566136800/jo-lle-gergis/terrible-truth-climate-change#mtr.

Goliger, A.M., Milford, R.V., 1998. A review of worldwide occurrence of tornadoes. In: Journal of Wind Engineering and Industrial Aerodynamics 74-76 (1998), pp. 111-121.

Grayson, M., Pang, W.C., Schiff, S., 2012. Three-dimensional probabilistic wind-borne debris trajectory model for building envelope impact risk assessment. In: Journal of Wind Engineering and Industrial Aerodynamics, 102 (2012), pp. 22-35.

Gurley, K., Davis, R., Ferrera, S.P., Burton, J., Masters, F., Reinhold, T., Abdullah, M., 2006. Post 2004 hurricane field survey — an evaluation of the relative performance of the standard building code and the Florida Building Code. ASCE structures congress. St. Louis, 2006.

Henderson, D., et al., 2018. Damage and loss to Australian engineered buildings during recent cyclones. International Workshop on Wind-Related Disasters and Mitigation Tohoku University, Sendai, Japan. March 11-14, 2018.

Herseth, A., Smith, T.L., Overcash, G., 2012. FEMA's Coastal Construction Manual Update – Wind Resistant Design. In: Advances in Hurricane Engineering. Learning from Our Past. ASCE.

Hoerner, S. F. 1965. Fluid-dynamic drag, Hoerner Fluid Dynamics, Midland Park, N.J.

Holmes, J.D., 2015. Wind Loading of Structures. CRC Press, Taylor & Francis Group.

Holmes, J.D., Baker, C.J., Tamura, Y., 2006. Tachikawa number: A proposal. In: Journal of Wind Engineering and Industrial Aerodynamics 94 (2006), pp. 41-47.

Holmes, J.D., Kwok, K.C.S., Ginger, J.D., 2012. Wind Loading Handbook for Australia and New Zealand. Australasian Wind Engineering Society, Sydney.

Hu, Z., Maxit, L., Cheng, L., 2021. Acoustic design and analyses of a double Skin Façade system. In: Applied Acoustics 173 107727.

Intergovernmental Panel on Climate Change (IPCC), 2018. Special Report: Global Warming of 1.5°C.

Intergovernmental Panel on Climate Change (IPCC), 2022. Climate Change 2022. Mitigation of Climate Change. Working Group III contribution to the WGIII Sixth Assessment Report of the Intergovernmental Panel on Climate Change.

International Building Code (IBC) 2021. International Building Code Building. International Code Council (ICC).

International Organization for Standardization 2018. Contributing to the UN Sustainable Development Goals with ISO standards. ISO Central Secretariat.

ISO 16932:2007 Glass in building - Destructive-windstorm-resistant security glazing.

ISO 22496:2021. Windows and pedestrian doors — Vocabulary, International Organization for Standardization, Geneva, Switzerland.

ISO 4354:2009. Wind actions on structures, International Organization for Standardization, Geneva, Switzerland.

ISO 7892:1988. Vertical building elements – Impact resistance tests – Impact bodies and general test procedures, International Organization for Standardization, Geneva, Switzerland.

Jacobson, M. Z., Delucchi, M. A., Cameron, M. A., Coughlin, S. J., Hay, C. A., Manogaran, I. P., Shu, Y., von Krauland, A.-K., 2019. Impacts of Green New Deal Energy Plans on Grid Stability, Costs, Jobs, Health, and Climate in 143 Countries. In: One Earth, 1(4), pp. 449- 463.

JIS R 3109, 2018. Glass in Building – Destructive-Windstorm-Resistant Security Glazing – Test Method. Japanese Industrial Standard.

Kopp, G.A., 2009. A Wind Tunnel Study to Observe the Characteristics of Loose-Laid Gravel Blow-Off from a Flat Roofed Low-Rise Building under Wind Load, Boundary Layer Wind Tunnel Laboratory Report BLWT-3-2009. University of Western Ontario, London, Canada.

Kopp, G.A., 2018. Flight Characteristics of Wind-Borne Debris. ASCE, 2018, pp. 39-52.

Kopp, G. A., Hong, E., Gavanski, E., Stedman, D., and Sills, D. M. L., 2017. Assessment of wind speeds based on damage observations from the Angus (Ontario) tornado of June 17, 2014. In: Canadian Journal of Civil Engineering 44(1), pp. 37-47.

Kordi, B., 2009. Aerodynamics of windborne plate debris. Ph.D. thesis. Department of Civil and Environmental Engineering, Faculty of Engineering Science, University of Western Ontario.

Kordi, B., Kopp, G.A., 2008. A Wind Tunel Study of Roof Shingle and Tile Flight. Report BLWT-SS10-2008. Alan G. Davenport Wind Engineering Group. Western Univeristy.

Kordi, B., Kopp, G.A., 2009. "The debris flight equation" by C.J. Baker. In: Journal of Wind Engineering and Industrial Aerodynamics 97, pp. 151-154.

Kordi, B., Kopp, G.A., 2011. Effects of initial conditions on the flight of windborne plate debris. In: Journal of Wind Engineering and Industrial Aerodynamics 99, pp. 601-614.

Kordi, B., Traczuk, G., Kopp, G.A., 2010. Effects of wind direction on the flight trajectories of roof sheathing panels under high winds. In: Wind and Structures 13 vol.2, pp. 145-167.

Kuligowski, E.D., Lombardo, F.T., Phan, L., Levitan, M. L., Jorgensen, D.P. 2014. Final Report, National Institute of Standards and Technology (NIST) Technical Investigation of the May 22, 2011, Tornado in Joplin, Missouri. National Construction Safety Team Act Reports (NIST NCSTAR).

Laboy, S., Dmith, D., Fernandez, G., Masters, F., 2012. Residential Fenestration Vulnerability to Windborne Debris. In: Advances in Hurricane Engineering: Learning from Our Past. ASCE, 2012.

Legambiente, Rapporto 2020 "Il clima è già cambiato".

Letchford, C., 2018. Current Standards for Wind-Borne Debris Testing and Protection. Wind-Borne Debris Hazards. ASCE, pp. 83-93.

Lieblein, J. (1974). "Efficient methods of extreme-value methodology." NBSIR 74-602, National Bureau of Standards, Washington, DC.

Lin, L.H., Hinman, E., Stone, H.F., Roberts, A.M., 2004. Survey of window retrofit solutions for blast mitigation. In: Journal of Performance of Constructed Facilities, ASCE 2004.18, pp. 86-94.

Lin, N., Holmes, J. D., Letchford, C. W., 2007. Trajectories of Wind-Borne Debris in Horizontal Winds and Applications to Impact Testing. In: Journal of Structural Engineering 133, pp. 274-82.

Lin, N., Letchford, C., Holmes, J.D., 2006. Investigation of plate-type windborne debris. Part I. Experiments in wind tunnel and full scale. In: Journal of Wind Engineering and Industrial Aerodynamics 94, pp. 51-76.

Lin, N., Letchford, C., Holmes, J.D., 2006. Investigation of plate-type windborne debris. Part I. Experiments in wind tunnel and full scale. In: Journal of Wind Engineering and Industrial Aerodynamics 94, pp. 51-76.

Lo, Y.L., Wu, Y.T., Fu, C.L., Y., Y.C., 2020. Wind load reduction effects on inner buildings by exterior porous façades. In: Building and Environment 183(2020), 107148.

Lu, S., X. Bai, X. Zhang, W. Li, and Y. Tang, 2019. The impact of climate change on the sustainable development of regional economy. In: Journal of Cleaner Production 233, pp. 1387-1395.

Marshall, T.P., Gilvary, K., Kestner, J., 2012. Hurricane Andrew 20 Years Later: What Have We Learned? 30th Conference on Hurricanes and Tropical Meteorology, Jacksonville, April 16th – 20th, 2012.

Maruyama, T., 2011. Simulation of Flying Debris Using a Numerically Generated Tornado-like Vortex. In: Journal of Wind Engineering and Industrial Aerodynamics 99, pp. 249-256.

Mason, M., Haynes, K., 2010. Historical Case Studies of Extreme Events – Adaptation. Lessons from Cyclone Tracy. National Climate Change Adaptation Research Facility, Gold Coast.

Mehta, K. 2013. Development of the EF-scale for tornado intensity. In: Journal of Disaster Research Vol.8 No.6, 2013, pp. 1034-1041.

Mejorin, A., Rigone, P., Kopp, G.A., Trabucco, D., 2020. Wind-borne debris resistant façades: The European case of flying debris - roof tiles. In: 15th Conference on Advanced Building Skins 26-27 October 2020 Conference Proceedings, Bern, Switzerland, pp. 50-60.

Mejorin, A., Trabucco, D., 2017. Resilienza del curtain wall: analisi delle normative internazionali per contrastare i cambiamenti climatici. In: L'Ufficio Tecnico n. 11-12/2017, pp. 82-89.

Mejorin, A., Trabucco, D., Stelzer, I., 2019. Cyclone-Resistant Façades. Best practices in Australia, Hong Kong, Japan, and the Philippines. CTBUH Research Report, Images Publishing.

Mejorin, A., Trabucco, D., Stelzer, I., Nakada, R., Rooprai, M.S., 2018a. Cyclone-Glazing and Façade Resilience for the Asia Pacific Region. Council on Tall Buildings and Urban Habitat, p. 122.

Mejorin, A., Trabucco, D., Stelzer, I., Nakada, R., Rooprai, M.S., 2018b. "Cyclone-Glazing and Façade Resilience for the Asia Pacific Region: Market Study and Code Survey". In: CTBUH Journal 2018 Issue II, pp. 42-47.

Miami Dade County, 2006. Post Hurricane Wilma assessment.

Minor, J.E., 1974. "Analysis of the Window Damaging Mechanism in Windstorms". Ph.D. thesis. Texas Tech University.

Minor, J.E., 1994. Wind-borne debris and the building envelope. In: Journal of Wind Engineering and Industrial Aerodynamics 53(1994), pp. 207-227.

Minor, J.E., 2005. Lessons learned from failures of the building envelope in windstorms. In: Journal of Architectural Engineering 11 (1), pp. 10-13.

Minor, J.E., 2009. Glazing systems to resist windstorms on special buildings. Woodhead Publishing C&S Engineering, pp. 217-231.

Minor, J.E., Mehta, K.C., McDonald, J.R., 1972. Failures of structures due to extreme winds. In: Journal of the Structural Division 98 (11), pp. 2455-2471.

Moghim, F., 2014. Wind-Borne Debris Trajectory in High Winds: Application to the Protection of Tall Building Façades. Ph.D. thesis, Northeastern University, Boston, Massachusetts.

Moghim, F., Caracoglia, L., 2012. A Numerical Model for Wind-Borne Compact Debris Trajectory Estimation: Part 1 – Probabilistic Analysis of Trajectory in The Proximity of Tall Buildings. In: Journal of Engineering Structures 38, pp. 153-62.

Munich RE, 2021. Record hurricane season and major wildfires – The natural disaster figures for 2020. Accessed on October 16th, 2022. https://www.munichre.com/en/company/media-relations/media-information-and-corporate-news/media-information/2021/2020-natural-disasters-balance.html.

Munich RE, 2022. Hurricanes, cold waves, tornadoes: Weather disasters in USA dominate natural disaster losses in 2021. Accessed on October 16th, 2022. https://www.munichre.com/en/company/media-relations/media-information-and-corporate-news/media-information/2022/natural-disaster-losses-2021.html.

Murphy, K., 1984. Big Blow Up North: A History of Tropical Cyclones in Australia's Northern Territory. University Planning Authority, Darwin.

Netherlands Standardization Institute 2011. NEN 6707: Fixing of roof coverings - Requirements and determination methods, Delft, Netherlands.

Nishimura, T., Taniguchi, T., Maruyama, T., 2009. Analysis on Trajectories of Wind-borne Debris and Impact Test of Building Components. GBRC Technical report, vol. 34, pp. 14-24.

Northern Tornadoes Project, 2022. Event Summary for Dunnville. Accessed on October 31st, 2022. Dunnville, ON - Nov 15, 2020 - Event Summary Map (arcgis.com).

NSCP, 2015. National Structural Code of the Philippines 2015. Association of Structural Engineers of the Philippines Inc..

Patterson, M., 2022. Resilience by design: building façades for tomorrow. Transformative Technologies and Research Trajectories. In: Woodhead Publishing Series in Civil and Structural Engineering. Elsevier.

Peterka, J. A., Cermak, J. E., Cochran, L. S., Cochran, B. C., Hosoya, N., Derickson, R. G., Harper, C., Jones, J., and Metz, B., 1997. Wind Uplift Model for Asphalt Shingles. In: Journal of Architectural Engineering, pp. 147-155.

Piscitelli, F.M., Ruiz, J.J., Negri, P., Salio, P., 2022. A multiyear radar-based climatology of supercell thunderstorms in central-eastern Argentina. In: Atmospheric Research 277.

Piscitelli, L.R., 2019. Serviceability and post-failure behavior of laminated glass structural elements. Firenze University Press.

Pomaranzi, G., Daniotti, N., Schito, P., Rosa, L., Zasso, A., 2020. Experimental assessment of the effects of a porous double skin façade system on cladding loads. In: Journal of Wind Engineering and Industrial Aerodynamics 196 (2020), 104019.

Powell, M.D., Huston, S.H., 1996. Hurricane Andrew's Landfall in South Florida. Part II: Surface Wind Fields and Potential Real-Time Applications. In: Weather and Forecasting 11(3).

Prevatt, D. O., Desai, D., 2018. Overview and Field Data. Wind-Borne Debris Hazards. ASCE, pp. 3-17.

Redland Technology 1991. Fixing studies for MRTI normal weight tiles - SBCCI submission. Redland Technology.

Rockel, B., & Woth, K. (2007). Extremes of near-surface wind speed over Europe and their future changes as estimated from an ensemble of RCM simulations. In: Climatic Change 81, pp. 267-280.

SBCCI 1999. SSTD 11-99: Test Standard for Determining Wind Resistance of Concrete or Clay Roof Tiles. Southern Building Code Congress International.

Sisco, M. R., V. Bosetti, and E. U. Weber, 2017. When do extreme weather events generate attention to climate change? In: Climatic Change, 143(1–2), pp. 227-241.

Shahrzad, S., Berardi, U., 2022. Parametric optimization of multifunctional integrated climate-responsive opaque and ventilated façades using CFD simulations. In: Applied Thermal Engineering 204 (2022), 117923.

Skews, B. W., 1990. Autorotation of rectangular plates. In: Journal of Fluid Mechanics 217 (1990), pp. 33-40.

Smith, D.J., Masters, F.J., Chowdhury, A.G., 2016. Investigating a wind tunnel method for determining wind-induced loads on roofing tiles. In: Journal of Wind Engineering and Industrial Aerodynamics 155, pp. 47-59.

Smith, D.J., Morrison, M., 2019. Full-Scale Wind Tunnel Testing of North American and Australian Tile Roofing Systems. Research Report. Insurance Institute for Business & Home Safety (IBHS).

Southern Building Code Congress International (SBBCI), 1997. SSTD 12-94 Test Standards for Determining Impact Resistance from Windborne Debris.

Standards Australia 2002. AS 2050: Installation of roof tiles. Standards Australia.

Tachikawa, M., 1983. Trajectories of flat plates in uniform flow with application to wind-generated missiles. In: Journal of Wind Engineering and Industrial Aerodynamics 14, pp. 443-453.

Testing Application Standard (TAS) 201-94. Impact Test Procedures. Florida Building Code.

Testing Application Standard (TAS) 202-94. Criteria for Testing Impact & Non-impact Resistant Building Envelope Components Using Uniform Static Air Pressure. Florida Building Code.

Testing Application Standard (TAS) 202-94. Criteria for Testing Products Subject to Cyclic Wind Pressure. Florida Building Code.

Trabucco, D., Mejorin, A., Miranda, W., Nakada, R., Troska, C., Stelzer, I., 2017. Cyclone Resistant Glazing Solutions in the Asia-Pacific Region. GPD 2017 Proceedings, Finland, 2017, pp. 64-69.

UNI 11018:2003. Rivestimenti e sistemi di ancoraggio per facciate ventilate a montaggio meccanico.

UNI 9460:2008 Discontinuously laid roof coverings - Criteria for design, execution and maintenance of roofing made either of clay or concrete roofing tiles.

UNI EN 13830:2020 Facciate continue.

UNI EN 14351-1:2016 Finestre e porte.

United Nations (UN), 2015. Transforming our world: the 2030 Agenda for Sustainable Development.

United Nations (UN), 2020. The Sustainable Development Goals Report 2020.

United Nations (UN), 2022. The Sustainable Development Goals Report 2022.

United Nations Environmental Programme (UNEP), 2017. Global Resource Information Database (GRID) network. Tropical cyclone frequency data.
http://preview.grid.unep.ch/index.php?preview=graphs&cat=1&lang=eng

Visscher, B.T., and Kopp, G.A., 2007. Trajectories of roof sheathing panels under high winds. In: Journal of Wind Engineering and Industrial Aerodynamics 95, pp. 697-713.

Walker, G.R. 2010. A Review of the Impact of Cyclone Tracy on Building Regulations and Insurance. In: Australian Meteorological and Oceanographic Journal 60, pp. 199-206.

Walker, G.R., Reardon, G.F., 1987. Technical Report No. 29 - A Discussion of Criteria for the Structural Design of Buildings to Resist Tropical Cyclones. Cyclone Testing Station, Townsville, Australia.

Weber, E. U., 2015: Climate Change Demands Behavioral Change: What Are the Challenges? In: Social Research 82(3), pp. 561-580.

Williams, D.J., Redgen, B.N., 2012. Investigation into Australian Impact Testing Methods and Criteria for Glass Façades. Ph.D. Thesis. Faculty of Science and Engineering, Queensland University of Technology.

Wills, J.A.B., Lee, B.E., Wyatt, T.A., 2002. A model of wind-borne debris damage. In: Journal of Wind Engineering and Industrial Aerodynamics 90, pp. 555-565.

World Economic Forum, 2022a. The Global Risk Report 2022, 17th Edition. Insight Report, World Economic Forum.

World Economic Forum, 2022b. China's Climate Challenge: Financing the Transition to Net Zero. Insight Report, World Economic Forum.

WSEC (Wind Science and Engineering Center), 2006. A recommendation for an enhanced Fujita scale. Texas Tech University, Lubbock, Texas, pp.95.

Zhang, S., Nishijima, K., Maruyama, T., 2014. Reliability-based modeling of typhoon induced wind vulnerability for residential buildings in Japan. In: Journal of Wind Engineering and Industrial Aerodynamics 124, pp. 68-81.

Zhang, X., Hao, H., 2013. Laboratory test and numerical simulation of laminated glass window vulnerability to debris impact. In: International Journal of Impact Engineering 55, pp. 49-62.

Zhang, Y., Wei, K., Shen, Z., Bai, X., Lu, X., & Soares, C. G., 2020. Economic impact of typhoon-induced wind disasters on port operations: A case-study of ports in China. In: International Journal of Disaster Risk Reduction, 101719.

Zeng, Z., Li, X., Li, C., Zhu, Y., 2012. Modeling ventilation in naturally ventilated double-skin façade with a venetian blind. In: Building and Environment 57, pp. 1-6.

Appendix A - Wind-Borne Debris Trajectory Calculation

In this Appendix, the validation of the numerical model used to solve the non-dimensional equations of motion (Equations 2.10, 2.11, 2.12) for a plate-like debris (Wills et al. 2002) is presented, according to Baker's (2007) non-dimensional form for the variables ($\bar{x}$, $\bar{z}$, $\bar{\theta}$). In the calculation, the rotational and static components of the drag, lift, and moment coefficients (C_{DR}, C_{LR}, C_{MR}, C_{DS}, C_{LS}, C_{MS}) follow the definition of Kordi (2009) which is based on Tachikawa's (1983) experiments (Equations 2.13, 2.14, 2.15, 2.19, 2.20, 2.21). The static normal coefficient on the plate C_N is defined in Equation 2.18. Therefore, using a 4th-order Runge-Kutta scheme, the flight trajectories of square plates in a uniform flow have been calculated, considering the quasi-steady theory, and compared to the experiments of Tachikawa (1983). The comparison between Tachikawa (1983) and the calculated trajectory for a plate with l = B = 4 cm, h = 0.2 cm, ρ_m = 1,120 kg/m³, U = 9.18 m/s, θ = 15°, static and rotational coefficients based on Kordi (2009) is reported in Figure 65, Figure 66, Figure 67, Figure 68, Figure 69, Figure 70, Figure 71, Figure 72. The results are limited to the representation of a two-dimensional model where the trajectory of the plate is, accordingly, contained in a two-dimensional space. For the calculation, the flight of the wind-borne debris has been analyzed assuming S_0 = 0.47 (Skews 1990), based on Kordi et al. (2011) approach.
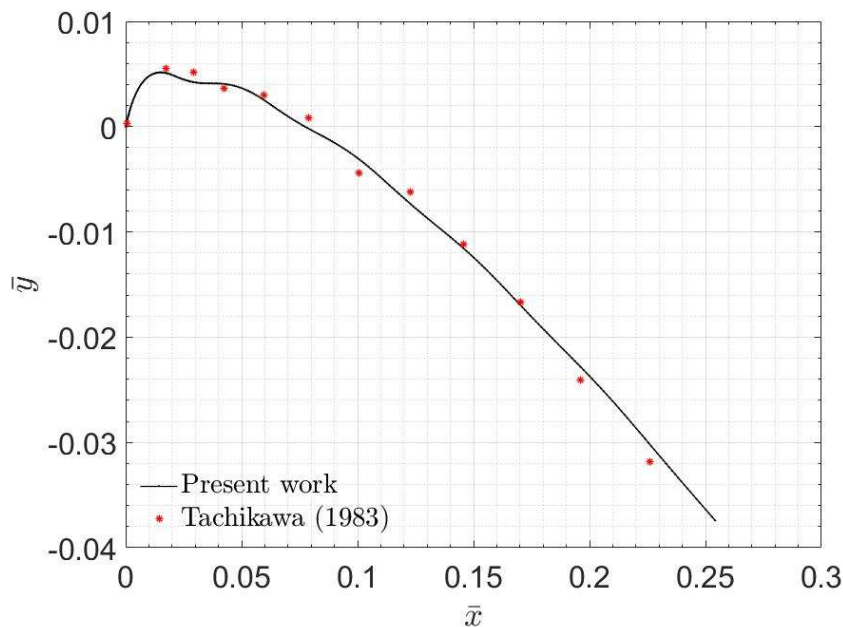

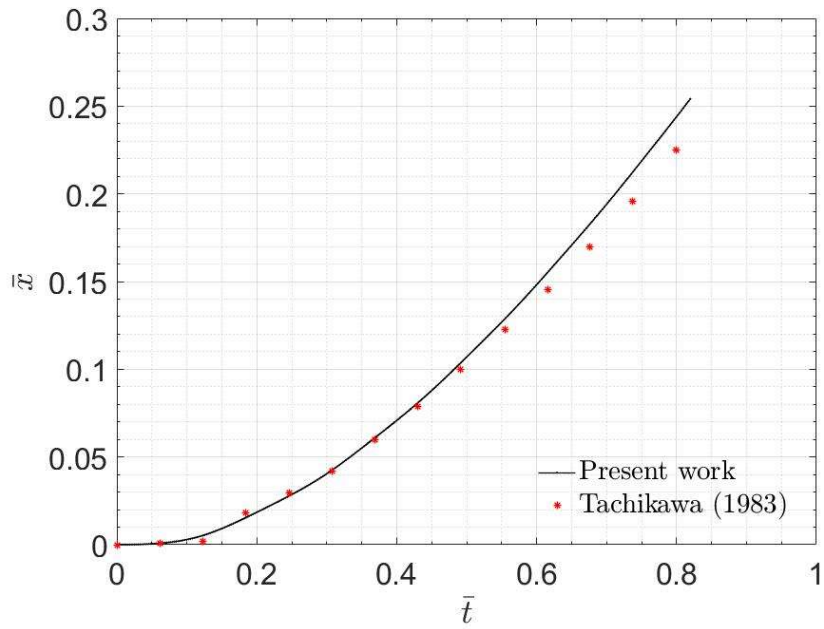**Figure 65 - Non-dimensional trajectory.**

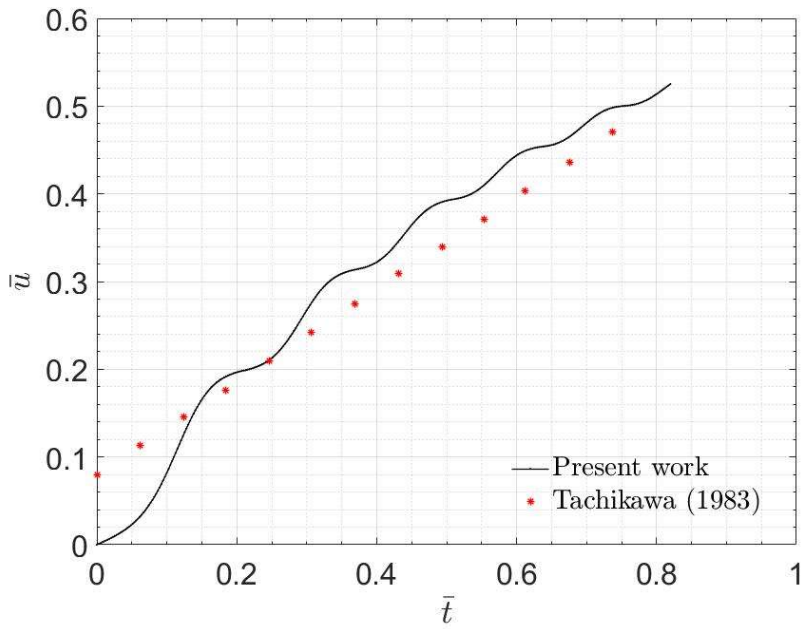**Figure 66 - Non-dimensional horizontal distance vs. non-dimensional time.**

Figure 67 - Non-dimensional horizontal velocity vs. non-dimensional time.
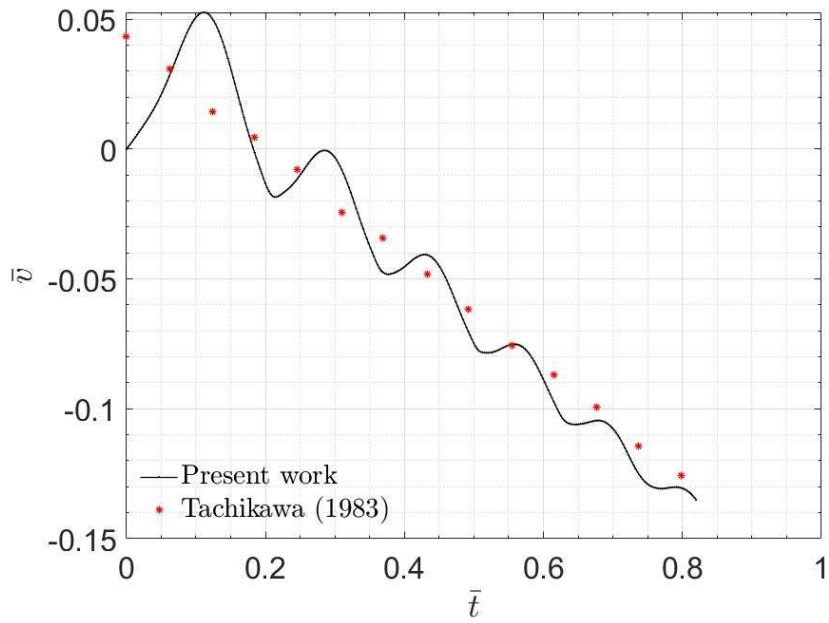
Figure 68 - Non-dimensional vertical velocity vs. non-dimensional time.
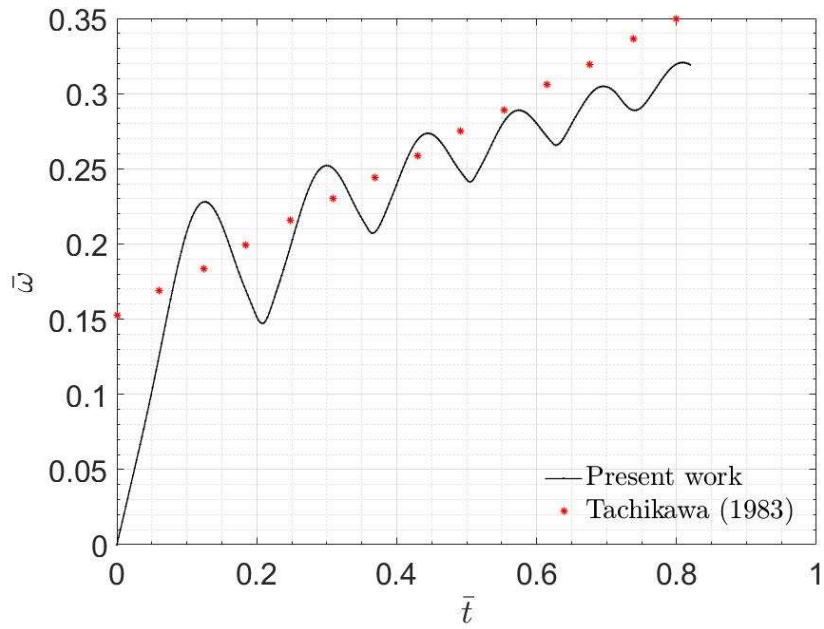

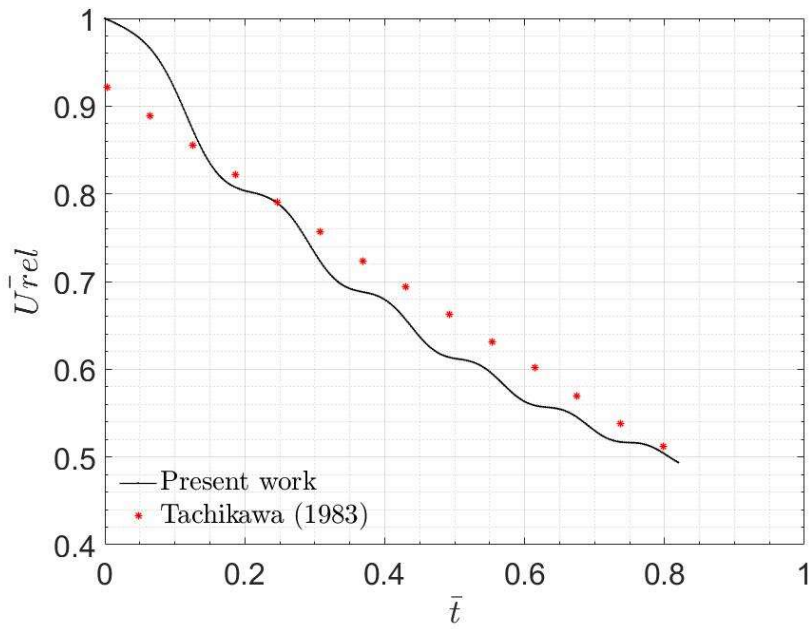**Figure 69 - Non-dimensional angular velocity vs. non-dimensional time.**

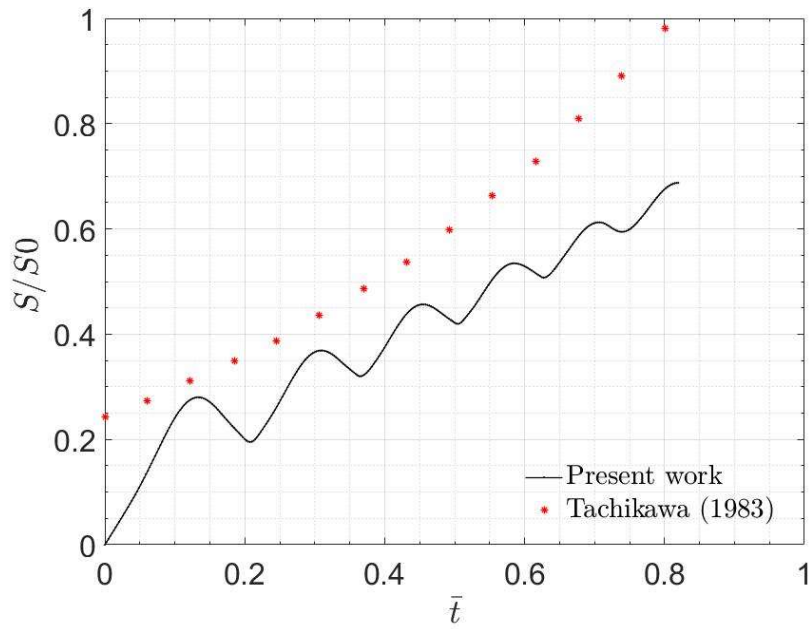**Figure 70 - Non-dimensional relative velocity vs. non-dimensional time.**

Figure 71 - Ratio of the spin parameter to the spin parameter at the point of stable autorotation vs.

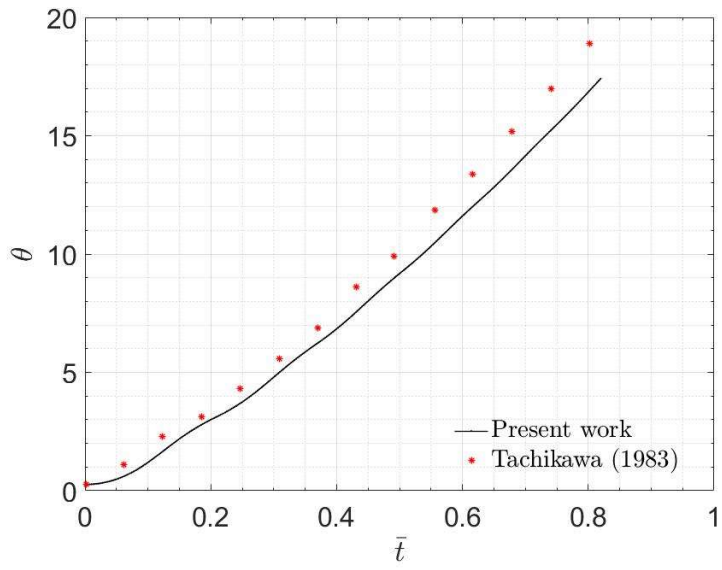**non-dimensional time.**

Figure 72 - Angular displacement (in rad) vs. non-dimensional time.

Appendix B - 3-s Gust Design Wind Speed Conversions

Most of the discussed assessments of the wind-induced force on building components took as reference building code ASCE 7-22 (2022) since in the U.S. there are test requirements for wind-borne debris façade protection. The design requirements of ASCE 7-22 (2022), where the basic wind speed for building design is expressed as a 3-sond gust wind speed, are particularly significant when it comes to wind-borne debris analysis. Wind-borne debris failure and consequent fly relate to the instantaneous velocity and, therefore, the mechanism is linked to wind gusts occurrence (Moghim 2014). A 10-minute mean wind speed does not look in line with the wind-borne debris wind speeds that can be reached after failure.

The studies on wind-borne debris failure analysis can be the reference also for other than the U.S. contexts, where different design wind speeds are considered for building design (i.e. 10-min wind speed). The thesis does account for 3-s gust wind speeds for building design purposes (V_b, V_{b_ini}). When it comes to the European context, the Eurocode 1 (2005) takes into consideration wind loads that are based on a mean wind speed, averaged over 10 minutes. When other wind speeds are used in the design process, such as the mean wind speed averaged over 10 min or 1 h, the following conversion formulae can be used, with reference to ISO 4354 (2009):

$$V_{T=10min} = 0.69 \, V_{T=3s} \qquad\qquad\qquad\qquad\qquad (\text{B. 1})$$

$$V_{T=1h} = 0.65 \, V_{T=3s} \qquad\qquad\qquad\qquad\qquad (\text{B. 2})$$

where:

$V_{T = 3s}$ = 3-second gust wind speed

$V_{T = 10 \, min}$ = 10-minute mean wind speed

$V_{T = 1 \, h}$ = 1-hour mean wind speed

Curriculum Vitae

Name: Angela Mejorin

Post-secondary   Tor Vergata Univerisity of Rome
Education and   Rome, Italy
Degrees: 2007-2010 B.A.

                              Tor Vergata Univerisity of Rome
                              Rome, Italy
                              2010-2012 M.Sci.

                              Politecnico di Torino
                              Turin, Italy
                              2013-2014 M.Eng.

                              Iuav University
                              Venice, Italy
                              2018-2022 Ph.D.

                              Western Univerisity
                              London, ON, Canada
                              2020-2022 Ph.D.

Related Work   Teaching Assistant
Experience   Western University, London, ON, Canada
                              2021-2022

                              Teaching Assistant
                              Iuav University of Venice, Italy
                              2017-2021

                              Research Fellow
                              CTBUH at Iuav University of Venice, Italy
                              2017-2018

Publications:

Mejorin, A., Trabucco, D., 2022. Curtain walling resiliency for tall buildings: standards, testing, and solutions. In: Sustainable High-Rise Buildings: Design, technology, and innovation. Edited by: Al-Kodmany, K., Du, P., Ali, M.M.. The Institution of Engineering and Technology, pp.143-170.

Mejorin, A., Rigone, P., Kopp, G.A., Trabucco, D., 2020. Wind-borne debris resistant façades: The European case of flying debris - roof tiles. In: 15th Conference on Advanced Building Skins 26-27 October 2020 Conference Proceedings, Bern, Switzerland, pp. 50-60.

Mejorin, A., Trabucco, D., Stelzer, I., 2019. Cyclone-Resistant Façades. Best practices in Australia, Hong Kong, Japan, and the Philippines. CTBUH Research Report, Images Publishing.

Mejorin, A., Trabucco, D., Stelzer, I., Nakada, R., Rooprai, M.S., 2018a. Cyclone-Glazing and Façade Resilience for the Asia Pacific Region. Council on Tall Buildings and Urban Habitat.

Mejorin, A., Trabucco, D., Stelzer, I., Nakada, R., Rooprai, M.S., 2018b. "Cyclone-Glazing and Façade Resilience for the Asia Pacific Region: Market Study and Code Survey". In: CTBUH Journal 2018 Issue II, pp. 42-47.

Mejorin, A., Miranda, W., Trabucco, D., 2018. Exceptional atmospheric events resilience of the curtain wall. In: Techne - Journal of Technology for Architecture and Environment, (15), pp. 323-330.

Trabucco, D., Mejorin, A., Miranda, W., Nakada, R., Troska, C., Stelzer, I., 2017. Cyclone Resistant Glazing Solutions in the Asia-Pacific Region. In: Glass Performance Days 2017 Conference Proceedings, Tampere, Finland, 2017, pp. 64-69.